

Density functional studies of the crystallization of hard polymeric chains

Citation for published version (APA):

Sushko, N. B. (2003). *Density functional studies of the crystallization of hard polymeric chains*. [Phd Thesis 1 (Research TU/e / Graduation TU/e), Applied Physics and Science Education]. Technische Universiteit Eindhoven. <https://doi.org/10.6100/IR567681>

DOI:

[10.6100/IR567681](https://doi.org/10.6100/IR567681)

Document status and date:

Published: 01/01/2003

Document Version:

Publisher's PDF, also known as Version of Record (includes final page, issue and volume numbers)

Please check the document version of this publication:

- A submitted manuscript is the version of the article upon submission and before peer-review. There can be important differences between the submitted version and the official published version of record. People interested in the research are advised to contact the author for the final version of the publication, or visit the DOI to the publisher's website.
- The final author version and the galley proof are versions of the publication after peer review.
- The final published version features the final layout of the paper including the volume, issue and page numbers.

[Link to publication](#)

General rights

Copyright and moral rights for the publications made accessible in the public portal are retained by the authors and/or other copyright owners and it is a condition of accessing publications that users recognise and abide by the legal requirements associated with these rights.

- Users may download and print one copy of any publication from the public portal for the purpose of private study or research.
- You may not further distribute the material or use it for any profit-making activity or commercial gain
- You may freely distribute the URL identifying the publication in the public portal.

If the publication is distributed under the terms of Article 25fa of the Dutch Copyright Act, indicated by the "Taverne" license above, please follow below link for the End User Agreement:

www.tue.nl/taverne

Take down policy

If you believe that this document breaches copyright please contact us at:

openaccess@tue.nl

providing details and we will investigate your claim.

Density functional studies of the crystallization of hard polymeric chains

PROEFSCHRIFT

ter verkrijging van de graad van doctor aan de
Technische Universiteit Eindhoven, op gezag van de
Rector Magnificus, prof.dr. R.A. van Santen, voor een
commissie aangewezen door het College voor
Promoties in het openbaar te verdedigen
op dinsdag 23 september 2003 om 16.00 uur

door

Nazar Bohdanovich Sushko

geboren te Lviv (Lemberg), Oekraïne

Dit proefschrift is goedgekeurd door de promotoren:

prof.dr. M.A.J. Michels
en
prof.dr. D. Frenkel

Copromotor:
dr.ir. P. van der Schoot

Druk: Universiteitsdrukkerij Technische Universiteit Eindhoven

CIP-DATA LIBRARY TECHNISCHE UNIVERSITEIT EINDHOVEN

Sushko, Nazar

Density functional studies of the crystallization of hard polymeric chains /
by Nazar Sushko. - Eindhoven : Technische Universiteit Eindhoven, 2003. - Proefschrift.-
ISBN 90-386-1765-8

NUR 924

Trefwoorden: polymeren / kristallisatie / Green functies methodes / dichtheidsfunctionaal-
theorie / elastische moduli / rekstroming.

Subject headings: polymers / crystallization / Green's function methods / density func-
tional theory / elastic moduli / elongational flow.

Contents

1	General introduction	1
1.1	General overview	1
1.2	The role of polymer models	6
1.3	Overview of theoretical methods	8
1.3.1	Mesoscopic equilibrium theories	8
1.3.2	Growth theories	9
1.3.3	Computer simulations	10
1.3.4	Landau-de Gennes theory	10
1.4	Outline of the thesis	11
2	Overview of classical DFT	13
2.1	General principles	13
2.2	Studies of the freezing	17
2.2.1	Thermodynamic perturbation expansion	17
2.2.2	Weighted-density approximation	18
2.2.3	Effective-liquid approximation	20
2.2.4	Fundamental measure theory	21
2.3	Results and comparison of different DFT types	21
2.4	Applications to polymers	23
3	DFT of the crystallization	25
3.1	Introduction	25
3.2	Model	27
3.3	Formalism	29
3.4	Description of the melt	30
3.5	Description of the crystal	31
3.6	Calculation method	32
3.7	Results and discussion	34
3.8	Conclusion	38
3.9	Appendix A	40
3.10	Appendix B	41

4	DFT for the elastic moduli	45
4.1	Introduction	45
4.2	DFT of a model polymeric solid	49
4.3	Elastic moduli from DFT	52
4.4	Calculation method	55
4.5	Results and discussion	60
4.6	Conclusions	66
5	On the role of connectivity in the relative stability	69
6	Theory of the crystallization in an orienting field	77
6.1	Introduction	77
6.2	Polymeric density functional theory	79
6.3	Solidification into the close-packed-crystal geometry	83
6.4	Results and discussion	86
6.5	Conclusions	90
6.6	Appendix	92
7	Beyond the polymeric reference interaction site model	95
8	Summary and proposals for future work	103
8.1	Summary and conclusion	103
8.2	Outlook	105
	Bibliography	107
	Samenvatting	115
	Acknowledgements	119
	Curriculum Vitae	121
	List of publications	123

Chapter 1

General introduction and scope of the thesis

ABSTRACT

In this chapter we give a brief overview of the phenomenon of polymer crystallization. A comparison of the different theoretical methods used to describe this phenomenon is given. We also point out the scope of the thesis.

1.1 General overview of the crystallization of polymers

Large molecules that are constructed from many small, repeating units are usually referred to as polymers. The ability of some of these materials to crystallize has a large industrial significance [1]. Crystalline polymers are important in the development and manufacture of many products in our every-day life. However, the physics of polymer crystallization is quite complex, and is not fully understood even after many years of intense study. The aim of this thesis is to contribute to this field, by combining the statistical theory of polymers and descriptions of the crystallization of simple (atomic) liquids. Before going into the details of our theoretical approach we first briefly describe what is known about the process of polymer crystallization. We also explain in more detail the aim of this thesis, and give its scope.

It is well known that in some temperature ranges polymers solidify into a glassy or rubbery state, but that under the right conditions they can also arrange into regular lattice structures or, in other words, crystallize [1]. The first serious studies of polymeric crystals were

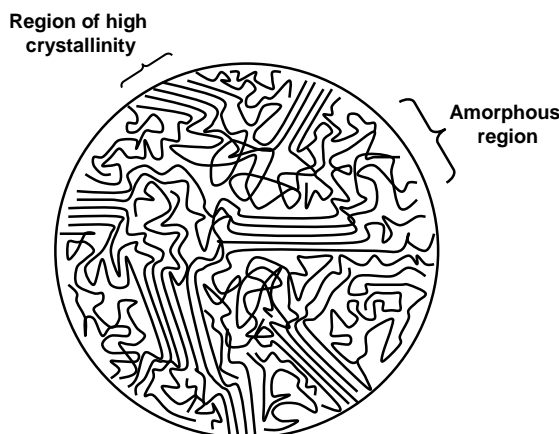


Figure 1.1: Fringed micelle model. One of the first attempts to explain crystalline polymers.

done using the X-ray diffraction technique [1]. Polymeric crystal melting and recrystallization can also be observed by differential scanning calorimetry, because these processes are accompanied by the absorption or the release of latent heat [1]. Studies show that most polymeric crystals formed are never fully crystalline. Some parts of the polymeric solid do not order into a regular crystal lattice, but form amorphous regions. In a typical polymeric crystal the degree of crystallinity lies in the range of 30 – 70% [1].

There have been many attempts to explain this [1]. For instance, the so-called fringed-micelle model was proposed by Hermann, Gerngross and Abitz in 1930 to explain the polymer crystallization phenomenon [2] and it was expanded significantly by Flory [3, 4, 5]. The model is based on the assumption that during crystallization some regions of the polymeric melt align and form bundles. The lateral growth of these regions is caused by the attaching of stretched parts of neighboring chains to these bundles. The presence of entanglements, however, prevents the sample from complete crystallization. The term ‘fringes’ is used to denote the amorphous parts of the sample, which connect different crystalline regions (see Figure 1.1). However, experimental observations showed this theory to be erroneous [6]. Indeed, the fringed-micelle model cannot predict the supramolecular crystalline structures observed in experiments (see below). Its modification can still be used to explain several phenomena occurring during crystallization, but in general this theory fails to explain experimental results.

In 1938, Storcks [6] observed that the total length of the polymeric chains can be much greater than the thickness of the polymeric film, which he studied by the electron diffraction method. He concluded that the polymeric chains have to be folded in order to form the crystal structure. In the early 1950’s Schlesinger and Leeper [7], and later Jaccodine [8], found experimental evidence in support of this conclusion using light microscopy and refractive-index measurements. They discovered that polymeric chains crystallized from

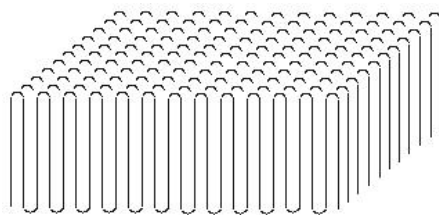


Figure 1.2: Lamellar model. Crystallizing polymers form layered structures called lamellae.

dilute solution are able to fold and form so-called ‘lamellar’ crystals (see Figure 1.2). The experiments conducted by Keller [9], Till [10], and Fischer [11] confirmed that the formation of lamella is the dominant structural mode in most polymeric crystals. With atomic force microscopy one is able to directly observe the lamellae formation [12]. On a larger scale, the amorphous and crystalline material can aggregate to form the supramolecular structures known as spherulites [1, 13] (Figure 1.3). Spherulites are the most common supramolecular structural elements of polymeric crystals when the crystallization happens from the melt or from solution under quiescent conditions, that is, in the absence of flow or any other mechanical deformation. The symmetric structures observed in spherulites cannot be explained using the fringed-micelle model, and the lamellar model seems to be a more plausible explanation. Another interesting structure was found when the polymeric melt was put under influence of an orientating hydrodynamic flow field [13]. In this case the formation of different supramolecular structures, so-called shish-kebab-like structures, is observable (Figure 1.4).

The kinetics of crystallization is very complex and plays a crucial role in the structure of crystalline polymeric solids. Usually, it is possible to distinguish the following three regimes in the crystallization process: homogeneous (or heterogenous) nucleation, secondary nucleation and growth, and secondary crystallization [13]. Nucleation is the process of random birth of small crystalline regions within the liquid polymeric sample. Later the crystal structure develops around the initial nuclei. This process is associated with the radial growth of the spherulites, but it is not the final stage of crystallization. The slow crystallization behind the crystal front caused by crystal thickening, the formation of secondary crystal lamellae and crystal perfection is known as a secondary crystallization. This process usually starts when the growth of the spherulites is limited by contact with other spherulites.

There is a controversial and interesting alternative to views that the nucleation and growth process prevails in solidifying polymer melt, which was found by some experimentalists and deserves to be mentioned [14]. They found a peak in the intensity of the small-angle X-ray scattering at an early time, well before any signal in wide-angle X-ray scattering that is usually associated with the formation of lamellae. This result might be an indication

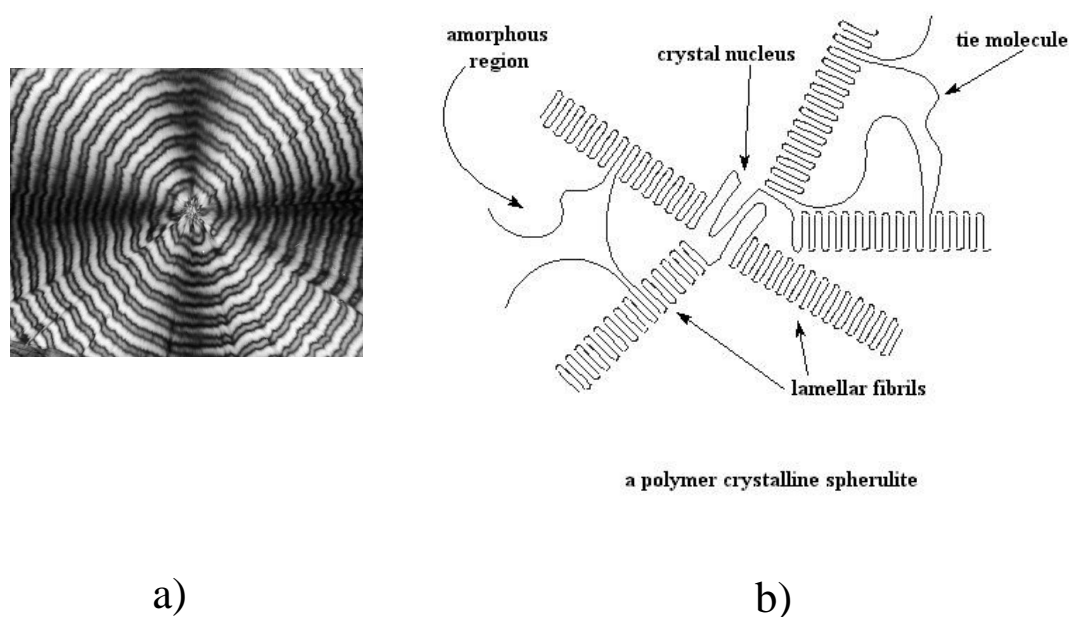


Figure 1.3: (a) Polarized photomicrograph of polyolefin showing a spherulite (from Gedde [1]); (b) Schematic depiction of spherulite. Spherulites consist of many lamellae separated by amorphous regions.

of spinodal decomposition and a hidden liquid-liquid demixing instability caused by the coupling between density and chain conformation. However, it should be mentioned that there is little experimental evidence of this phenomenon, and the evidence that exists has not been unequivocally confirmed [15]. The possibility of the spinodal mode (probably caused by a hidden mesomorphic phase) is hotly debated in literature and not clearly understood [16].

There are basically two dominating ideas to explain why polymers can crystallize. The first idea relies on the interplay between entropy and enthalpy as two main driving forces in the polymer crystallization. In the crystalline state the configuration entropy of the chains is small, because they are arranged into an ordered crystal lattice and into a locked-in position. On the other hand, this regular arrangement into the crystal lattice maximizes the attractive forces between the chains. The balance between entropy loss and enthalpy gain changes with the temperature, and defines the crystallization conditions. The second idea is due to Flory [17], who stated that packing entropy and chain stiffness determine the configuration of the polymeric system, and that enthalpic contributions only change the location of the transition as is now generally accepted to be the case for low-molecular weight materials. Here, we presume that enthalpy has an influence on the ordering transition of polymers, but its role is minor, and entropy dominates. Experimental results, showing the almost athermal behavior of the melting densities (see Figure 1.5), as well as computer simulations [18], support this assumption.

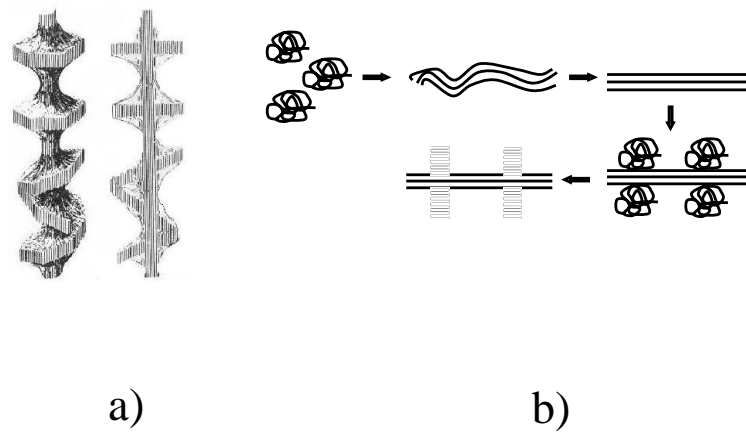


Figure 1.4: (a) Schematic drawing of the shish-kebab structure; (b) Schematic picture of orientationally induced crystallization. At the initial stage some chains are stretched from the coils under influence of an external orienting field. Then the growth of shish-kebab-like structure is observed.

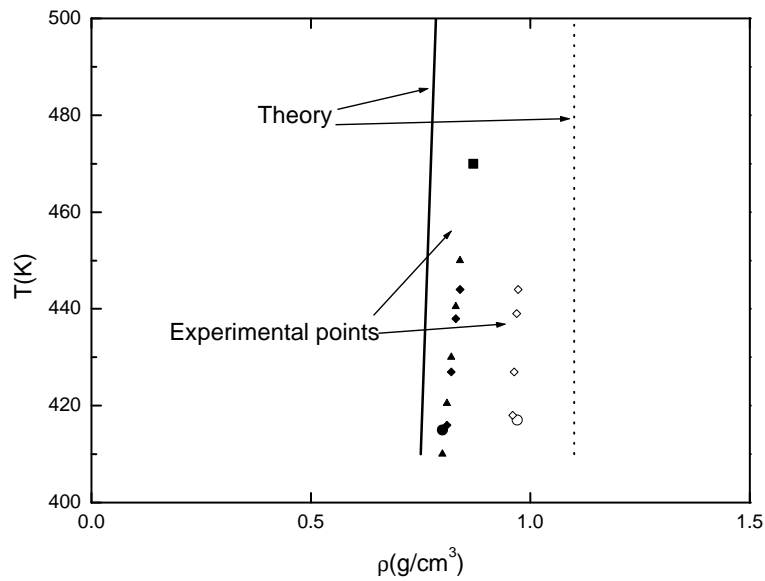


Figure 1.5: Polyethylene phase diagram. The lines are from theory of McCoy and co-workers and the symbols are experimental points. The temperature dependence of the crystallization density is inessential. (After McCoy *et. al.* [19].)

Clearly, the phenomenon under consideration is highly complex, and physical models need to be involved in order to better understand the physical processes behind it. In the next

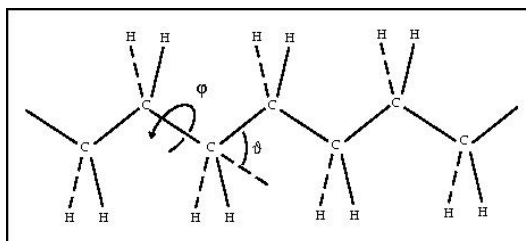


Figure 1.6: The atomic structure of polyethylene showing the two angles: the torsional angle φ and the angle θ between two consecutive bonds.

section we discuss the importance of simplified polymeric models in theoretical studies of polymers in general, and in studies of the polymer crystallization processes in particular.

1.2 The role of polymer models in studies of polymers

A typical polymer molecule consists of many repeating units with many degrees of freedom. See, *e.g.*, Figure 1.6, which shows the atomic structure of polyethylene. If we wish to describe the physical properties of a system consisting of such geometrically complex molecules, the involvement of some approximative physical models that can properly pattern after chemically realistic structures is necessary, because at present it is impossible to describe all the details of such molecules. Also, and perhaps more important, if there are indeed universal features to polymer crystallization, then one would expect that one can do without some of the chemical details. The relation between the detailed molecular structure and the crystallization processes is still being debated.

Bunn [20], and later Wunderlich [21] noticed that the stiffness and interchain attraction, which we presume here to play a minor role, are the driving forces for the solidification of a polymeric system. Thus, chain stiffness should play a key role in the polymeric models that are invoked to understand the crystallization phenomenon. Another important aspect of polymeric models is ‘coarse-graining’ that leaves out (seemingly) unimportant chemical details. In the coarse-grained model some parts of the polymer are represented by a single (usually spherical) object. This approximation has proven its usefulness in studies of polymeric melts and polymeric solutions in which the relevant length scales are larger than the effective length of the polymeric bond. In polymeric crystals the thickness of the lamellae is usually larger than the effective length of the polymeric bond. This would imply that coarse-grained models can be applied to the investigation of polymeric crystals as well. On the other hand, the crystallographic structure of polymeric crystal is microscopic. The variety of the lattice types for different polymers observed may be determined by the microscopic details of polymers. Thus, the coarse-grained polymeric models might run into difficulties in the description of this variety. However, as we show in Chapter 5,

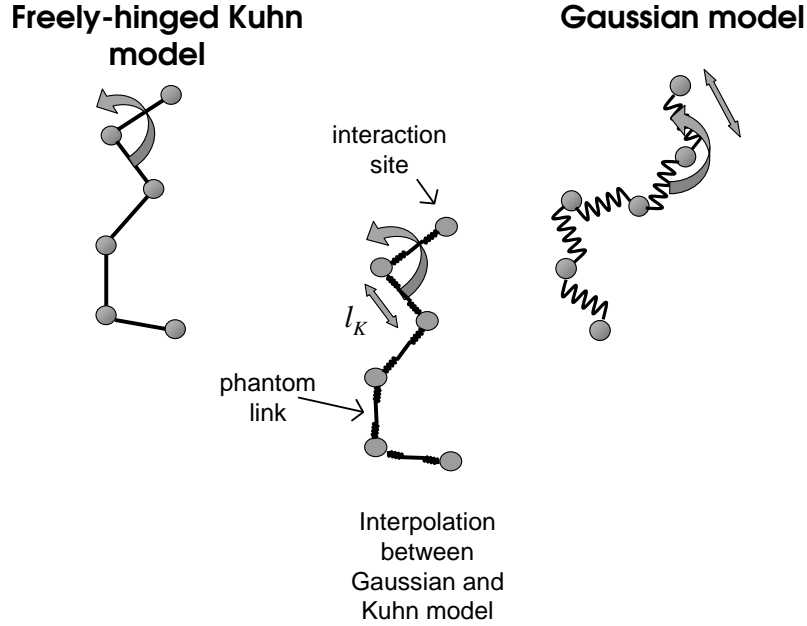


Figure 1.7: Three polymeric models under consideration: freely-hinged Kuhn model with stiff bonds, Gaussian model, and model, which interpolates between the previous two.

using the simplest coarse-grained polymeric models with varying bond stiffness (see below), and assuming the predominance of entropic contributions to the free energy, it is possible to predict different lattice types in polymeric solids. Indeed, lattice frustration effects, described in Chapter 3, can be one of the explanations of the different lattice types in polymer crystals.

The simplest known idealized model is the freely-hinged (jointed) chain, which was introduced for polymers by Kuhn in 1936 (Figure 1.7). This model consists of N stiff uncorrelated bonds of the length l . This means that each bond can be oriented in all possible directions independently from all other bonds. The probability to find the next bead at the fixed position \mathbf{r}' if the previous one is at the position \mathbf{r} can be expressed as

$$g_{fh}(\mathbf{r} - \mathbf{r}') = \frac{1}{4\pi l^2} \delta(|\mathbf{r} - \mathbf{r}'| - l), \quad (1.1)$$

where $|\mathbf{r} - \mathbf{r}'|$ is the distance between two beads.

If the polymeric segments in the model are connected by harmonic springs of a root-mean-square extension l (Figure 1.7), this chain is often called Gaussian, because the probability that the bond, which starts at the position \mathbf{r} and ends at the position \mathbf{r}' , is a Gaussian function

$$g_G(\mathbf{r} - \mathbf{r}') = (2\pi l^2/3)^{-3/2} \exp[-3(\mathbf{r} - \mathbf{r}')^2/2l^2]. \quad (1.2)$$

We use in the studies presented in this thesis a new model that interpolates between the Gaussian and the freely-hinged chain (Figure 1.7). Here, the bond distribution probability of this chain is expressed as

$$g_i(\mathbf{r} - \mathbf{r}') = \frac{\sqrt{6}}{8\pi^{3/2}\xi|\mathbf{r} - \mathbf{r}'|l} \left(\exp \left[-\frac{3(|\mathbf{r} - \mathbf{r}'| - l)^2}{2\xi^2} \right] - \exp \left[-\frac{3(|\mathbf{r} - \mathbf{r}'| + l)^2}{2\xi^2} \right] \right). \quad (1.3)$$

In this case any single polymeric bond consists of a stiff part with length l and a spring of mean length ξ . In this model the effective length of the bond (Kuhn length) does not equal l and can be calculated from the relation $l_K = \sqrt{l^2 + \xi^2}$. In the limit, where $\xi \ll l$, this model behaves like a freely-hinged chain (Eq. (1.1)), whilst for $\xi \gg l$ it becomes equivalent to the Gaussian-chain model (Eq. (1.2)). We use all three models in our study. The Gaussian and Kuhn models were used to study crystallization by different authors [19, 22].

There is also a freely-hinged model with a fixed bond angle, also known as the freely rotating chain. Another important model is that in which the chain has fixed bond angles and an independent potential for the internal torsional bond rotation. Finally, one of the most detailed models is based on the rotational isomeric state (so-called RIS model). In this model, the polymeric chain has an interdependent discrete rotational potential, which was extensively studied by Flory [23]. In the rotational isomeric state model each polymeric bond has one, two or more discrete rotational states.

In our work we study only the simplest chains lacking angular correlations. However, we propose some ideas about possible future studies of polymeric models which show the coupling between the angular and positional degrees of freedom in Chapter 7. In the following section we give a short overview of the most important theoretical methods, that have been used in the past for studies of the crystallization of polymers.

1.3 Overview of theoretical methods in the description of the polymer crystallization

1.3.1 Mesoscopic equilibrium theories

As we argue in Section 1.4, equilibrium theories remain essential even in studies of the kinetically controlled phenomenon of polymer crystallization. Lattice models are appropriate tools for the equilibrium description of systems in which excluded volume plays a role. Flory [17] was the first who proposed a description of polymeric systems with rotational isomerism and volume interactions to study the melting transition. His model can easily be applied to every lattice type. He performed simple mean-field statistical mechanics calculations for the lattice model. In this model all sites are occupied by monomeric units of the polymeric chains, and the elements of two chains cannot occupy the same

lattice site. Flory found that stiffness and compact packing tendency are the two driving forces for the phase transition and that they are independent. He suggested that the packing entropy is the main cause for the phase transition, and that enthalpic effects only determine the location of this transition. In the crystal phase all chains are assumed to be stretched; in this sense the theory of Flory is close to the Onsager theory for liquid crystals [24]. Huggins, Gibbs and Di Marzio [25, 26] somewhat improved the original theory of Flory, although the theory remained highly simplified. However, these lattice theories cannot predict the density jump across the phase transition if the fraction of lattice sites occupied by the polymers is set equal to unity. Another problem is that the chains are stretched by hand in order to form a crystal structure. The controversial result of these descriptions is also that below the melting temperature these simple lattice models are in their ground states for all temperatures [27, 28, 29]. An entropy catastrophe, which means that the conformation entropy of the chains can be negative at temperatures below the temperature of melting, is a problematic feature of the lattice models. Because the simple lattice model may be insufficient to describe the polymeric melting transitions, extensions of the model have been made and a crystallographically realistic lattice model or a gridlock model was developed [30]. The gridlock concept means that the system is locked into a small set of ground states with no disorder over the whole temperature range, unless the polymer chain density is allowed to decrease [30]. These models somewhat improved the results of classical lattice theories for the phase transitions in polymeric systems [30], but they experience the similar disadvantages as the original theory of Flory.

Another equilibrium approach for the studies of polymer crystallization is the off-lattice density functional theory by McCoy *et al.* [19]. The theoretically predicted phase diagram (see Figure 1.5) agrees fairly well with the experimental results, albeit this theory has a set of disadvantages to be discussed in Chapter 3. In the following chapter we give a more detailed insight into density-functional methods and their application to polymers.

1.3.2 Growth theories

Equilibrium theories obviously cannot predict such kinetic phenomena as nucleation and growth processes for which kinetic theories have been set up. These kinetic theories can be separated into two classes, being theories of enthalpic nucleation and those of entropic nucleation. Lauritzen and Hoffman [31, 32] proposed a theory which explains the enthalpic aspects of crystallization. They described the surface nucleation by means of the growth of new stems on the face of the lamellae. The factors that determine this growth are the energetic barrier associated with nucleation and the thermodynamic driving force. This theory compares favorably with experimental data in two features, being the temperature dependency of the initial crystal thickness and the linear growth rate [1]. However, significant disagreement with the experimental data as regards the dependence of the persistence length (a measure of polymer stiffness) on temperature, caused the criticism of this theory [1]. Another assumption, which uses similar ideas as the previous one, is found in the

rate-theory model developed by Sadler and Gilmer [33, 34]. The difference with the previous method is in the cause for the free energy barrier, which in this theory is assumed to have an entropic origin, and in the applicability to the formation of rough surfaces. This theory predicts a temperature dependency of the linear growth rate that it is consistent with observations made by electron microscopy [1].

These methods can describe some of the main features of the kinetics of polymer crystallization. However, they contradict some experimental results. These methods have the assumption that the crystal is growing with a constant thickness of new stems, contrary to the experimental observations [35]. Another disadvantage of these methods is that the connectivity is described implicitly and, in general, they neglect internal details of polymers, such as stiffness, and the role of fluctuations.

1.3.3 Computer simulations

Another important way to study polymer crystallization is by computer simulation. The number of publications on molecular dynamics or Monte Carlo simulations of polymer crystallization is very large. Therefore, we mention only some results, which are important in the context of our studies.

Polson and Frenkel [36] performed molecular simulations of a system of Lennard-Jones chains. They found a solid-fluid transition within this system, and conclude that increasing the chain stiffness results in a stabilization of the crystal. Kinetic Monte Carlo simulation methods were used by Doye and Frenkel to study the growth of polymer crystals [37]. The thickness of the growing polymeric crystal was found to be sensitive to a change in temperature, which conforms the experimental results, but was not found in the earlier theoretical descriptions of Lauritzen and Hoffman or that of Sadler [37]. A very important result of computer studies of the phase transition is the appearance of folded chains which form lamellae [18, 38, 39, 40], or even the supramolecular structures like shish-kebabs in the case of flow induced crystallization [41]. Especially interesting, in the context of our work, is the result that repulsive interactions alone (without attractive interactions) provide a sufficient driving force to form chain-folded structures [18].

Computer simulations are a very powerful technique to study polymer systems. Unfortunately, at this moment these methods are limited by computer capabilities and cannot produce results for large polymeric samples and large molecular weights.

1.3.4 Landau-de Gennes theory

An alternative approach is due to Olmsted and co-workers [16]. Using the Landau-de Gennes theory of phase transitions, they proposed a simple phenomenological theory to explain the spinodal kinetics sometimes found in small-angle X-ray scattering experiments

after a quench to the crystalline state. They proposed a coupling between the density and the conformational state of the chains, leading to a metastable liquid-liquid spinodal within the equilibrium liquid-to-crystalline solid coexistence region. Although interesting, the theory provides no microscopic picture of crystallization. Indeed, information about the polymeric nature of the material is only put in via the phenomenological equation of state [16]. One should mention that an alternative possibility to the liquid-liquid binodal was found. Matsuyama *et. al.* [42] on the basis of the Flory-Huggins theory, found a new type of phase separation in semiflexible polymers. They found a hidden nematic binodal as a results of the partial stiffening of the chains during the phase transition.

1.4 Outline of the thesis

The structure of crystalline polymeric solids is believed to be determined essentially by kinetic processes [13]. But any kinetic theory, which is assigned to describe the crystallization processes, requires a free-energy landscape as an input, because it provides the driving force towards the crystalline state. Therefore, an equilibrium analysis of the phenomenon remains essential. Our aim is to study the driving forces of polymer crystallization as well as the role of connectivity in this process. Also we are interested in the mechanical properties of polymeric solids, and we try to understand the variety of lattice types in different polymeric crystals. Due to the complexity of the crystallization phenomenon we use a set of approximations in our theory: the systems under consideration are athermal, our theory describes ordering only at length scales small compared to the size of the chains, and, finally, in the crystal phase the bonds are not ordered (see Chapters 3-6 for details). Although far removed from experimental reality, we show that within the equilibrium framework it is possible to obtain a set of very useful conclusions regarding polymer crystallization. It appears that only entropy and packing effects are sufficient to stabilize the crystal phase. Another important conclusion is that connectivity has a minor role in the polymer crystallization at least in the limit where the chains are not fully stretched. We suspect that the bond correlations, which we neglect in our description, can stabilize the crystal phase even further and we leave this question open for future investigations.

The polymeric units in our models interact via a hard-core potential (see the following chapters for details). Since the density functional theory can predict the freezing of a system of hard spheres with high degree of accuracy, we believe that this theory is a very promising method to study the crystallization phenomenon in our models. We outline the major principles of this method in the next chapter after we give the outline of the thesis.

This thesis is organized as follows. In Chapter 2 we describe the main principles of classical density functional theory and give a short overview of the existing variations of this theory. In Chapter 3 we describe our formalism and study the crystallization of model polymers. We find that connectivity is responsible for the so-called lattice frustration effects. In the next chapter we study the mechanical properties of a model polymeric solid. We compare

our results with experimental data and find that our theory, which takes into account only entropic contributions, can show an order of magnitude agreement. In Chapter 5 we show that a variety in lattice types for known polymeric crystals can be described using our method. We find that chain stiffness and connectivity can determine the preferred lattice type for the polymeric crystal. The effect of an external orientational flow on the crystallization of polymeric chains is described in Chapter 6. It turns out that in elongational flow model polymers can crystallize more easily than in the absence of this flow. In Chapter 7 we propose a method to improve the description of the polymeric melt, which exhibits angular correlations. And, finally, in Chapter 8 we summarize our studies and make proposals for the future investigation of the fascinating and complex problem of polymer crystallization.

Chapter 2

Overview of classical density functional theories for the liquid and the solid state

ABSTRACT

In this chapter we outline the main principles of classical density-functional theoretical methods in simple liquids and present the main approaches in the context of the freezing transition. The application of density functional theories to polymers is discussed.

2.1 General principles of classical density functional theories

Systems of simple, atomic liquids can show significant spatial variations of the number density or the one-body distribution functions, *e.g.*, near the walls of a container, or near the interface to a co-existent gaseous or crystalline phase. It is not possible to treat these systems using conventional thermodynamical techniques for these rely on bulk properties of the phases. A new approach, which relies on the free energy functional of a single-particle density, has been developed.

Historically, this approach was applied first to quantum systems by Hohenberg and Kohn [43], and Kohn and Sham [44]. They stated that the ground-state free energy of a non-uniform electron fluid is an exclusive functional of the electron density, which corresponds to a single-particle density in the classical case. The principles of density functional theory

found applications not only in quantum, but also in classical systems [45]. The fundamental theorems which are the basis of the density functional theory (DFT) were first formulated by Hohenberg, Kohn [43] and Mermin [46]. These theorems state the following:

Theorem 1. For a given external field the intrinsic free-energy functional is a unique functional of the density.

Theorem 2. The grand potential functional reaches its minimum when the density profiles coincide with the equilibrium densities.

An outline of the proofs of these theorem, on the basis of a paper of Evans [47], is as follows.

Let us consider the grand canonical ensemble, and define $f(\mathbf{r}^N, \mathbf{p}^N)$ as the normalized probability that the system contains N particles with coordinates \mathbf{r}^N and momenta \mathbf{p}^N , which at equilibrium becomes equal to f_0 . At temperature T , we have

$$f_0 = \frac{1}{N!h^{3N}\Xi} \exp\left(-\frac{1}{k_B T}(H_N - \mu N)\right), \quad (2.1)$$

where H_N is the Hamiltonian, Ξ the grand partition function, μ the chemical potential, k_B Boltzmann's constant, and h Planck's constant. The probability f is normalized in the same way as f_0 , *i.e.*,

$$\sum_{N=0}^{\infty} \int \int d\mathbf{r}^N d\mathbf{p}^N f(\mathbf{r}^N, \mathbf{p}^N) = 1. \quad (2.2)$$

Let us *define* the functional Ω of f to be

$$\Omega[f] = \sum_{N=0}^{\infty} \int \int d\mathbf{r}^N d\mathbf{p}^N (H_N - \mu N + k_B T \ln N!h^{3N} + k_B T \ln f) f. \quad (2.3)$$

For the equilibrium probability density we can establish a link between the functional $\Omega[f]$ and the grand potential Ω by insertion Eq. (2.1) into Eq. (2.3)

$$\Omega[f_0] = -k_B T \ln \Xi = \Omega, \quad (2.4)$$

and hence

$$\Omega[f] = \Omega[f_0] + k_B T \sum_{N=0}^{\infty} \int \int d\mathbf{r}^N d\mathbf{p}^N (f \ln f - f \ln f_0). \quad (2.5)$$

There is a theorem [48] that states that if for two arbitrary integrable, positive configuration-space functions $F(\mathbf{r}^N)$ and $G(\mathbf{r}^N)$ the equality

$$\int d\mathbf{r}^N F(\mathbf{r}^N) = \int d\mathbf{r}^N G(\mathbf{r}^N) \quad (2.6)$$

holds, then the Gibbs inequality is satisfied, *i.e.*,

$$\int d\mathbf{r}^N F \ln F \geq \int d\mathbf{r}^N F \ln G. \quad (2.7)$$

Using this theorem it is easy to see that if $f \neq f_0$ then

$$\Omega[f] \geq \Omega[f_0]. \quad (2.8)$$

We define the Hamiltonian of the system as follows

$$H_N(\mathbf{r}^N, \mathbf{p}^N) = K_N(\mathbf{p}^N) + V_N(\mathbf{r}^N) + \int \sum_{i=1}^N \delta(\mathbf{r} - \mathbf{r}_i) \varphi(\mathbf{r}) d\mathbf{r} \quad (2.9)$$

with K_N the kinetic energy of the system, V_N the potential energy, $\varphi(\mathbf{r})$ the external field.

If we change the external field from $\varphi(\mathbf{r})$ to $\varphi'(\mathbf{r})$, the Hamiltonian changes as well into a new one, H'_N . Consequently, the equilibrium probability density f_0 changes into a new probability f'_0 . We define Ω' as a grand potential in the new external field. Due to the condition $f'_0 \neq f_0$ it is possible to define a new inequality from Eqs. (2.3) and (2.4)

$$\begin{aligned} \Omega' &= \sum_{N=0}^{\infty} \int \int d\mathbf{r}^N d\mathbf{p}^N (H'_N - \mu N + k_B T \ln N! h^{3N} + k_B T \ln f'_0) f'_0 \\ &< \int \int d\mathbf{r}^N d\mathbf{p}^N (H'_N - \mu N + k_B T \ln N! h^{3N} + k_B T \ln f_0) f_0. \end{aligned} \quad (2.10)$$

Therefore,

$$\Omega' < \Omega + \int \rho_0(\mathbf{r})(\varphi'(\mathbf{r}) - \varphi(\mathbf{r})) d\mathbf{r} \quad (2.11)$$

with $\rho_0(\mathbf{r})$ the local particle density

$$\rho_0(\mathbf{r}) = \sum_{N=0}^{\infty} \int \int d\mathbf{r}^N d\mathbf{p}^N f_0(\mathbf{r}^N, \mathbf{p}^N) \sum_{i=1}^N \delta(\mathbf{r} - \mathbf{r}_i). \quad (2.12)$$

If we interchange the primed and unprimed quantities and suppose that the local equilibrium density $\rho_0(\mathbf{r})$ remains the same in both external fields, we get

$$\Omega < \Omega' + \int \rho_0(\mathbf{r})(\varphi'(\mathbf{r}) - \varphi(\mathbf{r})) d\mathbf{r}. \quad (2.13)$$

We conclude that

$$(\Omega' + \Omega) < (\Omega + \Omega'), \quad (2.14)$$

which is a contradiction. This means that density $\rho_0(\mathbf{r})$ is determined by the external potential in a unique way and the equilibrium probability density f_0 is a unique functional of the local density $\rho_0(\mathbf{r})$. This is the proof of the Theorem 1. Now we prove the second theorem.

Let us define the free energy functional

$$F[\rho] = \sum_{N=0}^{\infty} \int \int d\mathbf{r}^N d\mathbf{p}^N (K_N + V_N + k_B T \ln N! h^{3N} + k_B T \ln f) f. \quad (2.15)$$

At equilibrium this reduces to [47]

$$F[\rho_0] = -k_B T \ln \Xi + \mu \int \rho_0(\mathbf{r}) d\mathbf{r} - \int \rho_0(\mathbf{r}) \varphi(\mathbf{r}) d\mathbf{r}.$$

The grand potential functional can be defined in terms of the free energy functional

$$\Omega[\rho] = F[\rho] - \mu \int \rho(\mathbf{r}) d\mathbf{r} - \int \rho(\mathbf{r}) \varphi(\mathbf{r}) d\mathbf{r}. \quad (2.16)$$

At equilibrium we get

$$\Omega[\rho_0] = -k_B T \ln \Xi = \Omega. \quad (2.17)$$

From Eq. (2.8) it follows that $\Omega[\rho_0] < \Omega[\rho]$. Thus, Ω is the minimum value of the grand potential functional, or, in other words, the existence of extremum of $\Omega[\rho]$ at equilibrium can be expressed as [47]

$$\left. \frac{\delta \Omega[\rho]}{\delta \rho(\mathbf{r})} \right|_{\rho=\rho_0} = 0. \quad (2.18)$$

In this, not very rigorous way, we proved the theorems mentioned at the beginning of this section. More rigorous derivations can be found elsewhere [47, 48, 49]. See also [50, 51].

Using the thermodynamical relation between the grand potential, Ω , and the Helmholtz free energy, \mathfrak{F} , at equilibrium, we find that

$$\mathfrak{F} = F_{int}[\rho_0] + \int \rho_0(\mathbf{r}) \varphi(\mathbf{r}) d\mathbf{r}. \quad (2.19)$$

The first term in the right-hand-side of Eq. (2.19) is the so-called ‘intrinsic’ free energy [47] and the second term depends on the external potential. Differentiating the Eq. (2.16) with respect to the density at equilibrium we get

$$\mu = \mu_{int}[\rho_0, \mathbf{r}] + \varphi(\mathbf{r}), \quad (2.20)$$

where the intrinsic chemical potential $\mu_{int}[\rho_0, \mathbf{r}] = \left. \frac{\delta F[\rho]}{\delta \rho(\mathbf{r})} \right|_{\rho=\rho_0}$.

The free energy functional can be divided into an ideal part and a part which arises from the interactions between the particles, the so-called excess free energy

$$F[\rho] = F_{id}[\rho] + F_{exc}[\rho]. \quad (2.21)$$

We identify the following important quantity

$$C^{(p)}(\mathbf{r}_1, \dots, \mathbf{r}_p) = -\frac{1}{k_B T} \delta^{(p)} F_{exc} / \prod_{i=1}^p \delta \rho(\mathbf{r}_i), \quad (2.22)$$

which is the p -particle direct correlation function of the system. The formalism described above provides an elegant variational technique for the calculation of the equilibrium density of inhomogeneous classical fluids. However, there is no general recipe to compute the excess free energy, which is a vital ingredient of any DFT. All present DFT types contain uncontrolled approximations in that respect. Despite this problem, the DFT is probably the best modern method for the description of inhomogeneous systems. We present different incarnations of DFT in the following sections.

2.2 Studies of the freezing of simple liquids by means of density functional theories

2.2.1 Thermodynamic perturbation expansion (Ramakrishnan and Yussouff theory)

The theory of the freezing transition for classical fluids in the framework of DFT was developed by Ramakrishnan and Yussouff (RY) [52]. The original RY type of DFT at present has many modifications [53, 54]. Within this method the free energy functional of a solid is perturbationally expanded around a free-energy functional of a homogeneous liquid. The grand potential of the crystal relative to that of the melt equals

$$\Delta\Omega = \Delta F - \int d\mathbf{r} [\mu_S \rho_S - \mu_L \rho_L], \quad (2.23)$$

where ΔF is the difference in the Helmholtz free energies of the crystal and liquid phases, μ_S the chemical potential of the crystal and μ_L the chemical potential of the reference liquid state. We use symbols ρ_S for the mean density of the crystal phase and ρ_L for that of the homogeneous liquid. According to Eq. (2.21) ΔF can be written as $\Delta F = \Delta F_{id} + \Delta F_{exc}$. Haymet and Oxtoby [54] modified the original RY DFT and showed that

$$\begin{aligned} \frac{1}{k_B T} \frac{\Delta\Omega}{\rho_L V} &= \frac{1}{\rho_L V} \int d\mathbf{r} \rho(\mathbf{r}) \ln \rho(\mathbf{r}) / \rho_L \\ &\quad - \frac{1}{\rho_L V} \sum_{p=2}^{\infty} \frac{1}{p!} \int \dots \int C_L^{(p)}(\mathbf{r}_1, \dots, \mathbf{r}_p) \prod_{i=1}^p d\mathbf{r}_i (\rho(\mathbf{r}_i) - \rho_L) \\ &\quad - \frac{1}{k_B T} \frac{1}{\rho_L V} (\mu_S - \mu_L) \int d\mathbf{r} \rho(\mathbf{r}) - \frac{1}{\rho_L V} \int d\mathbf{r} (\rho(\mathbf{r}) - \rho_L), \end{aligned} \quad (2.24)$$

where the excess free energy of the solid phase is thermodynamically expanded around the excess free energy of the uniform liquid, V is the volume of the system, T denotes the absolute temperature and k_B Boltzmann's constant. The functional derivatives in the expansion are substituted by the direct correlation functions of the uniform liquid $C_L^{(p)}(\mathbf{r}_1, \dots, \mathbf{r}_p)$ following Eq. (2.22).

The coexistent densities of the solid and liquid at the freezing transition can be obtained by minimization of Eq. (2.24) with respect to the local density profiles $\rho(\mathbf{r})$. A sensible approximation that can be made, is substitution of the exact density distribution by a sum of Gaussians,

$$\rho(\mathbf{r}) = (\pi\epsilon^2)^{-3/2} \sum_{\{\mathbf{R}\}} \exp[-(\mathbf{R} - \mathbf{r})^2/\epsilon^2], \quad (2.25)$$

where $\{\mathbf{R}\}$ denotes the set of real-space lattice vectors of the crystal, and ϵ is a measure of the width of the Gaussian density distribution around each lattice point (see, however,

[55]). The densities of both crystal and liquid phases and the width of the Gaussian are determined by a free-energy minimization. Eq. (2.24) takes on a simple form if the density profiles in crystal are assumed to be only weakly overlapping [53, 56, 57]. This assumption turns out to be accurate for a wide range of solid densities and Gaussian widths [53].

The functional in Eq. (2.24) requires the direct correlation function of a uniform liquid as an input. Usually the four-body and higher-order correlation functions in the second term of Eq. (2.24) are left out, and the three-body one approximated by its value at zero wave vector. (Haymet [54] has shown for hard spheres that only the zero wave vector part of the three-body term is important in Eq. (2.24), because the non-zero \mathbf{q} contributions have an oscillatory character and cancel each other out.) The two-body direct correlation function can be obtained from a suitable closure of the Ornstein-Zernike equation that links the direct correlation function to the total correlation function. The hard-sphere two-body direct correlation function is an exact analytic solution of this equation with the Percus-Yevick closure and is used as input to Eq. (2.24) [49]. The three-body direct correlation function can be obtained from the two-body direct correlation function, at least near zero wave vector. This theory is computationally convenient and produces quite good agreement for the freezing densities for hard-sphere systems in comparison with the results of computer simulations. We adopt this type of DFT as a basis for our polymeric theory and present it in the next chapter.

2.2.2 Weighted-density approximation

The second type of DFT is the so-called weighted-density approximation (WDA) [58, 59] in which the solid is treated as an inhomogeneous liquid. This approach tries to avoid the perturbative description of a solid. The excess free energy of a solid phase is written as follows

$$F_{exc}[\rho_S] = \int d\mathbf{r} \rho(\mathbf{r}) f_{exc}^L(\bar{\rho}(\mathbf{r})), \quad (2.26)$$

where $f_{exc}^L(\bar{\rho}(\mathbf{r}))$ is the excess free energy per particle of a uniform liquid, which can be obtained, *e.g.*, from the equation of state of that fluid. The weighted solid density, $\bar{\rho}(\mathbf{r})$, is expressed as

$$\bar{\rho}(\mathbf{r}) = \int d\mathbf{r}' \rho(\mathbf{r}') w(\mathbf{r}' - \mathbf{r}, \bar{\rho}(\mathbf{r})) \quad (2.27)$$

with $w(\mathbf{r}' - \mathbf{r}, \bar{\rho}(\mathbf{r}))$ the normalized weighting function $\int d\mathbf{r} w(\mathbf{r}, \bar{\rho}) = 1$. It is technically complicated to compute the weighting function from the previous equation and some assumptions need to be made. The exact expression for the direct correlation function of the solid is

$$C_S^{(2)}(\mathbf{r}', \mathbf{r}, \rho_S) = -\frac{1}{k_B T} \left(\frac{\delta^2 F_{exc}[\rho_S]}{\delta \rho_S(\mathbf{r}) \delta \rho_S(\mathbf{r}')} \right). \quad (2.28)$$

The choice of the weighting function should satisfy the condition that for the direct correlation function of the uniform liquid

$$C_L^{(2)}(\mathbf{r}' - \mathbf{r}, \rho_L) = -\frac{1}{k_B T} \left(\frac{\delta^2 F_{exc}[\rho_S]}{\delta \rho_S(\mathbf{r}) \delta \rho_S(\mathbf{r}')} \right) \Big|_{\rho_S(\mathbf{r})=\rho_L}. \quad (2.29)$$

The following virial type of expansion was involved in order to compute the weighting function [58]

$$\begin{aligned} w(\mathbf{r}, \rho_L) &= w_0(\mathbf{r}) + w_1(\mathbf{r})\rho_L + w_2(\mathbf{r})\rho_L^2 + \dots \\ C_L^{(2)}(\mathbf{r}, \rho_L) &= c_0(\mathbf{r}) + c_1(\mathbf{r})\rho_L + c_2(\mathbf{r})\rho_L^2 + \dots \end{aligned} \quad (2.30)$$

and is usually truncated after the second order in the density. The approximation thus made is still rather crude and has similar weak points as the previous type of DFT, *i.e.*, the perturbative expansion of the thermodynamic quantities. Moreover, there is a lack of information about the convergence of the above series.

A different method, circumventing Eq. (2.30), was proposed by Curtin and Ashcroft [59]. The next equation directly follows from Eq. (2.29)

$$-k_B T \widehat{C}_L^{(2)}(q, \rho_L) = 2 \frac{\partial f_{exc}^L(\rho_L)}{\partial \rho_L} \widehat{w}(q, \rho_L) + \rho_L \frac{\partial}{\partial \rho_L} \left(\frac{\partial f_{exc}^L(\rho_L)}{\partial \rho_L} [\widehat{w}(q, \rho_L)]^2 \right), \quad (2.31)$$

where the hats denote the Fourier transform and q is the length of the wave vector. This equation is used to calculate the weighting function. Then the weighted solid density and excess free energy follow; the latter can subsequently be minimized with respect to solid density.

A technical improvement of the WDA was made by Denton and Ashcroft [60], who invented the modified WDA (MWDA). They replace equation (2.26) for the excess free energy by

$$\frac{1}{\rho_S V} F_{exc}[\rho_S] = f_{exc}^L(\tilde{\rho}) \quad (2.32)$$

with $\tilde{\rho}$ the uniform weighted solid density, which is

$$\tilde{\rho} = \frac{\int d\mathbf{r} \int d\mathbf{r}' \rho(\mathbf{r}) \rho(\mathbf{r}') \tilde{w}(\mathbf{r} - \mathbf{r}', \tilde{\rho})}{\int d\mathbf{r}'' \rho(\mathbf{r}'')}. \quad (2.33)$$

The new equation for the weighting function in the Fourier space is much simpler than Eq. (2.31) and adopts the form

$$-k_B T \widehat{C}_L^{(2)}(q, \rho_L) = 2 \frac{\partial f_{exc}^L(\rho_L)}{\partial \rho_L} \widehat{w}(q, \rho_L) + \rho \frac{\partial^2 f_{exc}^L(\rho_L)}{\partial^2 \rho_L} \delta_{q,0}. \quad (2.34)$$

The results of the MWDA for the hard-sphere system have very good agreement with computer simulations. This method requires as input the direct correlation function, which can again be obtained by means of the Ornstein-Zernike equation for classical fluids, in addition it requires the excess free energy per particle. The latter can be calculated from the equation of state.

2.2.3 Effective-liquid approximation

The third type of DFT involves an effective-liquid approximation (ELA), suggested by Baus and Colot [61] who also wanted to avoid the perturbative expansion of the excess free energy. The expression for the excess free energy in this method is written as

$$F_{exc}[\rho_S] = F_{exc}[\rho_L] + \tag{2.35}$$

$$-k_B T \int d\mathbf{r} \int d\mathbf{r}' \int_0^1 d\lambda \int_0^\lambda d\lambda' C^{(2)}(\mathbf{r}, \mathbf{r}' \rho_L + \lambda' \Delta\rho) \Delta\rho(\mathbf{r}) \Delta\rho(\mathbf{r}'),$$

where ρ_L is density of a uniform liquid reference state, $\Delta\rho(\mathbf{r}) = \rho_S(\mathbf{r}) - \rho_L$ is the density difference between reference density and the solid density ρ_S . The last one is achieved gradually as $\rho_L + \lambda\Delta\rho$, $0 \leq \lambda \leq 1$.

The direct correlation function of the solid phase is now approximated by the direct correlation function $C_L^{(2)}(\mathbf{r} - \mathbf{r}', \bar{\rho}(\rho_L))$ of the effective liquid of density $\bar{\rho}$

$$\frac{1}{k_B T} F_{exc}[\rho_S] = \frac{1}{k_B T} F_{exc}[\rho_R] \tag{2.36}$$

$$- \frac{1}{2} \int d\mathbf{r} \int d\mathbf{r}' C_L^{(2)}(\mathbf{r} - \mathbf{r}', \bar{\rho}(\rho_L)) \Delta\rho(\mathbf{r}) \Delta\rho(\mathbf{r}').$$

Baus and Colot [61] made the following choice of $\bar{\rho}(\rho_L)$. They postulated that the position of the main peak of the static structure factor of the effective liquid of density $\bar{\rho}$ corresponds to the smaller reciprocal lattice vector of the solid of average density ρ_L . If we expand the density of the effective liquid around the density of uniform fluid, we obtain the Ramakrishnan and Yussouff free energy functional.

A modification of this theory has been suggested by Baus [62]. He introduced a new excess free energy, which is just Eq. (2.35) with $\rho_L = 0$, giving

$$\frac{1}{k_B T} F_{exc}[\rho_S] = - \int d\mathbf{r} \int d\mathbf{r}' \int_0^1 d\lambda \int_0^\lambda d\lambda' C_L^{(2)}(\mathbf{r} - \mathbf{r}', \lambda' \tilde{\rho}) \rho_S(\mathbf{r}) \rho_S(\mathbf{r}'). \tag{2.37}$$

The effective-liquid density $\tilde{\rho}$ is then determined self-consistently in terms of $\rho_S(\mathbf{r})$ and $C_L^{(2)}$ from the expression for the excess free energy per particle of the solid, which is the same as the one for an effective liquid

$$\frac{1}{\rho_S V} F_{exc}[\rho_S] = f_{exc}^L(\tilde{\rho}) \equiv -k_B T \tilde{\rho} \int d\mathbf{r} \int_0^1 d\lambda \int_0^\lambda d\lambda' C_L^{(2)}(\mathbf{r}, \lambda' \tilde{\rho}). \tag{2.38}$$

This method is often referred as modified effective-liquid approximation (MELA). The results of MELA are superior to the ones of ELA. It is possible to establish a link with

between MWDA and MELA if the weighting function is written as

$$\tilde{w}(\mathbf{r}, \tilde{\rho}) = \frac{\int_0^1 d\lambda \int_0^\lambda d\lambda' C_L^{(2)}(\mathbf{r}, \lambda' \rho)}{\int d\mathbf{r}' \int_0^1 d\lambda \int_0^\lambda d\lambda' C_L^{(2)}(\mathbf{r}', \lambda' \rho)}. \quad (2.39)$$

In this case the excess free energy can be written as in Eqs. (2.26) and (2.27).

2.2.4 Fundamental measure theory

The fourth type of DFT is the fundamental measure theory (FMT) developed by Rosenfeld [63]. Later this method was modified to study the hard-sphere crystal by Tarazona [64]. The method does not rely on the extrapolation from the homogeneous fluid toward inhomogeneous crystal, as implemented in the previous methods. The FMT is based on functional interpolation between the zero-dimension (0D) limit for the excess free energy and properties of 3D bulk. The excess free energy is expressed as [64]

$$\frac{1}{k_B T} F_{exc}[\rho] = \sum_D^{\nu=1} \int d\mathbf{r} \varphi_\nu[\rho] \prod_{i=1}^{\nu} \int d\mathbf{R}_i w(\mathbf{R}_i) \rho(\mathbf{r} + \mathbf{R}_i) K_\nu^D, \quad (2.40)$$

where D denotes the spacial dimension, R is the radius of the hard sphere, $\varphi_\nu[\rho]$ the ν 's derivative of the 0D excess free energy, $w(\mathbf{R}_i)$ a normalized delta-function shell with the radius of the monomer and, finally, K_ν^D a geometrical factor. The expression for the geometrical factors can be obtained from the exact 0D results for it.

This method has a number of advantages. The free energy can be minimized without any additional constraints on the unit-cell geometry. Results of minimization of the free energy in this method reproduce the Percus-Yevick equation of state and direct correlation function for the hard-sphere fluid. A comparison with the results of computer simulations for the hard-sphere crystal is very good, better than any of the previously described methods. This method is able to reproduce details of the unit cell density distribution in the crystal such as anisotropy and normalization. The values of the Lindemann ratio, which is a measure of the mean square deviation of the monomer from the lattice-site position, are in better agreement with computer simulations than the ones obtained by means of previous methods.

2.3 Results and comparison of different DFT types

The simplest possible model of a fluid is a system of hard spheres. This model is suitable for systems for which the hard-core potential dominates the physics in hand. In this section

	$\rho_L\sigma^3$	$\rho_S\sigma^3$	L
Monte Carlo simulations [65]	0.943	1.041	0.126
RY [53]	0.985	1.126	0.059
WDA [59, 60]	0.915	1.045	0.093
MWDA [60]	0.909	1.035	0.097
ELA [61]	0.993	1.083	0.074
MELA [62]	0.924	1.027	0.098
FMA [66]	0.938	1.031	0.101

Table 2.1: The dimensionless liquid $\rho_L\sigma^3$ and crystal $\rho_S\sigma^3$ densities, and the Lindemann ratio L of the fcc hard-sphere crystal at phase coexistence calculated using different DFT types.

we briefly discuss the results of different types of DFT for the freezing of the hard-sphere face-centered cubic (fcc) crystal and also give results for the elastic moduli of this crystal.

Table I shows the results for the freezing density and the Lindemann ratio for the hard-sphere system. As can be seen the results of FMA show the best agreement with computer simulations, however the largest deviation from the results of Monte Carlo simulations for all methods is about 10% in density.

The following Table presents the results for the elastic moduli of the hard-sphere crystal at phase coexistence. We present the recipe how to calculate the elastic moduli using the DFT method in the Chapter 5. Here we just compare results which were obtained by different methods. The results of the MWDA show the best agreement with simulations of Frenkel and Ladd [67]. The worst agreement with simulations and an even unphysical negative Poisson ratio were obtained by means of the RY DFT of Jarić and Mohanty [68]. We show that inclusion of the three-body direct correlation function and a larger number of reciprocal vectors in the calculation (RY2 row in Table 2) increases the accuracy of the elastic moduli significantly. Although the agreement with simulations for the elastic moduli is far from perfect, the value of the Poisson ratio ν is positive (RY2 row in Table 2) and is in good agreement with the results of Frenkel and Ladd [67]. We conclude that the RY DFT is maybe not the best one but is a quite suitable method to study hard-sphere systems. The calculational simplicity of this method is an important feature in the context of our studies and we derive in the same perturbative fashion polymeric corrections to the free energy in order to apply DFT to polymeric systems. We present our theory in details in the following chapter, but first we give a short overview of what has been done within the DFT framework for polymers.

	$C_{11}\sigma^3/k_B T$	$C_{12}\sigma^3/k_B T$	$C_{44}\sigma^3/k_B T$	ν
Molecular dynamics simulations [67]	68	18	46	0.35
RY1 [68]	-40	158	141	-0.22
RY2 [69]	139	43	66	0.31
WDA [70]	69	32	60	0.32
MWDA [71]	71	18	47	0.32
ELA [72]	125	41	49	0.31

Table 2.2: The dimensionless elastic moduli $C_{11}\sigma^3/k_B T$, $C_{12}\sigma^3/k_B T$, $C_{44}\sigma^3/k_B T$ and the Poisson ratio ν for the fcc hard-sphere crystal at a density $1.04\sigma^{-3}$ calculated from different DFT types. (The results are estimated from figures of the corresponding references.)

2.4 Applications to polymers

Despite the drawback of uncontrolled approximations, the DFT method seem to be a very powerful tool to study inhomogeneous atomic systems. One would assume that this carries over to polymeric systems. The biggest challenge comes from the complicated internal structure of the polymers themselves. Connectivity is not an easy aspect to describe within the framework of DFT. Quite a few attempts to study polymeric systems using the DFT technique can be found in the literature. We mention just a few.

Yethiraj and Woodward [73] developed the DFT for polymers, based on the WDA theory. They used a simple weighting function, which was assumed to be a constant for distances smaller than the hard-core diameter. Later Yethiraj [74] improved this theory and used more complicated weighting functions. He studied freely-hinged chains and freely rotating chains (see Chapter 1). This theory requires a direct correlation function as an input, which was calculated from the polymer interaction site model (PRISM, a generalization of the Ornstein-Zernike equation for polymers, see the following chapter for details). The excess free energy per particle was obtained from an empirical equation of state. The connectivity enters their calculation in the direct correlation function and excess free energy, which is not self-consistent in the sense that it is obtained from a semi-empirical equation of state. They studied short chains and found good agreement with computer simulation for the density profiles of freely-hinged chains at a hard wall and somehow worse agreement for the freely rotating model at high densities. We are not aware about studies of the freezing of polymeric systems using this theory. The theory seems very promising, but the lack of an accurate self-consistent equation of state for polymers is a serious complication. Such equations of state can be obtained from, *e.g.*, PRISM via the virial or compressibility route, but their accuracy (or lack of it) is a point of concern. Contrary to the hard-sphere case,

for which we have the highly accurate Carnahan-Starling equation of state, no equation of state of similar accuracy is available for melts of long polymers.

There are other studies of the polymeric systems using density-functional methods [19]. McCoy *et al.* [19] applied the polyatomic density-functional theory developed by Chandler, McCoy, and Singer [75, 76] to realistic polymeric models. They also used the direct correlation function of the polymeric melt as an input from the PRISM. The crystal phase was described in a local-density type of approximation [77, 78]. Their results for the crystallization densities of polyethylene and polytetrafluoroethylene agree with experimental data very well. However, the difference between the solid and liquid densities at freezing was overestimated in their calculations. Unfortunately, this theory requires a large number of fitting parameters as input, and only the direct correlation function of the melt contains all the information about the connectivity of the polymeric chain. McMullen and Freed [79] developed a formal DFT which is similar to the one of Chandler, McCoy, and Singer discussed here, with exception that intramolecular correlations are relegated to the excess free energy. We are not aware of any application of this theory to studies of polymeric models.

Another DFT for site-site pair correlation functions of polymeric melts was developed by Kierlik and Rosinberg [80]. This theory is based on Wertheim's perturbation theory of polymerization in the limit of full association, when all monomers are polymerized. The results of this theory for the pair correlation function of diatomic and linear tetra-atomic molecules are not in the agreement with the results of computer simulations. This discrepancy can be attributed to the neglect of the intramolecular excluded volume effects.

As can be seen each polymeric DFT possesses some disadvantages and/or inaccuracies. We decide to use the RY DFT as a basis for our polymeric DFT because of the following reasons. First, this theory does not require extensive calculations and can predict the freezing transition of hard spheres with a high accuracy. It is possible to extend this method to polymers. Second, we develop the corrections to the free energy, reflecting the effects of connectivity, in the same perturbative fashion as the main principles of this theory making the theory self-consistent. We present our formalism in the following chapter.

Chapter 3

Density functional theory of the crystallization of hard polymeric chains

ABSTRACT

We study how connectivity influences the crystallization of fully flexible model polymers by applying a recently advanced amalgamation of the Green-function description of polymers, and the density functional theory of simple liquids. Our calculations show that the model polymers only crystallize if the effective Kuhn length of the chains is sufficiently large compared with the range of the hard-core interaction between the segments. Also shown is the importance of bond-length fluctuations for the stability of the crystal phase.

3.1 Introduction

The crystallization of polymers is still poorly understood, despite intense research spanning many decades. A likely reason for this may be the importance of kinetic effects, which seem to predominate the crystallization of polymers [13]. It is not surprising, then, that a great effort has been put in studying this particular aspect of the problem, and less so the thermodynamic driving force leading the polymeric melt to the crystalline state. This is unfortunate, however, since a meaningful kinetic theory is difficult to set up without a reliable statistical-thermodynamic description of the problem at hand. Indeed, as has become clear from recent discussions [16], the presence of metastable states may play an important role in selecting kinetic pathways. The aim of this chapter is first and foremost

to create an understanding of how chain connectivity affects the stability of the crystal phase. As we shall see below, unconnected monomers appear to be easier to crystallize than freely hinged model polymers. This implies that angular correlations could play a more prominent role in promoting polymer crystallization than is often thought. The effects of angular correlations will be studied in a forthcoming publications.

Before going into the details of our calculations, let us briefly summarize the state of the art. There are essentially three modes of attack in dealing with the thermodynamics of the freezing transition in polymeric systems. These are the lattice-based models, the Landau-de Gennes types of approach and density functional theories. Of these, the most well known are the lattice-based theories pioneered by Flory [17]. He developed a simple mean-field theory to deal with the effect of inter-chain interactions, in combination with a (simplified) isomeric state model for the description of the loss of configurational free energy upon the freezing of the polymers. Flory found that, upon cooling, the stiffness of the chains increases, which, due to a concomitant increase in volume exclusion, in turn induces the transition to the crystalline state. Within the Flory theory the phase transition is entropically driven, and attractive interactions only perturb the location of the transition [19]. Another important conclusion to be drawn from the Flory theory is (at least in solution) that stiffer chains crystallize more readily than flexible ones, in accord with recent computer simulations [36] but also with experimental fact [1].

The advantage of the Flory theory is its simplicity. The theory remains conceptually important in that it has drawn attention to the relevance both packing effects and chain configurations. At the same time the Flory theory has a serious drawback, namely that when the fraction of lattice sites occupied by the polymers is set equal to unity, it cannot predict a density jump at the crystallization transition. Another problem is that it is not self-consistent in the sense that order is introduced on the lattice by hand.

Perhaps the most promising way to accurately describe both the thermodynamics of polymer crystallization and the structure of the crystal phase is given by the powerful tool known as density functional theory (DFT), pioneered by Ramakrishnan and Yussouff [52] for monatomic liquids. McCoy *et al.* [19] applied the polyatomic density-functional theory developed by Chandler, McCoy, and Singer [75, 76] to chemically realistic polymeric systems. For the description of the melt phase they used a polymeric reference state model or PRISM [22, 81, 82], whilst the crystal phase was described in a local-density type of approximation [77, 78]. The agreement of the theory with experimental data on the densities at which the polymers polyethylene and polytetrafluoroethylene crystallize was quite remarkable. Somewhat less good was the predicted phase gap, which was overestimated by a factor of about 3, as well the temperature dependence of the density. Also, the rather large discrepancy between the theoretical and experimental lattice parameters should cause some concern. We speculate that it could well be the lack of coupling between positional and orientational degrees of freedom in their theory that is at the root of the problem [83].

Our aim is not directly to improve on the work of McCoy and co-workers [19], although

our approach does go beyond PRISM as it treats the melt and crystal phase on an equal footing. Rather, our aim is first to try to attack the problem in a limit that is consistent with the model assumptions of that work, and study the bare effects of connectivity. This has not been done before at the level of a density functional theory. Although the model polymers we employ are unrealistic at small length scales, and we do take a step back from experiment, our approach intends to act as a stepping stone to come to a more realistic description of actual polymeric systems. Ultimately, we intend to extend our theory to include bond correlations, which within a PRISM-type theory is much more cumbersome [83].

The remainder of this chapter is organized as follows. In Section 2 we first briefly describe the model polymers considered. The formalism which we use for our calculations is explained in Section 3. Section 4 discusses the description of the polymeric melt and Section 5 that of the crystal phase. The calculation method is explained in the Section 6. The results of our numerical calculations are represented in Section 7, and conclusions are presented in Section 8. Some of the details of our derivation are explained in the Appendices A and B.

3.2 Model

Since our aim is to study the role of connectivity in polymer crystallization, we focus on simple, coarse-grained polymer models, in particular the Gaussian-chain model, the freely-hinged-chain model and an intermediate model that interpolates (in a way) between these two. The model chains are thought to consist of N identical segments, which in the Gaussian model are connected by Hookean springs with a root-mean-square extension a , in the freely-hinged model by rigid links of fixed length l , and in the intermediate model by links of root-mean-square length b . The step length of the intermediate model b itself depends on a mean bond length l and root-mean-square deviation ξ via $b = \sqrt{l^2 + \xi^2}$. For $\xi \ll l$ this intermediate model turns into freely-hinged chain model, and for $\xi \gg l$ into the standard Gaussian chain model with ξ playing the role of a . All models behave like random-flight chains in the long-chain limit, so for convenience we put $l_K \equiv a \equiv l \equiv b$, with l_K the Kuhn length of the chains. Note that this provides a reasonable description of the chains in the melt, for intra-chain correlations are screened and the chains behave ideally. As we shall see later, in the Section 7, varying the stiffness of the bond of the intermediate model allows us to study the effects of lattice frustration.

The pair interactions between the segments are modeled by a simple hard-core repulsive potential of range σ , independent of the segment ranking numbers, and independent of the chain configurations. The range of the potential need not be the actual diameter of the hard-sphere segments, because connectivity (in a way) renormalizes the pair interaction [84]. To be able to study the influence of this renormalization, we introduce a *segment*

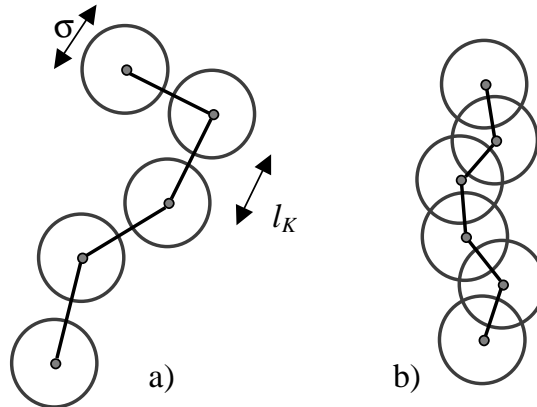


Figure 3.1: Schematic diagram of the influence of the segment fusion parameter $\Gamma \equiv l_K/\sigma$ on the model polymer. When $\Gamma > 1$ there is no overlap of neighboring segments within the chain (a), for $\Gamma < 1$ the segments 'fuse' (b).

fusion parameter defined as

$$\Gamma \equiv l_K/\sigma. \quad (3.1)$$

As it is unclear how connectivity renormalizes the local interaction, we keep Γ as a free parameter. Figure 3.1 makes clear why Γ may indeed be called fusion parameter; if $\Gamma > 1$ the hard cores of the neighboring segments along a chain do not overlap, whereas if $\Gamma < 1$ they do.

The polymeric model system is fully described by the fusion parameter Γ , the number of segments per chain N , and the effective packing fraction of the segments $\phi = \pi\rho\sigma^3/6$, where ρ denotes the number density of the segments. In the melt, the segments are (in the mean) homogeneously distributed, and the bonds connecting the segments randomly oriented. Because the interaction potential is isotropic and of the pair type, and because the links freely-hinged, orientational bond-order type correlations cannot build up. As a consequence, although in the crystal phase the segments do crystallize, *i.e.*, order positionally, there cannot be any associated long-range bond ordering within our model description. In other words, the chains in the crystal phase behave like random flights on a lattice. Although inaccurate, it is consistent within our treatment, and allows us to focus on the effects of connectivity alone.

In the following we first explain the general formalism with which we attack the problem in hand, and next describe how we apply this theory to describe the melt and crystal phases. Our treatment of the melt turns out to be equivalent to the so-called polymer reference interaction site model or PRISM theory, whilst that of the crystal is a DFT-type theory with corrections for bond connectivity. Those readers not interested in the technical details we refer directly to the results of our calculations presented in Section 7.

3.3 Formalism

In the mean-field approximation, the partition function \mathcal{Z} of a collection of M polymeric chains of N segments in a volume V is given by the product of the single-chain partition functions Z_N :

$$\mathcal{Z} = \frac{1}{M!} Z_N^M \quad (3.2)$$

The single-chain partition function can be written as the spatial integral over the positions of the ends of a single chain,

$$Z_N = \int d\mathbf{r} \int d\mathbf{r}' Z(\mathbf{r}', \mathbf{r}; N) \quad (3.3)$$

with $Z(\mathbf{r}', \mathbf{r}; N)$ the (conditional) partition function of a chain of N segments of which the ends are fixed at the positions \mathbf{r} and \mathbf{r}' . The latter quantity is often referred as the Green function of the polymer [85], and satisfies the following recursive equation

$$Z(\mathbf{r}', \mathbf{r}; N + 1) = \exp[-U_{scf}(\mathbf{r})] \hat{g} Z(\mathbf{r}', \mathbf{r}; N). \quad (3.4)$$

Here, $U_{scf}(\mathbf{r})$ denotes the self-consistent, molecular field a chain experiences from the presence of the other chains, and \hat{g} the so-called step operator [86].

If $f(\mathbf{r})$ is an arbitrary integrable function, the step operator is defined as

$$\hat{g}f(\mathbf{r}) \equiv \int d\mathbf{r}'' g(\mathbf{r}, \mathbf{r}'') f(\mathbf{r}'') \quad (3.5)$$

with the kernel $g(\mathbf{r}, \mathbf{r}'')$ the *a priori* probability that a bond that starts at \mathbf{r}'' , ends at \mathbf{r} . For the standard Gaussian chain in three spatial dimensions [86],

$$g(\mathbf{r}, \mathbf{r}') = g_G(\mathbf{r} - \mathbf{r}') = (2\pi l_K^2/3)^{-3/2} \exp[-3(\mathbf{r} - \mathbf{r}')^2/2l_K^2], \quad (3.6)$$

whilst for a the freely-hinged chain [86]

$$g(\mathbf{r}, \mathbf{r}') = g_{fh}(\mathbf{r} - \mathbf{r}') = \frac{1}{4\pi l_K^2} \delta(|\mathbf{r} - \mathbf{r}'| - l_K). \quad (3.7)$$

For the intermediate model we take the convolution $g_i(\mathbf{r}) \equiv g_G \circ g_{fh}(\mathbf{r}) \equiv \int d\mathbf{r}'' g_{fh}(\mathbf{r} - \mathbf{r}'') g_G(\mathbf{r}'')$ of the kernel of a freely-hinged model with a bond length l and that of a Gaussian model with root-mean-square bond length ξ , giving

$$g(\mathbf{r}, \mathbf{r}') = g_i(\mathbf{r} - \mathbf{r}') = \frac{\sqrt{6}}{8\pi^{3/2}\xi|\mathbf{r} - \mathbf{r}'|l} \left(\exp\left[-\frac{3(|\mathbf{r} - \mathbf{r}'| - l)^2}{2\xi^2}\right] - \exp\left[-\frac{3(|\mathbf{r} - \mathbf{r}'| + l)^2}{2\xi^2}\right] \right). \quad (3.8)$$

Note that for all models $g(\mathbf{r}, \mathbf{r}')$ is normalized, *i.e.*, $\hat{g}1 \equiv 1$, and that the ‘initial’ condition associated with the operator equation (3.4) is $Z(\mathbf{r}', \mathbf{r}; 1) \equiv \delta(\mathbf{r}' - \mathbf{r})$.

In units of thermal energy, the free energy of our system of chains is given by

$$F = -\ln \mathcal{Z}, \quad (3.9)$$

which at this point is still an implicit function of the as yet unknown molecular field U_{scf} . The molecular field may be fixed by following a procedure pioneered by Lifshitz [87]. First, we subtract from Eq. (3.9) the internal energy of the system, to give the contribution of the configurational free energy, F_{conf} , to the free energy

$$F_{conf} = F - \int d\mathbf{r} U_{scf}(\mathbf{r}) \rho(\mathbf{r}). \quad (3.10)$$

Here, $\rho(\mathbf{r})$ denotes the number density of segments, itself a functional of the conditional partition function

$$\rho(\mathbf{r}) \equiv M Z_N^{-1} \int d\mathbf{r}' \int d\mathbf{r}'' \sum_{s=1}^N Z(\mathbf{r}', \mathbf{r}; 1, s) Z(\mathbf{r}, \mathbf{r}''; s, N). \quad (3.11)$$

The next step is to surmise that the actual free energy \mathfrak{F} must be the sum of Eq. (3.10) and an excess free energy F_{exc} describing the interactions between the segments and a possible coupling to an external field,

$$\mathfrak{F} = F_{conf} + F_{exc}. \quad (3.12)$$

For any choice of F_{exc} , we can establish the conditions for phase coexistence by subsequently equating the chemical potentials $\mu = \delta\mathfrak{F}/\delta\rho(\mathbf{r})$ and the pressures $P = -\mathfrak{F} + \mu \int d\mathbf{r} \rho(\mathbf{r})$ of both phases. This, however, is not straightforward, for we would have to solve Eqs. (3.3) through (3.12) self-consistently. A much more efficient way to achieve the same, is to make the connection with liquid-state (integral equation) theory. As will become clear below, we then do not need to specify F_{exc} of the melt state. The free energy of the crystal state relative to that of the melt can be calculated perturbationally from that of the melt using the theory described above.

3.4 Description of the melt

To make the connection with liquid-state theory, we seek to derive an Ornstein-Zernike-type equation between the total correlation function of two segments on different chains $h(\mathbf{r}, \mathbf{r}')$, and the associated two-particle direct correlation function $C^{(2)}(\mathbf{r}, \mathbf{r}') \equiv \delta^2 F_{exc} / \delta\rho(\mathbf{r}) \delta\rho(\mathbf{r}')$. This is possible by calculating the response of the density field to an externally applied potential, and linking the response function to the static structure factor with the help of the well-known Yvon equation [83]. We find that the so-called polymeric reference

interaction site model or PRISM equation is consistent with the formalism described in the previous Section 3. See [83] or the Appendix A for details. This equation reads in Fourier space:

$$\widehat{h}(\mathbf{q}) = \widehat{\omega}(\mathbf{q})\widehat{C}^{(2)}(\mathbf{q}) + \rho_L\widehat{\omega}(\mathbf{q})\widehat{C}^{(2)}(\mathbf{q})\widehat{h}(\mathbf{q}), \quad (3.13)$$

where the hats indicate Fourier-transformed quantities, \mathbf{q} the wave vector and ρ_L the average melt density. The intramolecular correlations between segments on a single chain are described by the form factor $\widehat{\omega}$, which depends on the model used. For the models under consideration [88]

$$\widehat{\omega}(q) = \frac{1 - \widehat{g}^2 - \frac{2}{N}\widehat{g} + \frac{2}{N}\widehat{g}^{N+1}}{(1 - \widehat{g})^2}, \quad (3.14)$$

where $q \equiv |\mathbf{q}|$ and $\widehat{g}(q) \equiv \exp[-q^2 l_K^2/6]$ for the Gaussian model, $\widehat{g}(q) \equiv q^{-1} l_K^{-1} \sin ql_K$ for the freely-hinged chain, and $\widehat{g}(q) \equiv q^{-1} l^{-1} \sin ql \exp[-q^2 \xi^2/6]$ for the intermediate model. The last follows from the standard properties of the Fourier transform of the convolution of two functions.

Eq. (3.13) has to be implemented by a suitable closure. We use the well-known Percus-Yevick or PY closure, which was quite successfully applied by various authors to describe the structure of polymeric melts [19, 22]. The PY closure is defined by

$$\left. \begin{aligned} h(|\mathbf{r}| < \sigma) &= -1 \\ C^{(2)}(|\mathbf{r}| > \sigma) &= 0 \end{aligned} \right\}, \quad (3.15)$$

and describes hard-core interactions between the segments. With this closure, the PRISM integral equation (3.13) can be solved self-consistently. We applied the algorithm put forward by Honnell *et al.* [89], by assuming the direct correlation function to be a cubic polynomial, and solving numerically the system of nonlinear algebraic equations for the expansion coefficients. For this system of nonlinear equations we used the standard modification of the Powell hybrid method from the NAG[®] library (Mark 18, C05NBF). With the coefficients so obtained we calculated the direct correlation function.

3.5 Description of the crystal

To describe the crystal phase, we use an extension of the standard density-functional theory (DFT), set up within the local density approximation (LDA) developed by Ramakrishnan and Yussouff [52], and by Haymet and Oxtoby [54], for monatomic liquids, in the context of the freezing of hard spheres [53, 61]. The DFT can be derived from the theory of Section 3. We refer to references [52, 53, 61, 90] for details regarding the estimate of the excess free energy. The modification of the usual ideal free energy functional, needed to deal with the connectivity of the polymers, is outlined in Appendix B. Within our treatment, only those chain-connectivity corrections are included that are of leading order in the density modulation.

The expansion of the free energy gives us for the grand potential of the crystal relative to that of the melt,

$$\Delta\Omega = \Delta F - \int d\mathbf{r} [\mu_S \rho_S - \mu_L \rho_L], \quad (3.16)$$

where ΔF is the difference in the Helmholtz free energies of the crystal and melt phases, μ_S the chemical potential of the crystal and μ_L the chemical potential of the reference state (the melt); ρ_S is the mean density of the crystal phase and ρ_L as before that of the melt. ΔF can be written as $\Delta F = \Delta F_{conf} + \Delta F_{exc}$. As it turns out, at length scales relevant to the crystallization of the beads, ΔF_{conf} can be written as the sum of an ideal entropy of unconnected beads, and corrections coming from the connectivity of the beads.

Using standard DFT for ΔF_{exc} , which is identical to that of hard-sphere systems, and using the results of the Appendix B we find:

$$\begin{aligned} \Delta\omega \equiv \frac{1}{k_B T} \frac{\Delta\Omega}{\rho_L V} &= \frac{1}{\rho_L V} \int d\mathbf{r} \{ \rho(\mathbf{r}) \ln \rho(\mathbf{r}) / \rho_L - \Delta \} \\ &- \frac{1}{\rho_L V} \sum_{p=2}^{\infty} \frac{1}{p!} \int \dots \int C^{(p)}(\mathbf{r}_1, \dots, \mathbf{r}_p) \prod_{i=1}^p d\mathbf{r}_i (\rho(\mathbf{r}_i) - \rho_L) \\ &- \frac{1}{k_B T} \frac{1}{\rho_L V} (\mu_S - \mu_L) \int d\mathbf{r} \rho(\mathbf{r}) - \frac{1}{\rho_L V} \int d\mathbf{r} (\rho(\mathbf{r}) - \rho_L) \end{aligned} \quad (3.17)$$

with $C^{(p)}(\mathbf{r}_1, \dots, \mathbf{r}_p) = -\frac{1}{k_B T} \delta^{(p)} F_{exc} / \prod_{i=1}^p \delta \rho(\mathbf{r}_i)$ the p -particle direct correlation function of the melt. One recognizes in the first term on the right the usual ideal entropy. The next term Δ enters due to the existence of the (phantom) bonds. We find to quadratic order in density modulations

$$\Delta = \frac{1}{\rho_L} \int \int d\mathbf{r} d\mathbf{r}' g(\mathbf{r}, \mathbf{r}') [\rho(\mathbf{r}) - \rho_L] [\rho(\mathbf{r}') - \rho_L] \quad (3.18)$$

with g as before the kernel of the step operator. The other terms are connected with the excess free energy and mass conservation. We truncate the summation after the second term, because higher-order terms are presumably negligibly small, for they are known to be small for hard spheres [54].

3.6 Calculation method

For reasons of computational convenience we do not use the exact density distribution, obtained by minimizing the free energy, but rather approximate it by a sum of Gaussians,

$$\rho(\mathbf{r}) = (\pi\epsilon^2)^{-3/2} \sum_{\{\mathbf{R}\}} \exp [-(\mathbf{R} - \mathbf{r})^2 / \epsilon^2], \quad (3.19)$$

where we assume the crystal to be face-centered cubic. (We found that of all cubic lattices only the fcc lattice supports a stable solid phase for our model polymers, in common with systems of hard spheres [61].) In Eq. (3.19), $\{\mathbf{R}\}$ denotes all the real-space crystal-lattice vectors, and ϵ is a measure of the width of the Gaussian density distribution around each lattice point. The latter we fix by a free-energy minimization. As usual, the density modulations are assumed to be non-overlapping [53, 56, 57, 91]. It turns out to be useful to express the density modulations in their Fourier components $\zeta(\mathbf{q})$ [53],

$$\rho(r) = \rho_L \left[1 + \eta + \sum_{\{\mathbf{q}\}} \zeta(\mathbf{q}) \exp(i\mathbf{q} \cdot \mathbf{r}) \right] \quad (3.20)$$

with $\{\mathbf{q}\}$ the set of reciprocal lattice vectors of the fcc crystal, and $\eta = (\rho_S - \rho_L)/\rho_L$ the relative density jump across the crystallization transition. In the Gaussian approximation to the density profile we have

$$\zeta(\mathbf{q}) = (1 + \eta) \exp[-\mathbf{q}^2 \epsilon^2 / 4]. \quad (3.21)$$

Eq. (3.17) now simplifies to

$$\begin{aligned} \Delta\omega = & 1 - (1 + \eta)[3/2 + \ln \rho_L + 3/2 \ln \pi \epsilon^2] \\ & - \eta^2 - \sum_{\{\mathbf{q}\}} \hat{g}(\mathbf{q}) \zeta^2(\mathbf{q}) - \frac{1}{k_B T} (1 + \eta) (\mu_S - \mu_L) \\ & - \frac{1}{2} \eta^2 \hat{C}_L^{(2)}(0) - \frac{1}{2} \sum_{\{\mathbf{q}\}} \zeta(\mathbf{q})^2 \hat{C}_L^{(2)}(|\mathbf{q}|) - \frac{1}{6} \eta^3 \hat{C}_L^{(3)}(0, 0). \end{aligned} \quad (3.22)$$

The summation in Eq. (3.22) is over all reciprocal lattice vectors \mathbf{q} .

In Eq. (3.22) we neglected four-body and higher-order correlation functions, and approximated the three-body one by its value at zero wave vector. It exactly obeys [53]

$$\hat{C}_L^{(3)}(q, 0) = \frac{\partial \hat{C}_L^{(2)}(q)}{\partial \rho} \Big|_{\rho=\rho_L}. \quad (3.23)$$

Only the zero- \mathbf{q} part of $\hat{C}_L^{(3)}$ is included in Eq. (3.22), because Haymet [54] has shown that, at least for hard spheres, the non-zero \mathbf{q} contributions of $\hat{C}_L^{(3)}$ tend to cancel each other out.

For a fixed value of the fusion parameter Γ , the free energy Eq. (3.22) is a function of three quantities: the width ϵ of the density profile, and the mean densities ρ_S and ρ_L . Conditions for phase coexistence are found by setting $\mu_L = \mu_S$ in Eq. (3.22), minimizing $\Delta\omega$ with respect to ϵ and η , and finding the value of ρ_L for which $\Delta\omega = 0$. This way we ensure a balancing of the pressures of both phases, $P_L = P_S$, because in equilibrium $\Delta\Omega = -V(P_L - P_S)$. We found the minimum of the function $\Delta\omega$ using a standard quasi-Newton algorithm from the NAG[®] library (Mark 18, E04JYF). We used 5832 reciprocal lattice vectors and varied ρ_L with a step length of 10^{-5} units. We verified that this is quite sufficient to get a stable result for the minimum of $\Delta\omega$.

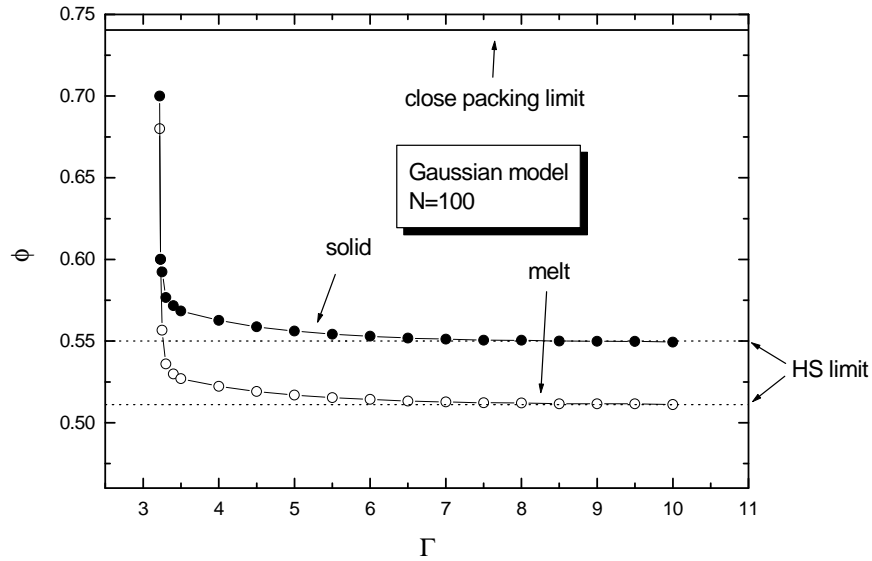


Figure 3.2: Packing fractions of the co-existing melt and crystal phases of the Gaussian model chains as a function of the fusion parameter $\Gamma = l_K/\sigma$. The chain length is $N = 100$. Also shown are the results for hard spheres (the HS limit $N = 1$, indicated by the dotted line).

3.7 Results and discussion

We now present the results of our calculations. Figure 3.2 shows the calculated phase diagram of the hard Gaussian chains for the case $N = 100$. Indicated is the (dimensionless) packing fraction $\phi = \pi\rho\sigma^3/6$ at the melt-crystal phase coexistence as a function of the fusion parameter Γ . For comparison we have also indicated the results for hard spheres ($N = 1$). The figure clearly shows that in the limit $\Gamma \rightarrow \infty$ the chains crystallize at the same density as hard spheres do. From Eq. (3.22) we understand that the reason for this is that all polymeric corrections become negligibly small in this regime, because these contain a function which decays fast with increasing values of Γ . Indeed, neighboring beads along a chain are then so far removed from each other on the crystal lattice that they no longer feel the influence of the connectivity. Packing effects dominate in this regime.

Lowering Γ we observe that the solidification density goes up. In other words, it becomes more difficult for the chains to crystallize. In fact, for $\Gamma \leq 3.25$ a crystal phase is no longer found for densities below close packing. The difficulty of crystallizing Gaussian chains in the low- Γ range was in fact already observed by McCoy and co-workers, and was attributed to the enormous amount of entropy stored in the melt [19]. Contrary to a previous conclusion by van der Schoot [83], the results of Figure 3.2 seem to bear out this conclusion.

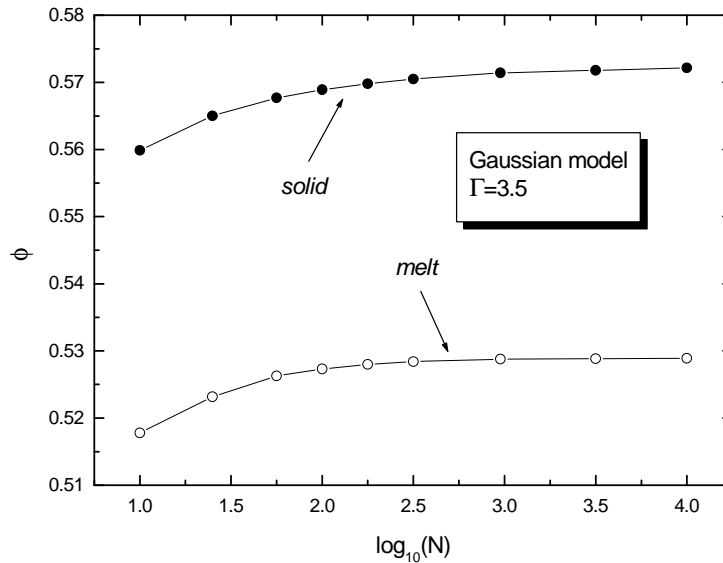


Figure 3.3: Packing fraction of the co-existing melt and crystal phases of Gaussian model chains as a function of the chain lengths N . The fusion parameter was fixed at a value of $\Gamma = 3.5$.

Shown in Figure 3.3 is the dependence on the length of the polymers of the densities at phase coexistence, again for the Gaussian model at fixed $\Gamma = 3.5$. Apparently, ϕ_L and ϕ_S quickly saturate with increasing degree of polymerization. Apparently, shorter chains are easier to crystallize, in accord with experimental observation [1]. A possible cause of this is that in our model calculations the configurational fluctuations and therefore also the entropy of the chains in the melt increase with increasing N .

Figure 3.4 shows the dependence of the Lindemann ratio L on the fusion parameter Γ . This ratio is defined as the root-mean-square deviation of the position of a particle from its lattice site divided by the nearest-neighbor distance. It is usually thought that if the Lindemann ratio of a crystal phase drops below about 0.1, this crystal melts [49]. The value of Lindemann ratio saturates for the large Γ at $L \approx 0.063$, what roughly corresponds to the hard-sphere result [53]. For small Γ the densities at co-existence are higher, so one would expect L to go down as there is less room for the beads to fluctuate around their lattice sites.

Results for the Gaussian and freely-hinged models are compared in Figure 3.5. Both models show a saturation of the crystallization density for large Γ , albeit that the results for the freely-hinged model do exhibit a seemingly irregular oscillatory behavior that we attribute to the effects of lattice frustration (explained in more details below)¹. We found

¹We have of course verified that numerical errors are not the cause of the oscillatory behaviour found for the freely-hinged model, by varying the precision of integration, the number of the reciprocal lattice vectors and the step of ρ_L .

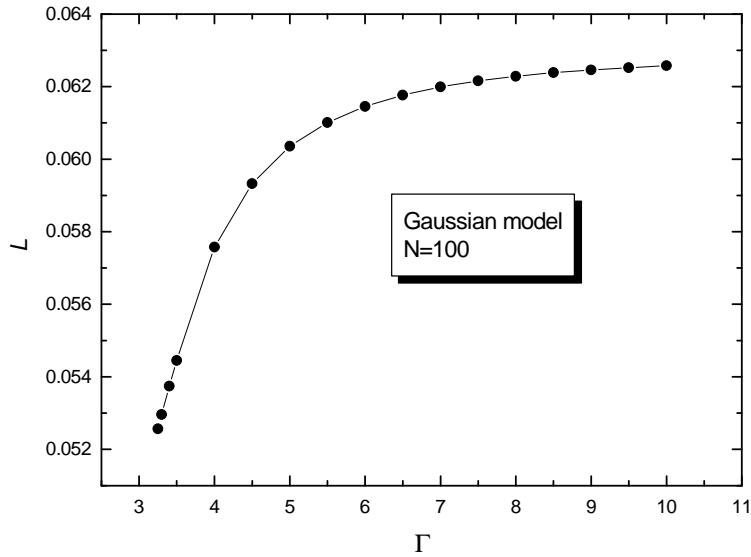


Figure 3.4: Lindemann ratio of the model polymer as a function of the segment fusion parameter $\Gamma \equiv l_K/\sigma$ on the model polymer. The chain length is $N = 100$.

the crossover to hard-sphere-like behavior for the freely-hinged model to occur at much larger Γ than for the Gaussian model. Note that both models predict the crystal phase to become absolutely unstable below a critical value of Γ , 3.25 for the Gaussian model and 2.45 for the freely-hinged model. The oscillatory behavior of the freely-hinged model is zoomed in the Figure 3.6, showing that the oscillations are not as erratic as they appear in Figure 3.5. We have indications that this behavior is caused by the interference of the properties of the crystal lattice and those of the polymeric chains. Indeed, if we rely on the Verlet rule [92] to estimate the solidification density, which uses only information on the structure of the melt, we retrieve the long-wavelength oscillations visible in the results of Figure 3.6. (See also Figure 3.9.)

That lattice frustration effects become important for stiff bonds is shown in Figure 3.7. The figure shows our results for the intermediate model for different values of the degree of bond stiffness ξ . The transition in behavior between the floppy Gaussian and the completely stiff freely-hinged models is clearly seen. For small ξ the bonds are stiff leading to a more oscillatory dependence of the packing density at freezing on the fusion parameter Γ , whilst for large-enough ξ it is smoother and Gaussian-like. The transition occurs roughly when $\xi \sim \epsilon$, *i.e.*, when root-mean-square deviation ξ is comparable to the width of the density field around a lattice site.

That lattice frustration may cause the freezing density of freely-hinged hard-bead chains with degree of bond stiffness $\xi < \epsilon$ to vary abruptly with varying Γ may be understood as follows. The optimal lattice distance is obviously set by the density and by the hard-core diameter σ . When the length of a bond does not fit the distance between two lattice points

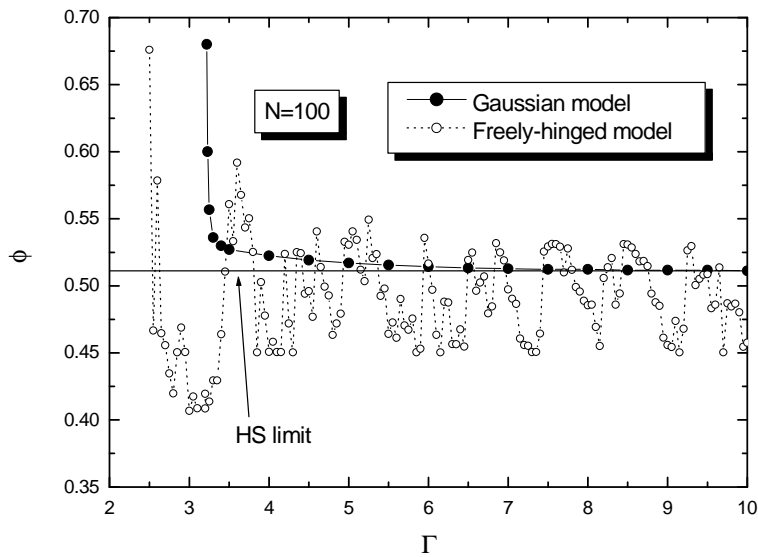


Figure 3.5: Packing fraction ϕ at freezing as a function of the fusion parameter Γ . Compared are results obtained for the Gaussian model, and those for the freely-hinged model. Also indicated are results for hard spheres ($N = 1$).

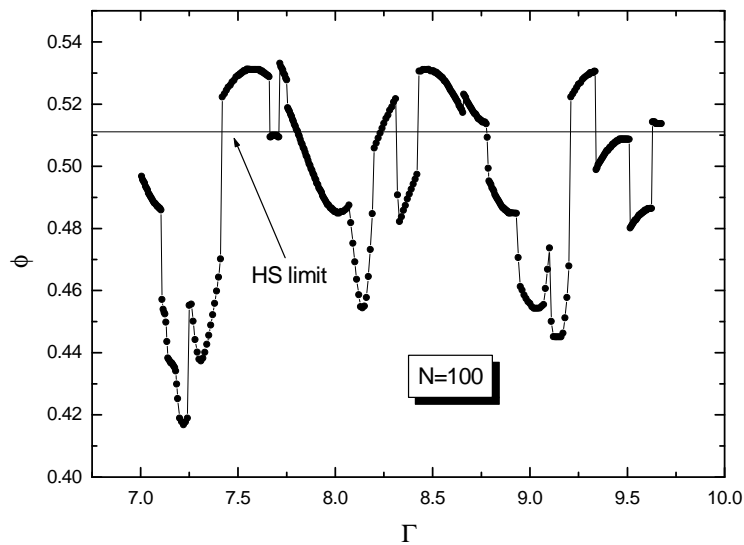


Figure 3.6: Packing fraction ϕ at freezing, as a function of the fusion parameter Γ for the freely-hinged model with a higher resolution than in the Figure 3.5. Also indicated are results for hard spheres ($N = 1$).

and the bonds are very stiff, the system must crystallize at a higher or lower density, such that the bond length does indeed become conjugate to the lattice constant (Figure 3.8). On

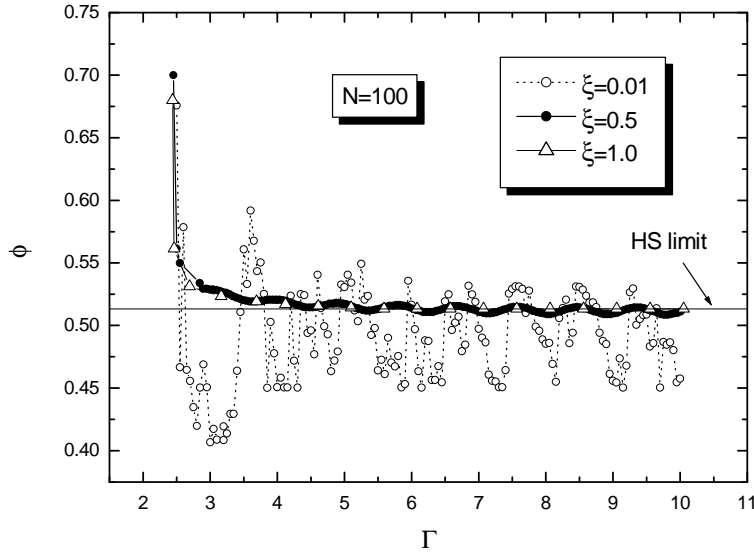


Figure 3.7: Packing fraction ϕ at freezing as a function of the fusion parameter Γ . Compared are results obtained for the intermediate model for the different value of degree of the stiffness ξ . Also indicated are results for hard spheres ($N = 1$).

the other hand, ξ is large enough to allow for the bonds to stretch, a match accommodating the lattice may be found without abruptly changing the lattice parameter too much.

Finally, in the last Figure 3.9 we demonstrate the usefulness of the phenomenological Verlet rule [92], applied to polymer crystallization. According to this rule, the freezing of simple liquids occurs for those conditions where the primary maximum of the static structure factor of the fluid reaches the value of 2.85. Figure 3.9 shows that this remains approximately true for our model polymers, although the rule's accuracy does deteriorate with decreasing values of Γ . We have no explanation for this. As already indicated, the Verlet rule cannot reproduce the strongly oscillatory dependence of the freezing density on the fusion parameter exhibited by the freely-hinged model, because it draws information from the fluid structure, not the crystal structure.

3.8 Conclusion

In our density functional theory we found model chains consisting of hard beads to be able to crystallize, but only if the effective Kuhn length exceeded the hard-core radius of the beads by a sufficient amount. We attribute this to the circumstance that only then the loss of configurational entropy upon freezing is sufficiently low to be compensated by the increased packing entropy. The latter is the driving force for the formation of the crystal

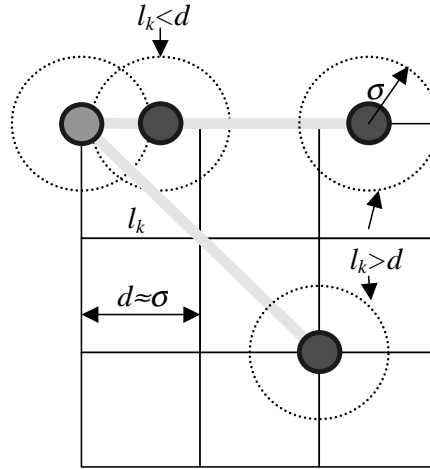


Figure 3.8: Illustration of the lattice frustration effect. When the length of the polymeric bond l_K is less than the distance between two neighboring lattice points in a close-packed crystal, what is always the case when $\Gamma = l_K/\sigma \leq d/\sigma \approx 1$, the system will find it very hard to crystallize because it would have to stretch the bonds. When $\Gamma \geq 1$, a different type of lattice frustration takes over. If the bonds cannot (in the mean) find two sites conjugate to their length, *i.e.*, two sites separated by a multiple bond length, the system has to either stretch or compress the bonds, or to adjust its density to change the lattice constant to the point where it does become possible to fit in the bonds. In the freely-hinged model, the bond length cannot be adjusted, only the density. The associated lattice-adjustment effect leads to the seemingly erratic dependence of the crystal density on the fusion parameter discussed in the main text.

phase. When the monomeric units of the model polymers are small on the scale of the bonds, the behavior of the chains is hard-sphere-like. Connectivity then plays a minor role in the crystallization of the polymeric chains. We observed that short chains crystallize more easily than long ones, because the loss of configurational entropy upon freezing is larger for long chains. This is not obvious, because in our model calculations the chains remain random walkers (albeit on a lattice), and the orientational freezing is only weak due to the lack of bond correlations.

We found lattice frustration to be important for models with sufficiently stiff bonds. This effect could play an important role in the crystallization of real polymers too, because $\xi \sim 0.01\sigma$ for realistic polymeric chain models often used in computer simulations [93]. It may well be that lattice frustration effects are in part responsible for the host of crystal lattice types observed for real polymers [1].

It seems likely that introducing a more realistic polymeric model, one that, *e.g.*, exhibits a finite bending energy, will stabilize the crystal phase over a larger range of bond lengths.

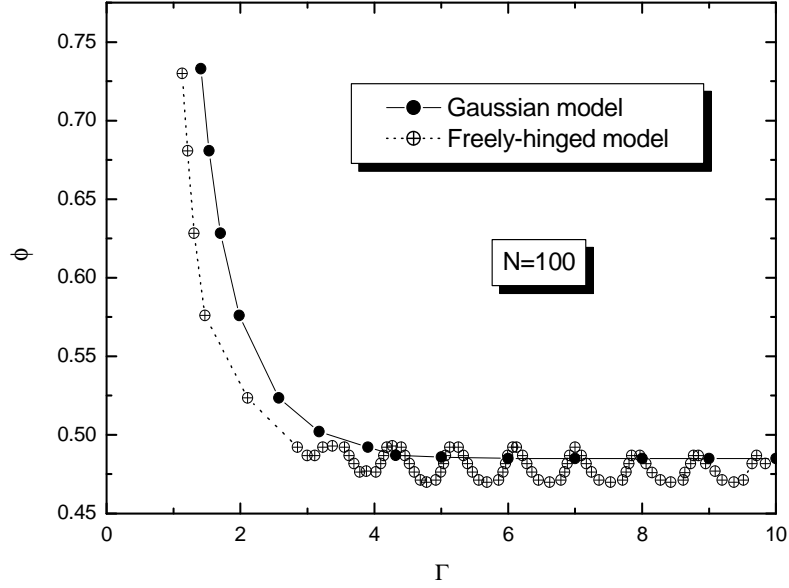


Figure 3.9: Packing fraction ϕ at freezing according to the Verlet rule as a function of the fusion parameter $\Gamma = l_K/\sigma$.

This we investigate in future work, using the Green-function formalism rather than PRISM. The reason is that the former can be more straightforwardly extended to include bond correlations than the latter [83].

3.9 Appendix: PRISM and the Green-function formalism

Here we show the equivalence of the Green-function formalism and PRISM theory for isotropic polymer models. For that purpose we switch on a position dependent external potential $\phi(\mathbf{r})$, acting on each segment. The excess free energy appearing in Eq. (3.12) can then be written as

$$F_{exc} = F_{int} + F_{pot} \quad (3.24)$$

with $F_{pot} = \int d\mathbf{r} \rho(\mathbf{r}) \phi(\mathbf{r})$ the free energy associated with the coupling of the segments to the external potential and F_{int} the free energy associated with the interactions between the beads. Therefore, the full free energy becomes (c.f. Eq. (3.12))

$$\mathfrak{F} = F_{conf} + F_{int} + F_{pot}. \quad (3.25)$$

Minimizing Eq. (3.25) we find, using Eq. (3.10) and the equality $\mu = \delta\mathfrak{F}/\delta\rho(\mathbf{r})$, that the self-consistent field obeys [94]

$$U_{scf}(\mathbf{r}) = \phi(\mathbf{r}) + \frac{\delta F_{int}}{\delta\rho(\mathbf{r})} - \mu, \quad (3.26)$$

where we note that U_{scf} will be treated as an external field, although obviously it is not [83]. (Note also that F in Eq. (3.10) only becomes a functional of ρ *after* the minimization.) We functionally expand the third term, assuming the external field to be sufficiently weak

$$\frac{\delta F_{int}}{\delta\rho(\mathbf{r})} = -C^{(1)}(\mathbf{r}) - \int d\mathbf{r}'' C^{(2)}(\mathbf{r} - \mathbf{r}'') \int d\mathbf{r}' \chi(\mathbf{r}'' - \mathbf{r}') \phi(\mathbf{r}') \dots, \quad (3.27)$$

with $C^{(1)}(\mathbf{r}) \equiv C^{(1)}$ the zero-field one-particle direct correlation function (which is a constant for the homogeneous systems), $C^{(2)}(\mathbf{r}, \mathbf{r}')$ the zero-field two-particle direct correlation function, and $\chi(\mathbf{r}, \mathbf{r}') \equiv \delta\rho(\mathbf{r})/\delta\phi(\mathbf{r}')$ the response function that we later identify with the structure factor. In Fourier space we thus find for weak fields

$$\widehat{U}_{scf}(\mathbf{q}) = \widehat{\phi}(\mathbf{q}) - \mu\delta(\mathbf{q}) - C^{(1)}\delta(\mathbf{q}) - \widehat{C}^{(2)}(\mathbf{q})\widehat{\chi}(\mathbf{q})\widehat{\phi}(\mathbf{q}) + \dots \quad (3.28)$$

The Yvon identity, which establishes the connection between the response of density $\widehat{\delta\rho}(q) = \rho(\mathbf{q}) - \rho_L\delta(\mathbf{q})$ in Fourier space and the structure factor $S(q)$, is given by

$$\widehat{\delta\rho}(q) = \widehat{\chi}(q)\widehat{\phi}(q) = -\rho_L S(q)\widehat{\phi}(q), \quad (3.29)$$

with ρ_L the density in the absence of the field. If we switch off the interactions and neglect the forward scattering associated with the delta peaks around $\mathbf{q} = 0$ [22], the self-consistent field in this case is simply $\widehat{U}_{scf}(\mathbf{q}) = \widehat{\phi}(\mathbf{q})$. We then find for the structure factor $S(q) = \widehat{\omega}(q)$, with $\widehat{\omega}(q)$ the form factor of the single chain. In other words, for non-interacting chains $\widehat{\delta\rho}(q) = -\rho_L\omega(q)\widehat{\phi}(q)$. From Eq. (3.29) we immediately read off that to get the response of the interacting system, we merely need to replace $\widehat{\phi}(q)$ by $\widehat{\phi}(q)(1 - \widehat{C}^{(2)}(q)\widehat{\chi}(q)) = \widehat{\phi}(q)(1 + \rho_L\widehat{C}^{(2)}(q)S(q))$, so that

$$S(q) = \frac{\widehat{\omega}(q)}{1 - \rho_L\widehat{C}^{(2)}(q)\widehat{\omega}(q)}, \quad (3.30)$$

which indeed is equivalent to the PRISM equation (3.13). Note the similarity of our arguments with that of the standard random-phase approximation [94]. A more elaborate derivation can be found in [83].

3.10 Appendix: Entropy of the crystal phase

In this appendix we derive the change in the configurational entropy of the chains up on freezing, based upon the theory of Section 3. Since within our model freezing entails

only processes at short wavelengths, it is justifiable to apply the so-called ground-state approximation [86]. In this approximation the spectrum is assumed to be discrete, and non-degenerate, so that one can order the eigenvalues $\Lambda_0 > \Lambda_1 > \Lambda_2 \dots$. Only is retained the first term of the formal expansion $Z(\mathbf{r}, \mathbf{r}') = \sum_{n=0}^{\infty} \Lambda_n^N \psi_n^+ \psi_n \sim \Lambda_0^N \psi_0^+ \psi_0$, with ψ_n^+ and ψ_n the eigenfunctions of the non-Hermitian operator equations $\hat{g}e^{-U_{scf}}\psi_n = \Lambda_n\psi_n$, $\hat{g}e^{-U_{scf}}\psi_n^+ = \Lambda_n\psi_n^+$. It is easy to see that $\psi_n^+ = e^{U_{scf}(\mathbf{r})}\psi_n$ [86]. As was argued in [83], the use of the ground-state approximation is justifiable because the direct correlation function as well as the self-consistent field are short ranged. Note that $\int d\mathbf{r} \psi_m^+(\mathbf{r})\psi_n(\mathbf{r}) = \delta_{n,m}$, *i.e.*, the eigenfunctions are normalized.

Multiplying both sides of the eigenvalue equation for ψ_0 with ψ_0^+ , and integrating over space, we find for the largest eigenvalue

$$\Lambda_0 = \int d\mathbf{r} \psi_0 \hat{g} \psi_0 \quad (3.31)$$

because of the normalization of ψ_0 and ψ_0^+ . The free energy thus becomes

$$F = -\ln \int d\mathbf{r} \int d\mathbf{r}' Z(\mathbf{r}, \mathbf{r}'; N) \sim MN \ln \Lambda_0, \quad (3.32)$$

where $MN = \int d\mathbf{r} \rho(\mathbf{r})$.

The eigenfunction in the very short wavelength limit can be obtained by recursive iteration, assuming the operator $e^{-U_{scf}(\mathbf{r})}\hat{g}$ to represent a contraction mapping [95]. Although easy to prove in the Banach space of normed scaling functions $f(\mathbf{r}/\sigma)$ in 3 spatial dimensions, at least for $l_K/\sigma > 1$, the general proof for arbitrary integrable functions $f(\mathbf{r})$ has so far evaded us². We truncate the recursive iterations after two iterations, giving

$$\psi_0(\mathbf{r}) \cong \frac{e^{-U_{scf}(\mathbf{r})}\hat{g}e^{-U_{scf}(\mathbf{r})}}{\int d\mathbf{r} e^{-U_{scf}(\mathbf{r})}(\hat{g}e^{-U_{scf}(\mathbf{r})})^2}. \quad (3.33)$$

Note that this expression obeys the normalization condition of the eigenfunctions. At the level of the ground-state approximation, the following relation now holds between the eigenfunctions and the density

$$\begin{aligned} \rho(\mathbf{r}) &= NM\psi_0^+\psi_0 \\ &= MN e^{-U_{scf}(\mathbf{r})}(\hat{g}e^{-U_{scf}(\mathbf{r})})^2 / \int d\mathbf{r} e^{-U_{scf}(\mathbf{r})}(\hat{g}e^{-U_{scf}(\mathbf{r})})^2. \end{aligned} \quad (3.34)$$

Reversely,

$$\psi_0(\mathbf{r}) = (MN)^{-1/2} e^{-U_{scf}(\mathbf{r})/2} \rho^{1/2}(\mathbf{r}) \quad (3.35)$$

²It turns out that for the Gaussian trial functions we use to describe the crystal phase, the recursive iteration converges very rapidly.

so that

$$U_{scf}(\mathbf{r}) = -\ln \rho(\mathbf{r}) + \ln \frac{NM(\widehat{g}\rho(\mathbf{r}))^2}{\int d\mathbf{r}\rho(\mathbf{r})(\widehat{g}\rho)^2}. \quad (3.36)$$

The largest eigenvalue obeys:

$$\Lambda_0 = \frac{1}{NM} \int d\mathbf{r}\rho(\mathbf{r})\widehat{g}\rho(\mathbf{r}'). \quad (3.37)$$

Using the Lifshitz procedure [87] Eq.(3.10) we obtain

$$F_{conf} = MN \ln \Lambda_0 - \int d\mathbf{r}\rho(\mathbf{r}) \left(-\ln \rho(\mathbf{r}) + \ln \frac{NM(\widehat{g}\rho)^2}{\int d\mathbf{r}\rho(\mathbf{r})(\widehat{g}\rho)^2} \right). \quad (3.38)$$

Expansion of the density around the liquid state $\rho(\mathbf{r}) = \rho_L + \Delta\rho(\mathbf{r})$, we find

$$\Lambda_0 \simeq (MN)^{-1} \int d\mathbf{r}(\rho_L^2 + \Delta\rho(\mathbf{r})\widehat{g}\Delta\rho(\mathbf{r})) + \dots \quad (3.39)$$

or equivalently,

$$\ln \Lambda_0 = \ln \rho_L + \frac{1}{\rho_L V} \int d\mathbf{r}\Delta\rho(\mathbf{r})\widehat{g}\Delta\rho(\mathbf{r}) + \dots$$

Neglecting the terms of higher than second order in $\Delta\rho$, we get for the free energy of setting up density modulations in a homogeneous melt

$$\Delta F_{conf} = \int d\mathbf{r}\rho(\mathbf{r}) \ln \rho(\mathbf{r}) - \int d\mathbf{r}\rho_L \ln \rho_L - \frac{1}{\rho_L} \int d\mathbf{r}\Delta\rho(\mathbf{r})\widehat{g}\Delta\rho(\mathbf{r}) + O(\Delta\rho^3). \quad (3.40)$$

For a homogeneous liquid, this expression becomes equal to zero as it should. Eq. (3.40) is only valid at small length scales relative to the size of the chains.

Chapter 4

Density functional theory for the elastic moduli of a model polymeric solid

ABSTRACT

We apply a recently developed density functional theory (DFT) for freely-hinged, hard polymeric chains to calculate the elastic moduli of an idealized polymeric solid lacking long-range bond order. We find that for such a model packing effects dominate the elastic behavior of the polymeric solid in a similar way as is the case in the hard-sphere crystal, which we re-examine. Our calculations show that the elastic stiffness of the model polymeric solid is essentially determined by how far one is removed from its melting point. The main role of the chain connectivity is to destabilize the solid relative to the equivalent solid of hard monomers. Comparison of our results with experimental data on semicrystalline polymers shows order-of-magnitude agreement.

4.1 Introduction

Considering the enormous technological and economic impact solid-state polymers have as construction materials, it is not entirely surprising that a considerable effort is being put into understanding the nature of the elastic behavior of polymeric solids. Scientifically the issue is also of some interest, as the elastic behavior is presumably closely connected with the complex (and often nonequilibrium) structure of the polymeric solid. Focusing our discussion on equilibrium theoretical studies of the elastic moduli of polymers, approaches of

various levels of sophistication can be distinguished. The simplest treat the solid as consisting of non-interacting, fully extended chains. More realistic treatments include interactions between neighboring chains within a force-field approximation. The most sophisticated but not necessarily the most accurate calculations rely on quantum-mechanical density functional theory. Before presenting an alternative to these approaches, representing a for polymers novel microscopic description of the elasticity of the solid phase, we first briefly discuss the conventional methods.

Treloar [96] considered the intrinsic elastic properties of individual, single chains, and found for the stiffness of a model solid of extended polyethylene chains in terms of the Young modulus a value of 182 GPa. This is quite close to the experimental values of 100 – 150 GPa found for highly stretched polyethylene fibres (such as Dyneema[®]) [97]. On the other hand, experimental values for so-called isotropic samples of polyethylene are typically less than 2 GPa. Clearly, other mechanisms than pure chain stretching need to be involved, at least for unstretched, partially crystallized samples. As is well-known, the degree of crystallinity for most solid polymeric materials is below 90% [1]. In these materials the chains are rarely fully extended, but are packed into folded structures; presumably the entanglements between the polymeric chains present in the melt are in some way frozen in upon solidification, and form glass-like solid regions throughout the sample.

Tashiro et al. [98, 99, 100] calculated the elastic moduli of chemically realistic polymeric solids beyond the single-chain approach using the force-field technique, in which a test chain is deformed in the presence of the force field from the neighboring chains that interact with this test chain. They assumed the crystal structure to be ideal, with the chains in the crystal fully stretched. The crystal densities obtained from the calculations are within 5% of the experimental values, and good agreement with experimental values of the Young's modulus of (stretched samples of) polyethylene, aromatic polyamides, poly-*p*-benzamide, and other crystalline polymers were obtained along the chain direction in the crystal, and somewhat less good perpendicular to that (but still of the same order of magnitude).

Finally, there are the quantum-mechanical studies of the elastic moduli of (again perfectly ordered) polymeric solids of, *e.g.*, crystalline polyethylene, and the novel rigid-rod polymer PIPD, based on quantum-mechanical density functional theory [101, 102]. The predictions of these (highly involved, “parameter-free”) calculations are quite reasonable when it comes to the Young's modulus along the chain direction, but fail for the bulk modulus with predictions that are several times larger than results known from experiment [101]. This is indicative of an incorrect description of interchain interactions. We further note that the crystal density used, *e.g.*, in reference [102], enter their calculations not self-consistently, but were put in by hand.

Apart from not considering the disordered regions typical of most crystalline polymers, all approaches mentioned so far either seriously underestimate or even completely ignore the role of entropy, although long ago Flory pointed out the importance of entropy in stabilizing a polymer crystal [17]. It is furthermore well established that for simple liquids entropic

packing-effects dominate the microscopic structure of the system, and the same appears to be true for polymers [19]. Thus, despite that the precise point of crystallization may (in reality) be determined by enthalpic effects, the structure of the solid phase is probably still entropy dominated. Note that hard-core models (in which entropy predominates) have been applied reasonably successfully in studies of the crystallization of colloidal particles and model atoms [103].

Here, we study the generic features of polymer elasticity and the role of packing effects by relying on model polymers with hard-core interactions between the beads. We apply *classical* liquid-state density functional theory (DFT) to calculate the elastic moduli of idealized polymeric crystals described in more detail below. Polymeric fluids have been studied using density functional methods in various contexts before. Perhaps the most relevant to the problem in hand is the work of McCoy and co-workers [19], which is an application of polyatomic DFT to chemically realistic polymeric systems. Our approach differs from that of McCoy and coworkers in that information about the connectivity not only enters through the direct correlation function of the polymers in the melt, but also through the contribution of polymeric corrections to the free energy of the crystal.

There are essentially four types of DFT for simple liquids [62]. The first relies on a thermodynamic perturbation expansion around a liquid state, *i.e.*, the thermodynamic properties of the solid are computed by means of a formal expansion around those of the liquid. This theory was developed by Ramkrishnan and Yussouff (RY) [52], and is straightforward to implement, *i.e.*, is computationally convenient. The second type of DFT applies a so-called weighted-density approximation (WDA) [59] in which the solid is treated as an inhomogeneous liquid. The third type of DFT involves an effective-liquid approximation (ELA) [61], which is a modification of the weighted-density approximation. The difference between WDA and ELA is rather technical and lies in the description of the crystal density in the excess free energy. The fourth type of DFT is the fundamental measure theory (FMT) developed by Rosenfeld [63], and later modified by Tarazona [64], which relies on functional interpolation between the zero-dimension limit for the excess free energy and the one of 3D bulk.

The latter three approaches are generally taken to be superior to the former, but are much more involved to implement for fluids of model polymers than for fluids of spherical particles. This in fact is the reason why we developed a polymeric version of the RY DFT in Chapter 3. Despite that WDA (or the more accurate “modified WDA”) and ELA give much better prediction for the elastic moduli of hard spheres, we show here that a RY-type theory is not as crude as is often thought [61, 71]. Taking into consideration the highly approximate nature of our model polymers, we argue that for our purposes this method is sufficiently accurate¹. The advantage of the RY DFT is that it is easily extended to

¹We feel that the modified WDA method applied to our problem is unlikely to produce a better agreement. The reason is that it relies on the input of an equation of state for long polymers, obtainable, *e.g.*, from PRISM, that is not as accurately known as that for monomers.

describe polymeric solids. At this point we contend with a qualitative analysis of the problem.

The method we follow to calculate the elastic moduli from the RY-type DFT is closely connected to the one advanced by Jarić and Mohanty [68], and by Jones [104], for hard spheres. Unfortunately, the results obtained by these authors for hard spheres are qualitatively incorrect. Not only do they obtain a negative Poisson ratio, which for most materials and in particular for hard-sphere solid is unphysical, their values of the various elastic moduli also differ significantly from ones obtained by means of computer simulations [67]. Jarić and Mohanty suggested that adding in the excess free energy functional terms higher than second order in the density inhomogeneities [53, 54] could improve these results [105]. We show here that these terms are indeed significant, and that a significant improvement over the original theory is possible. In addition we show that restricting the number of reciprocal lattice vectors used in calculations below a certain minimum can drastically affect the final results.

Our results for hard, polymeric chains indicate that in the hypothetical case where the bond order is completely suppressed, the role of chain connectivity is relatively small, and that interactions between the monomeric units dominate the elastic behavior of the solid phase. Connectivity merely changes the density at which the melt-solid phase transition takes place [106], and affects the elastic moduli by influencing the stability of the solid phase. For polymer models with stiff bonds that are less extensible or compressible, we expect that lattice frustration effects, which we found in a previous study [106], influence the elastic moduli. As we shall see, this turns out to be so.

The remainder of this chapter is organized as follows. In Section 2 we first present our model polymeric solid, and briefly discuss the main principles of our polymeric DFT. For more details the reader is referred to Chapter 3. The formal expressions for the elastic moduli from the density functional theory are given in Section 3. They differ from those previously derived for hard spheres [105] in that they contain an explicit dependence on the bonded interaction between the monomeric subunits of the polymers. In Section 4 we describe the calculation technique in detail, and show that the results for the simple case of hard spheres are in good agreement with the computer simulations [67], and improve upon the predictions of Jarić and Mohanty. The results for hard-chain crystals are given in Section 5. We find that the *direct* influence of the polymeric connectivity on the values of the elastic moduli is minor. The chain connectivity affects the values of the elastic moduli *indirectly* by changing the freezing density of the polymeric solid. We compare our results with the elastic moduli for real polymeric materials and find a surprisingly good agreement. The conclusions are presented in Section 6.

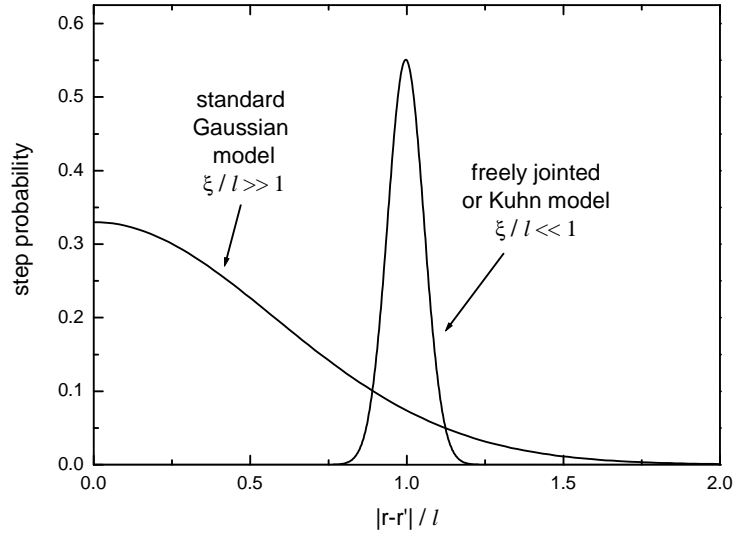


Figure 4.1: Step probability for two limiting cases of the polymer model under consideration: a standard Gaussian chain model with $\xi/l \gg 1$ and a freely-hinged model with $\xi/l \ll 1$, at fixed Kuhn length l_K .

4.2 Density functional theory of a model polymeric solid

The model polymers we consider are freely-hinged chains with an adjustable bond stiffness. Let $g(\mathbf{r}, \mathbf{r}')$ denote the probability that a bond that starts at position \mathbf{r}' ends at \mathbf{r} . The following bond probability interpolates between the standard Gaussian and Kuhn models [106]

$$g(\mathbf{r}, \mathbf{r}') = \frac{\sqrt{6}}{8\pi^{3/2}\xi|\mathbf{r} - \mathbf{r}'|l} \left(\exp \left[-\frac{3(|\mathbf{r} - \mathbf{r}'| - l)^2}{2\xi^2} \right] - \exp \left[-\frac{3(|\mathbf{r} - \mathbf{r}'| + l)^2}{2\xi^2} \right] \right), \quad (4.1)$$

where l is a mean length of the bonds, and ξ is a root-mean-square deviation to that. The effective Kuhn length l_K of the model depends on l and ξ via the relation $l_K = \sqrt{l^2 + \xi^2}$ [106]. As illustrated in Figure 4.1, our model behaves like a freely-hinged chain model for $\xi \ll l$ with fixed bond length $l_K = l$, whilst for $\xi \gg l$ it becomes equivalent to the Gaussian-chain model with a root-mean-square bond extension $l_K = \xi$.

The model polymers are assumed to interact via an isotropic volume exclusion between the beads, which are thought to “live” on a face-centered cubic (fcc) lattice. As argued elsewhere, the only crystal consistent with a freely-hinged-polymer model consisting of isotropic interaction sites, is one where the (phantom) bonds do not display any long-range order. Hence, in our description of the solid the polymers remain random walkers confined to an fcc lattice. (In the reference melt they are random walkers too, but in free,

continuous space.) We restrict our calculations of the elastic moduli to the fcc crystal, for it is the only stable structure among the set of all cubic lattices for the polymer model introduced above [106].

For reasons of computational convenience, the density distribution $\rho(\mathbf{r})$ of the material in the crystalline solid phase is often described by a lattice sum of narrow Gaussians. We, too, invoke this approximation, and write for the local segment density [68, 104]

$$\rho(\mathbf{r}) = \frac{\rho_S}{N_c \pi^{3/2} \det \mathbf{M}^{1/2}} \sum_{\{\mathbf{R}\}} \exp [-(\mathbf{R} - \mathbf{r}) \cdot (\mathbf{A} \cdot \mathbf{M} \cdot \mathbf{A}^\dagger)^{-1} \cdot (\mathbf{R} - \mathbf{r})], \quad (4.2)$$

where $\{\mathbf{R}\}$ indicates the set of all the real-space crystal-lattice vectors, \mathbf{M} a matrix describing the width of the Gaussian density profiles, \mathbf{A} the lattice-constant matrix with \mathbf{A}^\dagger its transpose, N_c the number of sites per unit cell, and ρ_S the average segment density of the crystal. In the strained crystal the Gaussian density profiles are assumed to be isotropic, which seems to be an accurate approximation [68]. We do not allow for the presence of vacancies, so

$$\rho_S = N_c \det \mathbf{A}^{-1}. \quad (4.3)$$

In the case of cubic symmetry the density profiles are locally isotropic, so [68]

$$M_{ij} = \alpha \delta_{ij}, \quad A_{ij} = a \delta_{ij} \quad (4.4)$$

with α the (dimensionless) square width of the local density profile, measured in units of the lattice constant a . Note that for the fcc lattice $N_c = 4$. In our calculations of the elastic moduli we rely on a description in terms of the reciprocal lattice vectors, which we now define. The reciprocal lattice matrix describing these vectors is given by

$$\mathbf{B} = 2\pi(\mathbf{A}^\dagger)^{-1}, \quad (4.5)$$

which for the case of cubic symmetry simplifies to

$$B_{ij} = b \delta_{ij} \quad (4.6)$$

with b the reciprocal-lattice constant for the fcc lattice.

In a previous chapter we advanced a density functional theory for the polymeric crystal [106], based on an expansion around the liquid or molten state. The grand potential $\Delta\Omega$ of the crystal relative to that of the melt was found to read

$$\begin{aligned} \frac{1}{k_B T} \frac{\Delta\Omega}{\rho_L V} &\equiv \Delta\omega = \frac{1}{\rho_L V} \int d\mathbf{r} \rho(\mathbf{r}) \ln \rho(\mathbf{r}) / \rho_L \\ &- \frac{1}{\rho_L^2 V} \int d\mathbf{r}' g(|\mathbf{r} - \mathbf{r}'|) [\rho(\mathbf{r}) - \rho_S] [\rho(\mathbf{r}') - \rho_S] \\ &- \frac{1}{\rho_L V} \sum_{p=2}^{\infty} \frac{1}{p!} \int \dots \int C^{(p)}(\mathbf{r}_1, \dots, \mathbf{r}_p) \prod_{i=1}^p d\mathbf{r}_i (\rho(\mathbf{r}_i) - \rho_L) \\ &- \frac{1}{k_B T} (\mu_S - \mu_L) \frac{1}{\rho_L V} \int d\mathbf{r} \rho(\mathbf{r}) - \frac{1}{\rho_L V} \int d\mathbf{r} (\rho(\mathbf{r}) - \rho_L), \end{aligned} \quad (4.7)$$

where for the density distribution $\rho(\mathbf{r})$ we insert the Gaussian profiles Eq. (4.2). Here, T denotes the temperature, k_B Boltzmann's constant, V the volume of the system, μ_S the chemical potential of the solid and μ_L that of the liquid reference phase, and ρ_S and ρ_L the segment densities of respectively the solid and liquid state. $C^{(p)}(\mathbf{r}_1, \dots, \mathbf{r}_p)$ is the p -particle direct correlation function of the liquid reference state, which we calculate with the aid of the polymeric reference interaction site model (so-called PRISM) [22], which we *derived* from an amalgamation of the Lifshitz theory of polymers and the theory of simple liquids [83, 106]. To this end we invoke the usual Percus-Yevick (PY) closure [22], mimicking a hard-core interaction between the beads.

The range of the hard-core interactions we denote by σ allows us to define the so-called fusion parameter $\Gamma \equiv l_K/\sigma$, measuring the strength of the coupling between the chain connectivity and the effective interactions between the beads. Note that chain connectivity enters our description through the second term of Eq. (4.7), as well as via the direct correlation functions in the third term². The second term is accurate only at length scales small compared to the size of the chains. This is one of the reasons why the long-range bond order cannot be established within our model description. (See also the discussion in Chapter 3.)

It is convenient to rewrite Eq.(4.7) in terms of a Fourier representation of the density distribution Eq. (4.2),

$$\rho(\mathbf{r}) = \rho_L \left[1 + \eta + \sum_{\{\mathbf{q}\}} \zeta(\mathbf{q}) \exp(i\mathbf{q} \cdot \mathbf{r}) \right] \quad (4.8)$$

with $\{\mathbf{q}\}$ the set of the reciprocal lattice vectors of the fcc lattice, $\eta = (\rho_S - \rho_L)/\rho_L$ the dimensionless density jump across the crystallization transition, and

$$\zeta(\mathbf{q}) = (1 + \eta) \exp \left[-\frac{1}{4} \mathbf{q} \cdot \mathbf{A} \cdot \mathbf{M} \cdot \mathbf{A}^\dagger \cdot \mathbf{q} \right]. \quad (4.9)$$

Inserting Eq. (4.8) into Eq. (4.7), and truncating the sum containing the direct correlation functions after the third term, we get an expression for the grand potential,

$$\begin{aligned} \Delta\omega = & 1 - (1 + \eta) \left(5/2 + \ln \frac{N_c \pi^{3/2} \alpha^{3/2}}{(1 + \eta)} - \frac{1}{k_B T} (\mu_S - \mu_L) \right) \\ & - \sum_{\{\mathbf{q}\}} \hat{g}(\mathbf{q}) \zeta^2(\mathbf{q}) - \frac{1}{2} \eta^2 \rho_L \hat{C}_L^{(2)}(0) - \frac{1}{2} \rho_L \sum_{\{\mathbf{q}\}} \zeta^2(\mathbf{q}) \hat{C}_L^{(2)}(|\mathbf{q}|) \\ & - \frac{1}{6} \eta^3 \rho_L^2 \hat{C}_L^{(3)}(0, 0), \end{aligned} \quad (4.10)$$

²Note that in the density differences in the connectivity correction term, ρ_S should be used instead of ρ_L , however the difference turns out to be negligible in comparison with our previous calculations [106]. This is because we are interested in the polymeric correction in the crystal, and the solid density should be used as the reference density in this case.

which we minimize with respect to the liquid density ρ_L , the parameter η and also the width of the density profile α^3 . In our density functional we include only the zero- q part of the three-body direct correlation function [53]

$$\widehat{C}_L^{(3)}(q, 0) = \frac{\partial \widehat{C}_L^{(2)}(q)}{\partial \rho} \Big|_{\rho=\rho_L}, \quad (4.11)$$

since only this term is believed to contribute significantly to the elastic moduli [105]. Higher order terms are usually deemed to be unimportant, although not much is known about whether this is true or not [53, 54].

The minimization of Eq. (4.10) was done by a standard quasi-Newton algorithm from the NAG[®] library (Mark 18, E04JYF). The number of reciprocal lattice vectors $\{\mathbf{q}\}$ needed to accurately describe the crystal phase was determined empirically (see Section 4). The conditions for coexistence between liquid and solid phases are found by equating the pressures and chemical potentials in both phases. In other words, we set $\Delta\omega = -\Delta P/k_B T \rho_L = 0$ and $\mu_S - \mu_L = 0$ in Eq. (4.7) to ensure phase coexistence, with ΔP the pressure difference in both phases.

In the next section we describe how the elastic moduli can be calculated from the density functional Eq. (4.10).

4.3 Elastic moduli from density functional theory

To calculate the elastic moduli of our polymer crystal, we use the method proposed for hard-sphere crystals by Jarić and Mohanty [68], and adapt it to our needs. We use the usual Einstein convention for the summation of the tensorial components, so Hooke's law may be written as

$$d\sigma_{ij} = C_{ijkl} d\epsilon_{kl} \quad (4.12)$$

with σ_{ij} the components of the stress tensor, ϵ_{ij} the components of the strain tensor and C_{ijkl} the components of isothermal elastic modulus tensor ($i, j = 1, 2, 3$). The stress tensor is the first derivative of the Helmholtz free energy F of a deformed crystal with respect to the strain ϵ_{ij} in the limit of zero strain, $\sigma_{ij} = V^{-1} \partial F / \partial \epsilon_{ij} |_{\epsilon=0}$. Jarić and Mohanty [68] showed that

$$C_{ijkl} = \frac{1}{V} \frac{\partial^2 F}{\partial \epsilon_{ij} \partial \epsilon_{kl}} \Big|_{\epsilon=0} + P [\delta_{ij} \delta_{kl} - \frac{1}{2} (\delta_{ik} \delta_{jl} + \delta_{jk} \delta_{il})] \quad (4.13)$$

with again P the external pressure and V the volume of the system. Eq. (4.13) may be obtained in an isothermal isobaric ensemble by formally expanding the elastic Gibbs free

³Note that our functional differs from the analogous one in [106] by factor η^2 because of a substitution of ρ_S by ρ_L in the second term in Eq. (4.7), which is negligibly small and does not affect the results of our calculations.

energy G_{el} for small strain, defined by [68]

$$G_{el} = (F_\epsilon - F) + P(V_\epsilon - V) = \frac{V}{2} \epsilon_{ij} C_{ijkl} \epsilon_{kl} + \dots, \quad (4.14)$$

where we drop all terms of higher than second order in the strain, C_{ijkl} is the second derivative of the elastic Gibbs free energy in respect of the components of strain tensor, and F_ϵ is the Helmholtz free energy and V_ϵ the volume, conditions under deformation as indicated by the subscript ϵ .

Since our DFT is most conveniently expressed in the grand canonical ensemble, we seek to represent the elastic Gibbs free energy G_{el} in term of the grand potential $\Delta\Omega$, which is defined relative to a liquid reference phase. Note that in the thermodynamic limit $\Omega_\epsilon = F_\epsilon - \mu_\epsilon n$ and $\Omega = F - \mu n$, and that the number of segments n in both the strained and unstrained crystals remains invariant under the deformation. Because we assume strain ϵ to be small, we expand to second order in ϵ the volume V_ϵ , the chemical potential μ_ϵ , and the Helmholtz free energy F_ϵ . We identify the work done on the liquid reference phase against the deformation under the pressure P_L as $\Omega_{\epsilon,L} - \Omega_L = -P_L(V_\epsilon - V)$. Adding and subtracting the term $P_L(V_\epsilon - V)$ to Eq. (4.14), and taking into account the expansions of V_ϵ , μ_ϵ , and F_ϵ in ϵ , we finally get [68]

$$G_{el} = \Delta\Omega_\epsilon + V_\epsilon(P - P_L). \quad (4.15)$$

For the unstrained system the grand potential $\Delta\Omega = k_B T \rho_L V \Delta\omega$ is given by Eq. (4.10). To obtain the free energy of the strained solid, we follow Jarić and Mohanty and assume the microscopic strain ζ and the macroscopic strain ϵ to be equal, $\zeta = \epsilon$ (see the arguments and discussion in [68]). These strains are generally thought to be different, and in fact to depend on the type of deformation [107]. At this point we ignore the issue, and discuss the effect of the non-equality of the microscopic and macroscopic strains in Section 4. The strained Gaussian width tensor \mathbf{M}_ϵ of the density profiles differs from the unstrained tensor \mathbf{M} by an amount $\Delta\mathbf{M} = \mathbf{M}_\epsilon - \mathbf{M}$, because of the nonaffine character of deformation below the unit-cell (Cauchy) scale [68, 104]. For the case of cubic symmetry we have $M_{\epsilon,ij} = \alpha_\epsilon \delta_{ij}$ and $\Delta M_{ij} = \Delta\alpha \delta_{ij}$ with $\Delta\alpha = \alpha_\epsilon - \alpha$.

We expand the expression for the elastic free energy around the unstrained state in terms of the strains ϵ , ζ , $\Delta\mathbf{M}$. Obviously, the zero- and first-order terms vanish (see again Jarić and Mohanty [68] for more details), hence only second order terms are important. We compute the elastic moduli from these quadratic terms using the results of the minimization of Eq. (4.7) for the unstrained case. We allow for the relaxation of the density profiles under the strain [104], implying that we need to minimize the functional Eq. (4.7) twice. The first minimization is with respect to the density of the reference liquid ρ_L , the relative density of the crystal η , and the equilibrium density profile width α . The second minimization is with respect to the variational parameter $\Delta\alpha$.

We thus arrive at the following variational form for the elastic energy G_{el}

$$G_{el} = \frac{V}{2} \boldsymbol{\epsilon} : \mathbf{C} : \boldsymbol{\epsilon} = \frac{V}{2} \epsilon_{ij} C_{ijkl} \epsilon_{kl} = \quad (4.16)$$

$$\min_{\Delta \mathbf{M}} \frac{V}{2} [\boldsymbol{\epsilon} : \mathbf{C}^{\epsilon\epsilon} : \boldsymbol{\epsilon} + 2\Delta \mathbf{M} : \mathbf{C}^{\alpha\epsilon} : \boldsymbol{\epsilon} + \Delta \mathbf{M} : \mathbf{C}^{\alpha\alpha} : \Delta \mathbf{M}],$$

where $\min_{\Delta \mathbf{M}}$ denotes a minimization with respect to the components of the tensor $\Delta \mathbf{M}$. We used following definitions for the tensors

$$\mathbf{C}^{\epsilon\epsilon} = C^{\epsilon\epsilon} + C^{\epsilon\zeta} + C^{\zeta\epsilon} + C^{\zeta\zeta} \quad (4.17)$$

$$\mathbf{C}^{\epsilon\alpha} = C^{\alpha\epsilon} + C^{\alpha\zeta} \quad (4.18)$$

$$\mathbf{C}^{\alpha\alpha} = C^{\alpha\alpha}. \quad (4.19)$$

The tensorial blocks of the elastic modulus tensor can be expressed in terms of the components B_{ij} of the reciprocal lattice matrix \mathbf{B} defined in Eq. (4.5) as [68]

$$C_{ijkl}^{\epsilon\epsilon} = \delta_{ij} \delta_{kl} k_B T \rho_L (\eta + 1)^2 \frac{\partial^2 \Delta \omega}{\partial \eta^2} \quad (4.20)$$

$$C_{ijkl}^{\epsilon\zeta} = C_{ijkl}^{\zeta\epsilon} = \frac{1}{2} \delta_{ij} k_B T \rho_L (\eta + 1) \left[\frac{\partial^2 \Delta \omega}{\partial \eta \partial B_{kp}} B_{lp} + \frac{\partial^2 \Delta \omega}{\partial \eta \partial B_{lp}} B_{kp} \right]$$

$$C_{ijkl}^{\epsilon\alpha} = C_{ijkl}^{\alpha\zeta} = -\delta_{ij} k_B T \rho_L (\eta + 1) \frac{\partial^2 \Delta \omega}{\partial \eta \partial M_{kl}} \quad (4.21)$$

$$C_{ijkl}^{\zeta\zeta} = \frac{1}{4} k_B T \rho_L \left[\frac{\partial^2 \Delta \omega}{\partial B_{ip} \partial B_{kq}} B_{jp} B_{lq} + \frac{\partial^2 \Delta \omega}{\partial B_{ip} \partial B_{kq}} B_{jp} B_{lq} \right. \\ \left. + \frac{\partial^2 \Delta \omega}{\partial B_{ip} \partial B_{lp}} B_{jp} B_{kq} + \frac{\partial^2 \Delta \omega}{\partial B_{jp} \partial B_{lq}} B_{ip} B_{kq} \right] \quad (4.22)$$

$$C_{ijkl}^{\zeta\alpha} = C_{ijkl}^{\alpha\zeta} = \frac{1}{2} k_B T \rho_L \left[\frac{\partial^2 \Delta \omega}{\partial B_{ip} \partial M_{kl}} B_{jp} + \frac{\partial^2 \Delta \omega}{\partial B_{jp} \partial M_{kl}} B_{ip} \right] \quad (4.23)$$

$$C_{ijkl}^{\alpha\alpha} = k_B T \rho_L \frac{\partial^2 \Delta \omega}{\partial M_{ij} \partial M_{kl}}. \quad (4.24)$$

The result of the minimization of Eq. (4.16) is the elastic modulus tensor

$$\mathbf{C} = \mathbf{C}^{\epsilon\epsilon} - \mathbf{C}^{\epsilon\alpha} : (\mathbf{C}^{\alpha\alpha})^{-1} : \mathbf{C}^{\alpha\epsilon}. \quad (4.25)$$

Since the elastic moduli tensor can be symmetrized for the fcc lattice, there are only three independent elastic moduli C_{11} , C_{12} , C_{44} (in the standard Voigt notation). In the Voigt notation the coefficients are transformed according to the rules $11 \rightarrow 1$, $22 \rightarrow 2$, $23 = 32 \rightarrow 4$, etc., so $C_{1122} \rightarrow C_{12}$ and so on [108].

In our actual calculations we rely on dimensionless quantities, such as the dimensionless segment density $\tilde{\rho} \equiv \rho\sigma^3$, the dimensionless real lattice constants $\tilde{a} \equiv a/\sigma$, the dimensionless reciprocal lattice constants $\tilde{b} \equiv b/\sigma$, and the dimensionless root-mean-square variation of the bond length $\tilde{\xi} = \xi/\sigma$, where σ denotes as before the effective diameter of the beads. The dimensionless moduli \tilde{C}_{ijkl} are defined as

$$\tilde{C}_{ijkl} = \frac{1}{k_B T \tilde{\rho}_L} C_{ijkl} \sigma^3. \quad (4.26)$$

In the next section we discuss the details of our calculations.

4.4 Calculation method

Performing the differentiations of equations (4.20 - 4.24), and using Eq. (4.10), we obtain the following expression for the elastic moduli of our model polymeric solid

$$\begin{aligned} \tilde{C}_{ijkl}^{\epsilon\epsilon} = & \delta_{ij}\delta_{kl} \left\{ (\eta + 1) - (\eta + 1)^2 \rho_L \hat{C}_L^{(2)}(0) \right. \\ & - \rho_L \sum_{\{\mathbf{q}\}} \hat{C}_L^{(2)}(|\mathbf{q}|) \zeta^2(\mathbf{q}) - \eta(\eta + 1)^2 \rho_L^2 \hat{C}_L^{(3)}(0, 0) \\ & \left. - \frac{2}{(\eta + 1)^2} \sum_{\{\mathbf{q}\}} \hat{g}(\mathbf{q}) \zeta^2(\mathbf{q}) \right\} \\ & - \frac{1}{2} \rho_L \sum_{\{\mathbf{q}\}} \left[\frac{\hat{C}_L^{\prime\prime(2)}(|\mathbf{q}|)}{|\mathbf{q}|^2} - \frac{\hat{C}_L^{\prime(2)}(|\mathbf{q}|)}{|\mathbf{q}|^3} \right] \zeta^2(\mathbf{q}) q_i q_j q_k q_l \\ & - \sum_{\{\mathbf{q}\}} \left[\frac{\hat{g}^{\prime\prime}(\mathbf{q})}{|\mathbf{q}|^2} - \frac{\hat{g}^{\prime}(\mathbf{q})}{|\mathbf{q}|^3} \right] \zeta^2(\mathbf{q}) q_i q_j q_k q_l \end{aligned} \quad (4.27)$$

$$\begin{aligned} \tilde{C}_{ijkl}^{\epsilon\alpha} = & -\frac{(\eta + 1)}{2\alpha} \delta_{ij}\delta_{kl} - \frac{1}{4} a^2 \rho_L \sum_{\{\mathbf{q}\}} \frac{\hat{C}_L^{\prime(2)}(|\mathbf{q}|)}{|\mathbf{q}|} \zeta^2(\mathbf{q}) q_i q_j q_k q_l \\ & - \frac{a^2}{2(\eta + 1)} \sum_{\{\mathbf{q}\}} \frac{\hat{g}^{\prime}(\mathbf{q})}{|\mathbf{q}|} \zeta^2(\mathbf{q}) q_i q_j q_k q_l \end{aligned} \quad (4.28)$$

$$\begin{aligned} \tilde{C}_{ijkl}^{\alpha\alpha} = & \frac{(\eta + 1)}{4\alpha^2} (\delta_{ik}\delta_{jl} + \delta_{il}\delta_{jk}) - \frac{1}{8} a^4 \rho_L \sum_{\{\mathbf{q}\}} \hat{C}_L^{(2)}(|\mathbf{q}|) \zeta^2(\mathbf{q}) q_i q_j q_k q_l \\ & - \frac{a^4}{4(\eta + 1)^2} \sum_{\{\mathbf{q}\}} \hat{g}(\mathbf{q}) \zeta^2(\mathbf{q}) q_i q_j q_k q_l. \end{aligned} \quad (4.29)$$

Here, the primed symbols indicate the derivatives with respect to $|\mathbf{q}|$. The contribution from the chain connectivity enters these expressions *directly* in terms that contain the Fourier transform of the step operator \hat{g} , and *indirectly* via the contribution of the direct correlation function $\hat{C}_L^{(2)}$. Note that in the polymer density functional theory proposed by McCoy *et al.*[19], connectivity would be included only via the direct correlation function of the melt obtained by PRISM. It turns out, however, that for our model, which lacks any long-range bond order, the contribution from the terms containing the step operator \hat{g} are relatively small, representing 2 – 3% of the actual values of the elastic moduli for all models. One would expect these to become more important if long-range bond ordering does take place.

To calculate the elastic moduli from Eqs. (4.27 - 4.29), we use the results of minimization of Eq. 4.10 for α, η and ρ_L , and those of the second minimization for $\Delta\alpha$, with the new density profile width $\Delta\alpha + \alpha$. We perform the summations over the reciprocal space in Eqs. (4.27 - 4.29) numerically. In passing, we note that the body-centered cubic (bcc) lattice is the reciprocal lattice to the fcc lattice. It is straightforward to calculate the reciprocal vectors of fcc lattice for the whole space using its general definition. Using the results of Eqs. (4.27 - 4.29), and with help of Eq. (4.25), we calculate the elastic moduli \tilde{C}_{11} , \tilde{C}_{12} , \tilde{C}_{44} for the fcc lattice.

To show that the calculation method we employ should produce quite reasonable results, we first apply it to the hard-sphere problem. Eqs. (4.16 - 4.29) can be applied to hard spheres or monomers by setting $\hat{g} = \hat{g}' = \hat{g}'' = 0$ and using for $C_L^{(2)}$ the known results from the PY closure [68]. It is useful to recall in this context that Jarić and Mohanty [68], and Jones [104], using the same type of DFT we use, obtained negative and therefore physically incorrect results for the so-called Poisson ratio (defined below). In reply to strong criticism of Frenkel and Ladd [67], provoked not only by the negative Poisson ratio, but also by a poor agreement of the theoretical moduli with results from the computer simulations, Jarić and Mohanty [105] suggested that inclusion of the three-body direct correlation function Eq. (4.11) should increase the accuracy of the elastic moduli. This indeed is the reason why we have included this term in our excess free energy Eq. (4.10).

Another important aspect of the calculation of the elastic moduli is the number of reciprocal vectors included in the sums of Eqs. (4.27 - 4.29), which in the calculation of Jarić and Mohanty may have been not sufficiently large [53]. Beforehand it is unclear how many of those need to be included in the calculations to obtain accurate values of the elastic moduli. To test this, we present in Figure 4.2 the (dimensionless) elastic moduli of the solid phase as a function of the number of reciprocal lattice vectors included in the sums of Eqs. (4.27 - 4.29). Results are shown for hard monomers at a density of $\tilde{\rho}_S = 1.12$, and for model polymers (with $\xi/l \gg 1$, $N = 100$, $\Gamma = 3.7$) at a density of $\tilde{\rho}_S = 1.14$, which in fact are the densities below which the solid melts. From the figure we conclude that the values of the moduli only level off when the number of reciprocal vectors included in the calculations exceeds approximately 20000 for both monomers and polymers. This value

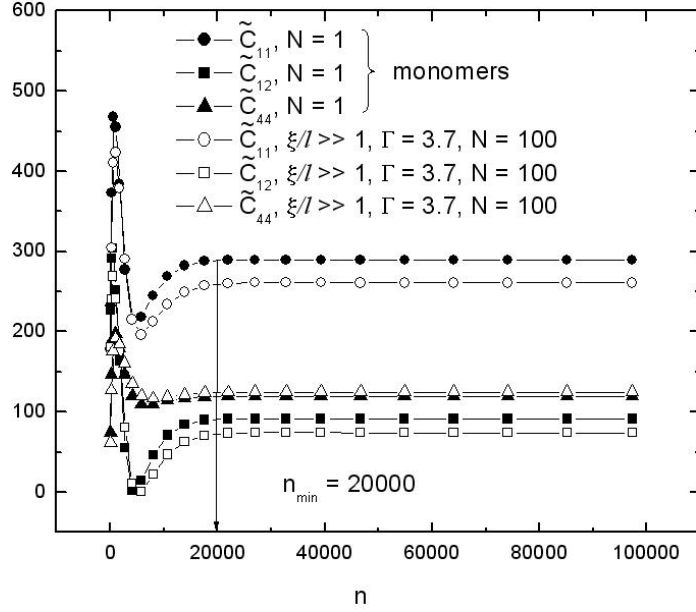


Figure 4.2: Dependence of the dimensionless elastic moduli \tilde{C}_{11} , \tilde{C}_{12} , \tilde{C}_{44} on the number of reciprocal lattice vectors n used in the summation in Eqs. (4.27-4.29) for the hard-sphere crystal at $\tilde{\rho}_S = 1.12$ (solid symbols), and for a polymeric crystal with $\Gamma = 3.7$, $\tilde{\rho}_S = 1.14$ and $N = 100$ (open symbols). The values of the moduli level off for $n > 20000$.

we use in the calculations discussed next. (We need to sum over only 5832 vectors to get saturated values of α, η and ρ_L in our minimization of Eq. (4.10).)

As regards the relaxing of the crystal under strain, we observe that although typical values of $\Delta\alpha$ are two to three order of magnitude smaller than α , the impact on the values of the elastic moduli is quite significant. Indeed, the moduli are typically smaller by a factor 4 for \tilde{C}_{11} and by a factor of 7 for \tilde{C}_{12} after the relaxation (*i.e.*, the second minimization as explained in the previous section), but not the shear modulus \tilde{C}_{44} , which remains the same within the precision of the calculation. In all our figures we show the values of elastic moduli after the relaxation.

In Figure 4.3 we compare our results for the hard-sphere fcc crystal with values obtained from molecular dynamics (MD) simulations [67]. Results of both methods indicate increasing moduli with increasing density, connected with the concomitant decreasing of the free volume available to the monomeric units. The agreement between MD and DFT is quite satisfactory, albeit far from perfect. This is especially true for \tilde{C}_{44} , which is the only directly accessible experimentally modulus. Whilst for all moduli the agreement between DFT and MD is fairly close to the freezing density, it deteriorates with increasing density. This, of course, is to be expected, and is connected with the expansion around the liquid reference state. Also shown are the results corrected for the assumption that the

macroscopic and microscopic strains are equal, which is exact only at zero initial stress. Corrections were made following Wallace [107]. For cubic crystals the solid pressure P_S needs to be added to the moduli C_{11} and C_{44} in order to correct them, whilst C_{12} remains unchanged. We estimated the pressure P_S from the relation $P_S = P_L + \Delta P$, where we use the Carnahan-Starling equation of state to obtain the pressure of liquid state P_L and the results of minimization of Eq. (4.7) for ΔP . The corrections do not improve our results, but rather make the comparison slightly worse, especially for the low-density regime below the crystallization point.

Contrary to Jarić and Mohanty [68], we do obtain a positive Poisson ratio $\nu \equiv (C_{12} + P_S)/(C_{11} + C_{12}) = (\tilde{C}_{12} + P_S\sigma^3/k_B T)/(\tilde{C}_{11} + \tilde{C}_{12})$. (The contribution of the pressure P_S to the Poisson ratio, estimated from the Carnahan-Starling equation of state and the results of minimization of Eq. (4.7), turns out rather small, of order 10%, even if we use corrected values for the elastic moduli.) A comparison of our DFT results for the Poisson ratio, and those of Frenkel's MD simulations is shown in Figure 4.4. Except for the highest density tested, our values are somewhat lower than those obtained by computer simulation [67]. We note that for most true solids, ν has a value between 1/4 and 1/3, implying a decrease in volume under tension. Our values of Poisson ratio are in this range.

In Figure 4.4 we have also given a comparison of the DFT and MD results for the bulk modulus $B \equiv (C_{11} + 2C_{12} + P_S)/3$ and the Young's modulus $E \equiv 9BC_{44}/(3B + C_{44})$, or rather their dimensionless counter parts $\tilde{B} = B\sigma^3/k_B T\tilde{\rho}_L$ and $\tilde{E} = E\sigma^3/k_B T\tilde{\rho}_L$. Again we observe good agreement at low densities, and less good agreement at higher densities.

A simple estimate of the Young's modulus may be obtained directly from the properties of the crystal phase, using its definition as the ratio of tensile stress and strain. In our DFT we assume the density distribution to be Gaussian with width α . Hence, the effective potential each bead experiences around each site is harmonic, implying a force constant equal to $2k_B T/\alpha a^2$. We thus find that the Young's modulus must be proportional to $1/\alpha a^3$, or in terms of the solid density ρ_S , and the Lindemann ratio $L = \sqrt{\alpha}$, as $E \sim k_B T\rho_S/L^2$. Recall that the Lindemann ratio is defined as the root-mean-square deviation of the position of a particle from its lattice site, divided by the nearest-neighbor distance. In Figure 4.4 we have plotted this estimate for E , using values of α and a obtained from DFT, proving it to be remarkably accurate when compared with the simulations, except again at the highest densities.

From the above we conclude that the method that we apply is reasonably accurate in the vicinity of the crystal freezing point of hard monomers, and that it should equally be suitable for the study of hard model polymers.

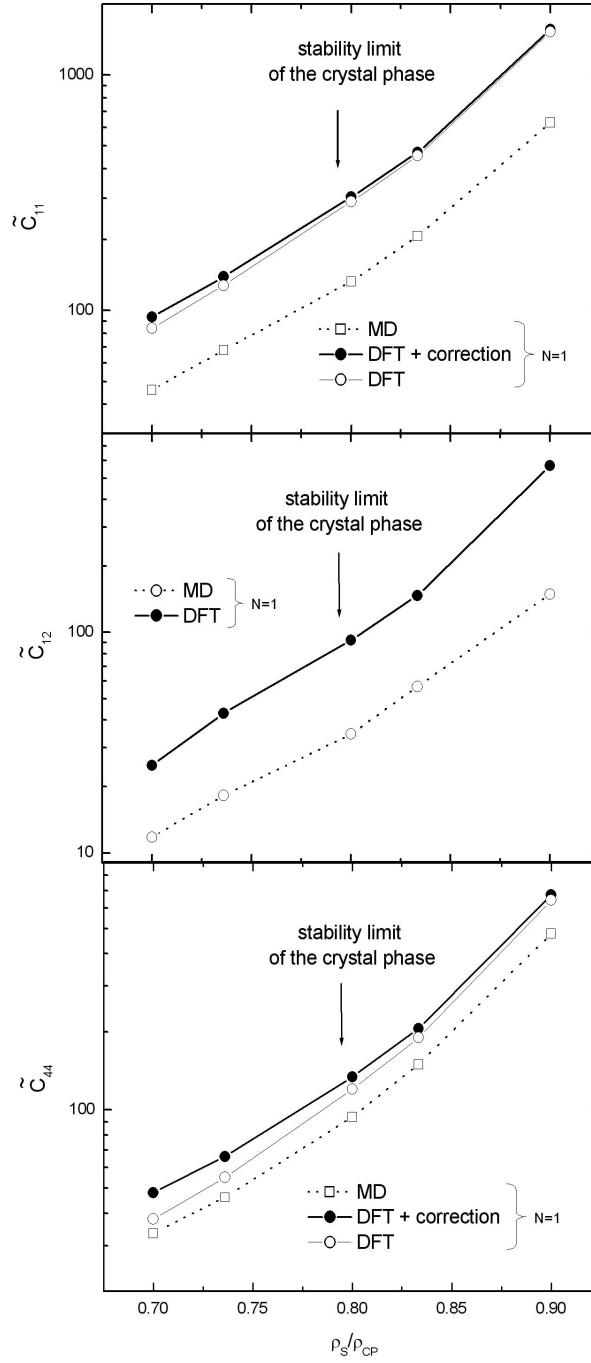


Figure 4.3: Density functional theoretical (DFT) results for the elastic moduli of the hard-sphere crystal as a function of reduced hard-sphere crystal density ρ_S/ρ_{CP} , where $\tilde{\rho}_{CP} = 1.422$ is the (dimensionless) density of the close-packed crystal. Also indicated are the results of molecular dynamics (MD) simulations of Frenkel and Ladd [67], and our corrected DFT results for the elastic moduli (see the main text).

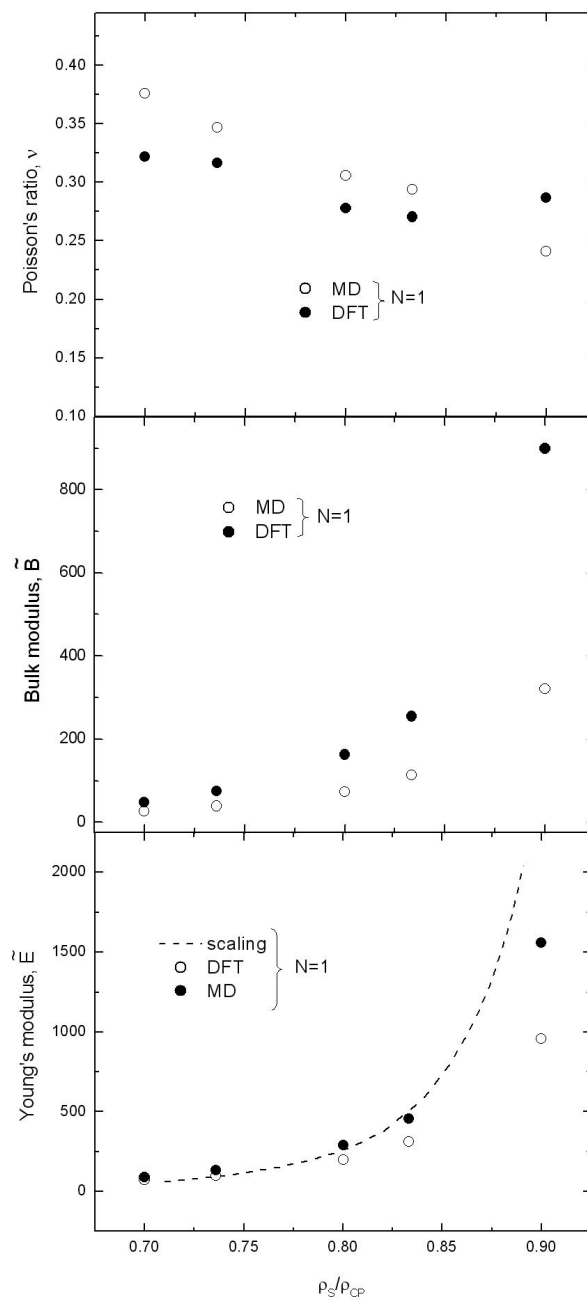


Figure 4.4: The Poisson ratio ν bulk modulus \tilde{B} and Young's modulus \tilde{E} as a function of reduced hard-sphere crystal density ρ_S/ρ_{CP} , where ρ_{CP} is the density of the close-packed crystal. The results of the DFT and of the molecular dynamics simulations of [67] are shown, as well as an estimate for the Young's modulus, discussed in the main text.

4.5 Results and discussion

We now describe the results we obtained for the model polymers, focusing on the dependence of the elastic moduli on the various system parameters. Results are presented for the

cases where: i) the fusion parameter Γ varies at fixed density ρ_S and degree of polymerization N , ii) the density varies at fixed fusion parameter, iii) the degree of the polymerization of the chains varies at fixed density and fusion parameter, and iv) the fusion parameter and segment density vary along the freezing line at fixed degree of the polymerization. In addition, we show how the presence of bonds between the beads influences the elastic response of the crystalline phase. As we shall see, the values of the elastic constants are primarily a function of how far one is removed from the melting point of the crystal.

Figure 4.5 shows how the (dimensionless) elastic moduli depend on the fusion parameter Γ for Gaussian-like chains of 100 monomeric units at a fixed density of the crystal of $\tilde{\rho}_S = 1.14$. (Results are shown for the limit $\xi/l \gg 1$.) We find that the values of the moduli increase monotonically with Γ , levelling off in the large- Γ regime. The reason for such a behavior is that by increasing the fusion parameter at fixed density, we move away from the equilibrium melting density, and in a way venture more deeply into the crystal phase (see also Figure 3.2 of Chapter 3). For large Γ the freezing density of the polymeric solid approaches a constant value with Γ , identical to the freezing density of hard spheres. This is caused by the dominance of packing effects in this regime [106]. We check the corrections to the elastic moduli for a non-zero initial stress for a number of selected values of the fusion parameter between 3.7 and 10 under condition of phase coexistence, using the pressure calculated from the virial and compressibility routes obtained from the PRISM formalism [109]. We calculated the pressure in a similar way as has been done for hard spheres to reproduce the Carnahan-Starling equation. The pressure is estimated as the sum of 2/3 of pressure obtained via the compressibility route and 1/3 of that obtained via the virial route. Corrected values were within 10 to 15% of the results for zero stress. In further calculations we do not use these corrections, because of their relatively small effect and the approximate nature of our polymeric models. (Another reason is that the calculations are computationally demanding.)

Now we fix the fusion parameter and investigate the influence of an increase in density on the elastic moduli. In Figure 4.6 we have plotted the elastic moduli again for the Gaussian limit of our model, $\xi/l \gg 1$, as a function of the ratio of the density ρ_S of the polymeric solid and that of a crystal phase at the freezing point ρ_S^c for fixed $\Gamma = 3.7$ and $N = 100$. For comparison also shown are our results for the hard-sphere crystal with $N = 1$. For both monomers and polymers, the elastic moduli become larger with increasing density, which we attribute to a reduction of the free volume. This reduction of the free volume in turn leads to an increased excluded-volume response to a deformation of the lattice.

For the metastable crystal below the coexistence point the behavior of the monomeric and the polymeric solids are almost identical, but more deeply in the crystal phase their elastic moduli diverge, albeit only modestly so. This could be due to the influence of the connectivity corrections, which are not linear in the density. It appears, at least in the Gaussian limit, that the *direct* influence of the connectivity on the moduli is indeed only small. This is quite a surprising conclusion, for the direct correlation functions of monomers and polymers are quite different and to leading order determine the elastic moduli. Somehow the

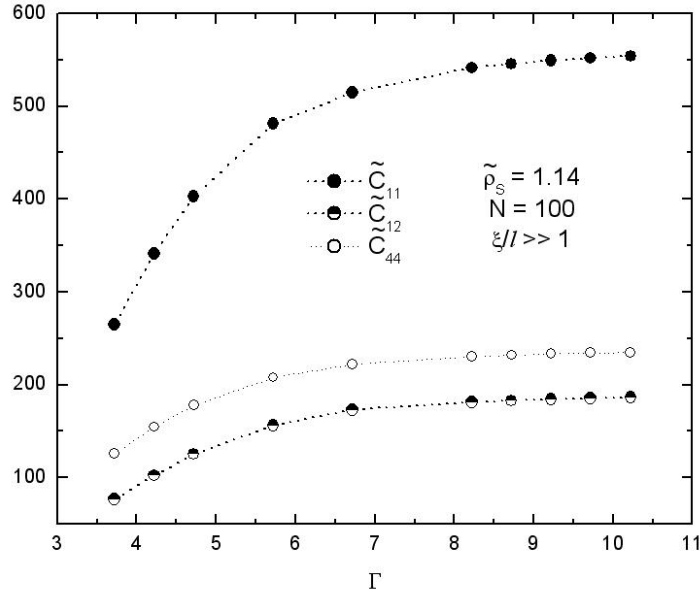


Figure 4.5: Elastic moduli of the Gaussian chain as a function of the fusion parameter Γ at fixed density $\tilde{\rho}_S = 1.14$ and degree of polymerization $N = 100$.

contribution from all terms containing the information about connectivity in Eqs. (4.27 - 4.29) cancel out.

In our previous work we found that shorter chains crystallize more easily than longer ones [106]. Hence, by decreasing the chain length at fixed fusion parameter and density, we effectively go deeper into the crystal phase. Figure 4.7 confirms this trend, showing the (normalized) elastic moduli versus the molecular weight of the chains for the Gaussian limit $\xi/l \gg 1$, at fixed density $\tilde{\rho}_S = 1.147$ and fusion parameter $\Gamma = 3.7$. The density was chosen such as to correspond to the freezing density of chains of length $N = 1000$. For clarity, and to prove our point that the elastic response of the polymer crystal depends only on how deep we are in the crystal phase, we have also plotted, in the inset, the density difference between the given density and the density at the melting point for the various molecular weights.

Finally, we demonstrate in Figure 4.8 that by increasing the stiffness of the bonds, the elastic moduli become sensitive to so-called lattice frustration effects, which also strongly influence the melting density of the crystal [106]. Shown are the elastic moduli as a function of the fusion parameter. We stress that, in contrast with situation of the Figure 4.5, the density is now not fixed, but varies with Γ (see Chapter 3). Compared are results for two cases, being the Gaussian case $\xi \gg l$, and the case where the chains behave more like freely-hinged chains with links that extend or compress by no more than half a segment diameter, *i.e.*, $\xi = 0.5\sigma$. An oscillatory dependence of the elastic moduli on Γ can be

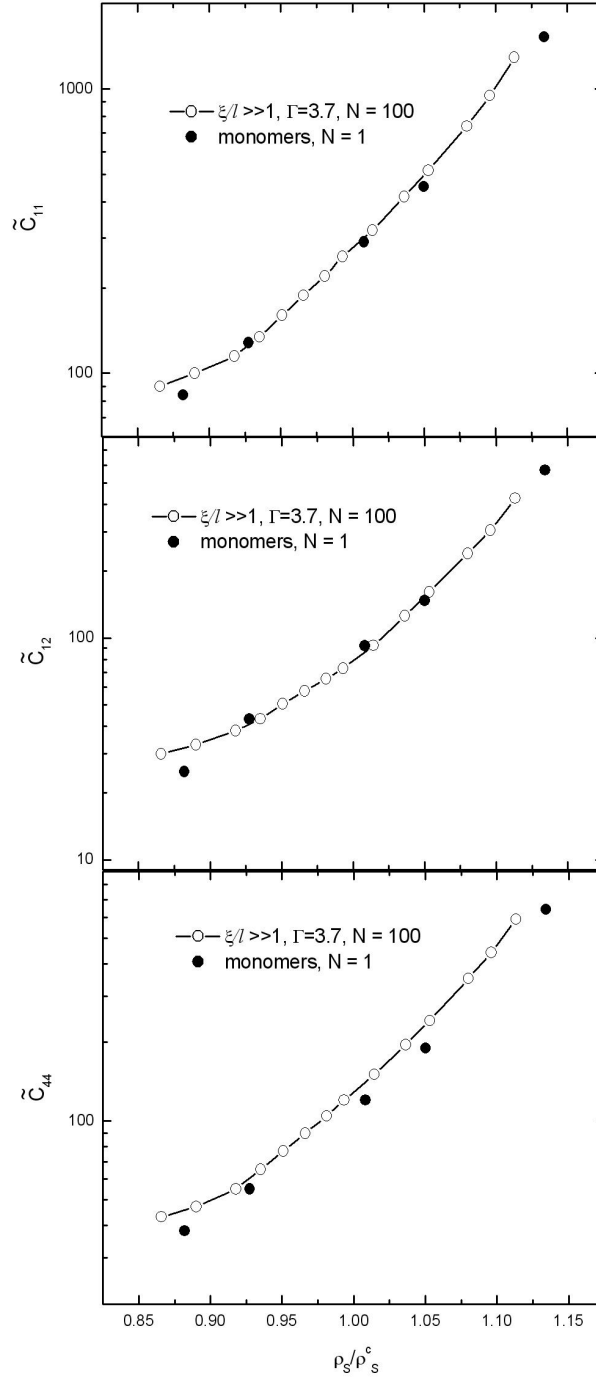


Figure 4.6: Elastic moduli of the Gaussian chain limit $\xi/l \gg 1$, as a function of reduced density ρ_S/ρ_S^c , where ρ_S^c is the density of the solid at coexistence with the melt, at fixed $\Gamma = 3.7$ and $N = 100$. Also shown are the values of the elastic moduli for the monomeric case with $N = 1$.

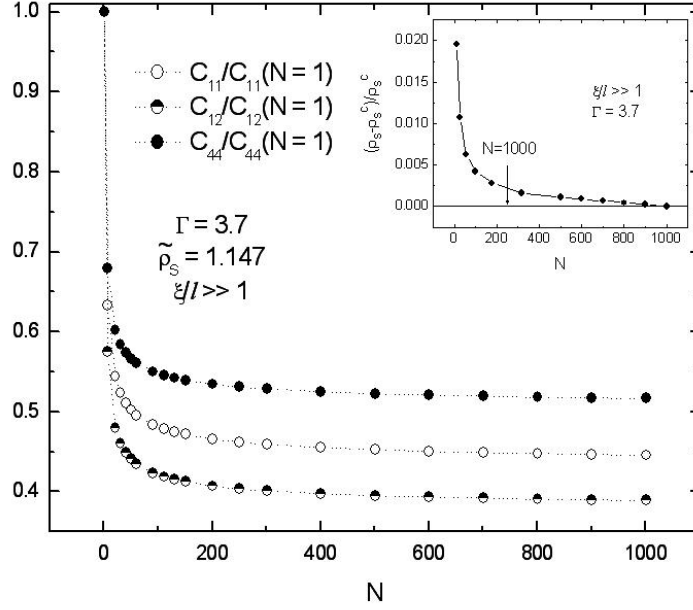


Figure 4.7: Elastic moduli in the Gaussian chain limit $\xi/l \gg 1$ divided by equivalent moduli of the monomers as a function of the degree of polymerization N for $\Gamma = 3.7$ and $\tilde{\rho}_S = 1.147$. The density difference between the given density and the density at the melting point are shown in the inset for the various molecular weights.

observed for the stiffer bonds, which reflects a similar behavior of the freezing and melting densities, see Chapter 3. These oscillations (which become less pronounced with increasing Γ) are due to a mismatch between the lattice constant and the effective length of the bonds. Note that the relative variation of the elastic moduli with this parameter remains relatively small since we now remain on the melting density for all Γ (cf. Figure 4.4). This confirms once more that the *direct* influence of connectivity on the values of the elastic moduli is small.

That the contribution from the bonded interaction to the elastic moduli must indeed be small if bond order is absent, can be demonstrated using a simple scaling estimate of the Young's modulus. Let us assume that the effective potential U_{eff} associated with each bond is harmonic, so that the kernel of the step operator approximately obeys $g \sim \exp[-U_{eff}/k_B T]$. (This is true close the minimum of the bonded-interaction potential.) It is then easy to show from Eq. (4.1) that the force constant equals $k_B T/\xi^2$. Using the same argument as in our estimate for the Young's modulus for monomers in the previous section, we find that the ratio between the contributions to the Young's modulus from the non-bonded interactions ($\sim 2k_B T/\alpha a^2$) and those from the bonded interactions ($\sim k_B T/\xi^2 a$) must be proportional to $(\Gamma/L)^2 (\xi/l_K)^2$. For the Gaussian-chain limit $\xi/l \gg 1$ this ratio is in order of $10^2 \Gamma^2$, whilst for chains that behave more like freely-hinged chains, it is $\sim \Gamma^2$.

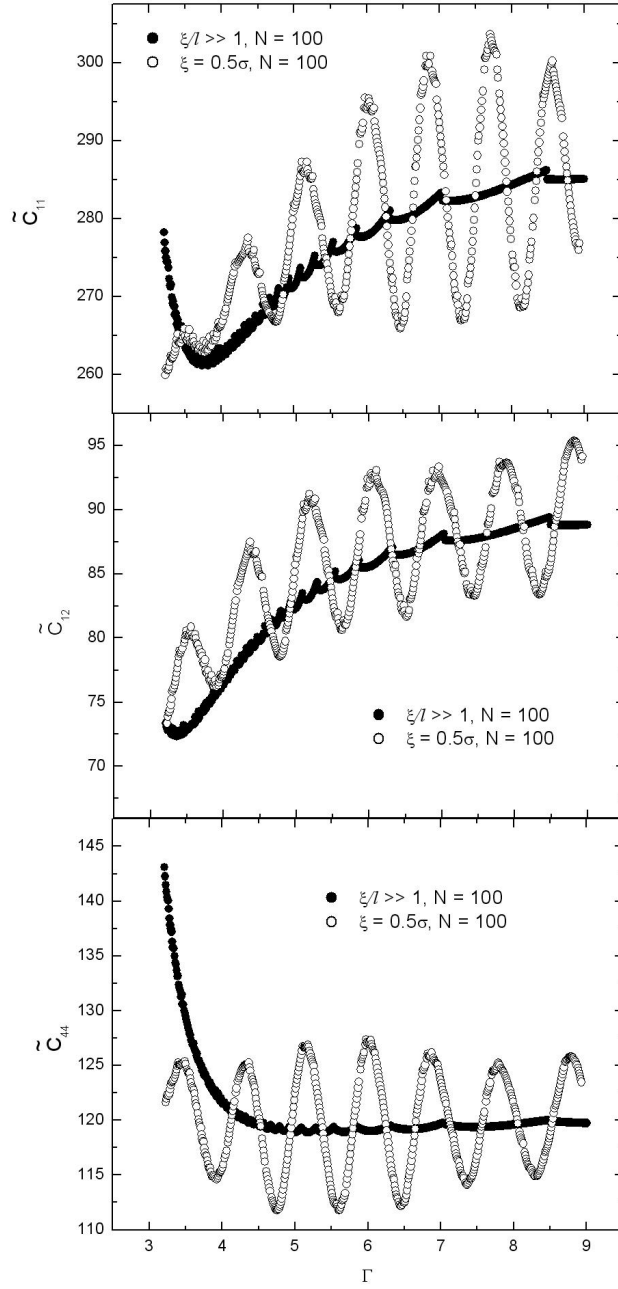


Figure 4.8: Elastic moduli \tilde{C}_{11} , \tilde{C}_{12} , and \tilde{C}_{44} as a function of the fusion parameter Γ . Compared are results for the Gaussian regime $\xi/l \gg 1$ with those of the stiff-bond regime, $\tilde{\xi} = 0.5$. Note the lattice frustration effect for the model with the stiff bonds.

Hence, for soft bonds the bonded interaction contribute less than a few percent to the Young's moduli, and for stiffer ones under, say, ten percent. This is in agreement with our more accurate DFT calculations.

Although our polymer model is crude, we nevertheless attempt to apply our predictions to actual experiment, and compare our predicted moduli with known values for polyethylene. For this purpose we need an estimate of the effective diameter of the beads in our model. The Kuhn length l_K of polyethylene in the melt equals roughly 7 diameters d of the excluded-volume sphere of each CH_2 group, with $d \approx 3.9 \text{ \AA}$ [19]. We may therefore conclude that the volume of a single bead within our coarse-grained model must be equal to the volume of 7 CH_2 groups, and estimate the effective diameter of the bead for our model from the volume of a single bead as $\sigma \approx 7.46 \text{ \AA}$. We fix the temperature at $T = 430K$ [19]. This gives for our estimate of the fusion parameter $\Gamma \approx 4$. The solid density calculated within such an estimate is 1.0 g/cm^3 , whilst the experimental value for the polyethylene solid is 0.996 g/cm^3 . The dimensionless liquid density, which we need to calculate the dimension-bearing elastic moduli, is $\tilde{\rho}_L \approx 0.9 - 1.0$ for $\Gamma \approx 4$, dependent on the parameter ξ .

The Poisson ratio of the polymeric solid that we find for $\Gamma \approx 4$ varies with density in the range $\nu = 0.22 - 0.26$, depending also on the precise value of the parameter ξ . These values are somewhat below the ones found for polyethylene in experiment, which are about $0.3 - 0.5$ [110]. The closer to the value of $1/2$, the lower the volume changes upon deformation. It may well be that the lack of bond ordering in our model is connected with the larger volume response upon external deformation than observed in real polymeric crystals.

The bulk modulus B we find for $\Gamma \approx 4$ varies between 3.3 and 4.6 GPa and the Young's modulus E between 2.8 and 4.3 GPa, depending again on the parameter ξ . This has to be compared with the Young's modulus of about 2 GPa found in experiment for isotropic polyethylene samples [111], and with experimental values for the bulk modulus that are of the same order of magnitude. The agreement could be co-incidental, but it turns out that our results compare favorably with experimental data on typical semicrystalline polymers [99].

It is quite surprising that our highly idealized polymeric model crystal can indeed describe the mechanical properties of real polymeric solids so well. A possible explanation is that in most (semicrystalline) polymeric solids the interchain interactions dominate the physics underlying their elasticity. Obviously in strongly stretched samples, which have much higher elastic moduli, especially along the chain direction, chain connectivity plays a much more prominent role. The aim of future works therefore is to incorporate long-range bond order self-consistently into the model description.

4.6 Conclusions

According to our density functional calculations, the elastic moduli of highly idealized polymeric solids are only fairly weakly dependent on the connectivity of the beads – packing effects seem to predominate. The *direct* influence of the polymeric corrections on

the moduli is small, representing less than 5% of the numerical values of these moduli. The main influence of the connectivity is *indirect* via the direct correlation function of the beads that may be seen as an effective interaction potential between pairs of beads. It appears that connectivity influences the values of the elastic moduli by stabilizing or destabilizing the crystal phase of our model polymeric solid.

We found that the elastic moduli increase with increasing crystal density because of the reduction of the available free volume upon closer packing, which leads to a stronger response to external deformation. Strong oscillations of the elastic moduli as a function of fusion parameter are also found. These are most likely caused by lattice-frustration effects, discovered by us in Chapter 3. The Poisson ratio we found is positive and somewhat smaller than the one obtained experimentally, *e.g.*, for polyethylene. Our values of the bulk and Young's moduli agree to within the same order of magnitude with the experimental values, which is an indication of the importance of the interchain interactions to the elasticity of polymeric solids.

In order to validate our polymeric DFT, we also examined the elastic moduli of hard-sphere crystals. We found that by adding the three-body direct correlation function to the expression for the grand potential, and by performing the summation over a large enough number of reciprocal-lattice vectors, the DFT significantly improved upon the original of Jarić and Mohanty [68]. Indeed, we found quite reasonable agreement with the computer simulations of Frenkel and Ladd [67].

We thank Joachim Wittmer (Lyon, France) for discussions and for suggesting the calculations presented in this chapter.

Chapter 5

On the role of connectivity in the relative stability of crystal types for model polymeric solids

ABSTRACT

We study the relative stability of two different lattice types for model polymeric solids, using a recently developed density functional theory (DFT) for freely-hinged, polymeric chains of hard globular segments. The most stable crystal-lattice type appears to be determined by the mean length and the stretching stiffness of the bonds as well as by the size of the segments. We discuss the possible implications of this for the crystallization of chemically realistic polymers.

According to current paradigm, the face-centered cubic (fcc) lattice is the preferred lattice type for the hard-sphere crystal. Theoretically, however, there still is some ambiguity as regards the optimal crystal symmetry for this type of system. In a remarkable paper, Alexander and McTague [112] argued on quite general grounds within a Landau type of approach that, irrespective of the type of interactions, spherical particles favor the body-centered cubic (bcc) lattice, not the fcc lattice. Recently, Groh and Mulder [55] showed with the help of (a highly approximate) density functional theory (DFT), that the relative stabilities of the bcc and fcc lattices are a function of the strength of the solid-phase order parameter, the latter type becoming more favorable when the order parameter is high. More sophisticated DFTs seem to point at the fcc crystal being the lowest free energy structure, but the differences in free energy of the fcc lattice and, *e.g.*, the hexagonally close-packed (hcp) lattice are minute. (In some DFTs the bcc structure is found to be mechanically stable for some densities [71]. However, it is thermodynamically metastable

or absolutely unstable with respect to the fluid in case for all hard-sphere DFTs as far as we are aware [62].) The crystallization of hard spheres has also been studied intensively by means of computer simulations [67, 113, 114, 115, 116]. These studies also indicate that it is hard to determine which lattice the most stable, although the most recent results demonstrate that the fcc structure is indeed favored for systems of hard spheres [115, 116]. In experiment, hard-sphere-like colloids seem to crystallize in a fcc crystal, as in fact do charged ones except at high ionic strength [117, 118]. (At low ionic strength a bcc structure seems to be preferred for the latter.)

Hard spheres are often considered convenient models for atoms or small molecules and by the same token chains of hard spheres are often treated as paradigmatic for actual polymer molecules [86, 94]. It seems useful, therefore, to investigate the impact of bonded interactions between hard spheres on their (preferred) crystal type. Of course, real polymeric crystals are very complex, and do not even necessarily represent the state of thermodynamic equilibrium. Almost each polymer has its specific crystal structure [111], which depends on the external conditions such as the applied pressure, the type of the chemical bonds and other characteristics related to the chemical details of these materials. Naively, one would perhaps expect the influence of the bonds on the stability of the polymeric crystal to be minor compared with that of the packing constraints imposed by the geometry of the molecules. By applying density functional theory we show here that the stiffness of the bonded interactions is in fact important to the formation of the polymeric solid, and can destabilize one crystal type in favor of another. A similar situation is found in computer simulation studies involving particles that interact via a (non-bonded) Yukawa potential, where an increase of the range of the potential was found to suppress the fcc lattice in favour of the bcc lattice [119].

Density functional theoretical methods have been extensively used in the study of crystallization of simple liquids [62]. For instance, Igloi *et al.* [120] used this method to study the relative stability of fcc and hcp lattices, first for hard-sphere systems (applying the Fourier approximation for the local segment density in the crystal) and later for simple liquid metals (using a direct correlation function of the liquid that was calculated *ab initio*, using quantum-mechanical methods) [121]. Their calculations predict correctly the preferred lattice type for Al and Mg at given external conditions of normal pressure and temperature. Other DFT studies were done for hard-sphere systems by Yussouff [122] (within the Fourier approximation), and by Baus and Colot [123] and by Laird *et al* [124]. (who used the Gaussian approximation for the local density distribution). They found the difference between the grand potentials for the fcc and hcp crystal structures at the same density near the freezing point to be very small (less than 0.05 in units of thermal energy per particle). By applying similar theoretical tools we find here that for polymeric chains of hard globular segments, this difference between the grand potentials can be increased by up to 0.07 in units of thermal energy *per segment*. Considering that the chains consists of many segments, such a stability gap must be viewed as huge.

In previous studies we considered the thermodynamic stability as well as the mechanical

properties of model polymeric solids by means of a polymer DFT, obtained from a self-consistent field-type argument [106, 69]. In our present investigation we use the same model polymer. The model polymer under consideration consists of beads interacting through a hard-core repulsive potential, and connected by freely-hinged bonds with an adjustable bond stiffness. The bonds are of a phantom nature, *i.e.*, can pass through each other. In our theory we define $g(\mathbf{r}, \mathbf{r}')$ as the normalized a-priori probability that a bond that starts at position \mathbf{r}' ends at \mathbf{r} . The following choice of bond probability interpolates between the standard Gaussian and Kuhn models [106]

$$g(\mathbf{r}, \mathbf{r}') = \frac{\sqrt{6}}{8\pi^{3/2}\xi|\mathbf{r} - \mathbf{r}'|l} \left(\exp \left[-\frac{3(|\mathbf{r} - \mathbf{r}'| - l)^2}{2\xi^2} \right] - \exp \left[-\frac{3(|\mathbf{r} - \mathbf{r}'| + l)^2}{2\xi^2} \right] \right), \quad (5.1)$$

where l denotes the mean length of a bond, and ξ the root-mean-square deviation about this mean length. The effective Kuhn length l_K of the model depends on l and ξ , and equals $\sqrt{l^2 + \xi^2}$. For $\xi \ll l$ our model turns into a freely-hinged chain with fixed bond length $l_K = l$. The other limiting case is for $\xi \gg l$, when our model behaves as the Gaussian-chain model with a root-mean-square bond extension $l_K = \xi$.

We denote the range of the (effective) hard-core interactions between the beads by σ . To describe how the chain connectivity renormalizes these interactions, we introduced in our previous work the so-called fusion parameter $\Gamma \equiv l_K/\sigma$ [106, 69]. For $\Gamma \ll 1$ neighboring beads along a chain overlap, whilst for $\Gamma \gg 1$ they do not. Our aim now is to study how the parameters Γ and ξ influence the stability of either hcp or fcc structures, and in particular which lattice is preferable for our athermal polymeric system. We note that for our model polymers the fcc crystal is the only stable cubic lattice type, and then only if $\Gamma \geq 3$ (see Chapter 3 for a discussion). The hcp crystal structure does not belong to the group of cubic lattices.

In our calculations we approximate the density distribution in the crystal phase by a sum of narrow Gaussians [106]

$$\rho(\mathbf{r}) = (\pi\epsilon^2)^{-3/2} \sum_{\{\mathbf{R}\}} \exp \left[-(\mathbf{R} - \mathbf{r})^2/\epsilon^2 \right] \quad (5.2)$$

with the width ϵ of the local density profile presumed to be much smaller than the distance between the lattice points, whose positions are given by the vectors \mathbf{R} . $\{\mathbf{R}\}$ is the set of all real-space crystal-lattice vectors. The equilibrium width of the density distributions ϵ we fix by a free-energy minimization. The unit cell of the fcc lattice is defined by the set of vectors

$$\begin{aligned} \mathbf{a}_1 &= (a/2)(\mathbf{j} + \mathbf{k}), \\ \mathbf{a}_2 &= (a/2)(\mathbf{i} + \mathbf{k}), \\ \mathbf{a}_3 &= (a/2)(\mathbf{i} + \mathbf{j}) \end{aligned} \quad (5.3)$$

with $\mathbf{i}, \mathbf{j}, \mathbf{k}$ the basis vectors in the Cartesian system of coordinates, and a the nearest-neighbor separation. The following vectors describe the hcp structure

$$\begin{aligned}\mathbf{a}_1 &= a\mathbf{i}, \\ \mathbf{a}_2 &= -(a/2)\mathbf{i} + (\sqrt{3}a/2)\mathbf{j}, \\ \mathbf{a}_3 &= c\mathbf{k},\end{aligned}\tag{5.4}$$

where $c/2$ denotes the separation of neighboring hexagonal planes.

Within the ground-state approximation, the grand-potential difference $\Delta\Omega[\rho(\mathbf{r})]$ of the crystal and a molten reference state reads [106]

$$\begin{aligned}\frac{1}{k_B T} \frac{\Delta\Omega}{\rho_L V} &\equiv \Delta\omega = \frac{1}{\rho_L V} \int d\mathbf{r} \rho(\mathbf{r}) \ln \rho(\mathbf{r}) / \rho_L \\ &\quad - \frac{1}{\rho_L^2 V} \int d\mathbf{r}' g(|\mathbf{r} - \mathbf{r}'|) [\rho(\mathbf{r}) - \rho_S] [\rho(\mathbf{r}') - \rho_S] \\ &\quad - \frac{1}{\rho_L V} \sum_{p=2}^{\infty} \frac{1}{p!} \int \dots \int C^{(p)}(\mathbf{r}_1, \dots, \mathbf{r}_p) \prod_{i=1}^p d\mathbf{r}_i (\rho(\mathbf{r}_i) - \rho_L) \\ &\quad - \frac{1}{k_B T} (\mu_S - \mu_L) \frac{1}{\rho_L V} \int d\mathbf{r} \rho(\mathbf{r}) - \frac{1}{\rho_L V} \int d\mathbf{r} (\rho(\mathbf{r}) - \rho_L),\end{aligned}\tag{5.5}$$

where for the density distribution $\rho(\mathbf{r})$ we insert the Gaussian profiles of Eq. (5.2). In Eq. (5.5), V is the volume of the system, μ_S the chemical potential of the solid and μ_L that of the liquid reference phase, and ρ_S and ρ_L are the segment densities of respectively the solid and liquid state. $C^{(p)}(\mathbf{r}_1, \dots, \mathbf{r}_p)$ is the p -particle direct correlation function of the liquid reference state, T the temperature, and k_B Boltzmann's constant. We calculate $C^{(p)}(\mathbf{r}_1, \dots, \mathbf{r}_p)$ from a generalized Lifshitz theory, formally equivalent to the so-called polymeric reference interaction site model (PRISM) [83]. To solve the PRISM equations we impose the usual Percus-Yevick (PY) closure, mimicking a hard-core interaction between the beads.

In the free-energy functional the information about the connectivity of the beads within a polymer enters via the second term in the right-hand-side of Eq. (5.5), which contains the step probability g , but also via the direct correlation functions in the third term. The term containing g is accurate only at length scales small compared to the size of the chains (see Chapters 3 and 4). As a result, the monomeric units do order positionally onto either the fcc or hcp lattice, but long-range *bond order* does not build up. (See again Chapters 3 and 4 for a discussion.)

For obvious reasons the calculations are more conveniently done in Fourier space, so we use the Fourier representation of the density distribution given in Eq. (5.2):

$$\rho(\mathbf{r}) = \rho_L \left[1 + \eta + \sum_{\{\mathbf{q}\}} \zeta(\mathbf{q}) \exp(i\mathbf{q} \cdot \mathbf{r}) \right]\tag{5.6}$$

with $\{\mathbf{q}\}$ the set of the reciprocal-lattice vectors of the fcc or hcp lattice, $\eta = (\rho_S - \rho_L)/\rho_L$ the fractional density change across the crystallization transition, and

$$\zeta(\mathbf{q}) = (1 + \eta) \exp[-\mathbf{q}^2 \epsilon^2 / 4]. \quad (5.7)$$

The expression for the dimensionless grand potential density $\Delta\omega$ reduces to

$$\begin{aligned} \Delta\omega = 1 - (1 + \eta) & \left(5/2 + \ln \rho_L + 3/2 \ln \pi \epsilon^2 - \frac{1}{k_B T} (\mu_S - \mu_L) \right) \\ & - \sum_{\{\mathbf{q}\}} \hat{g}(\mathbf{q}) \zeta^2(\mathbf{q}) - \frac{1}{2} \eta^2 \rho_L \widehat{C}_L^{(2)}(0) - \frac{1}{2} \rho_L \sum_{\{\mathbf{q}\}} \zeta^2(\mathbf{q}) \widehat{C}_L^{(2)}(|\mathbf{q}|) \end{aligned} \quad (5.8)$$

$$- \frac{1}{6} \eta^3 \rho_L^2 \widehat{C}_L^{(3)}(0, 0), \quad (5.9)$$

where, following Laird and co-workers [53], we include, apart from the usual two-body direct correlation function, only the zero- q three-body direct correlation function. This expression we minimize with respect to the liquid density ρ_L , the parameter η and the width of the density profile ϵ .

The minimization was done at the freezing point, using a standard quasi-Newton algorithm from the NAG[®] library (Mark 18, E04JYF). The conditions of mechanical and thermodynamical equilibrium were imposed by insisting on the equality of the pressures and chemical potentials in the liquid and solid phases (so $\Delta\omega = -\Delta P/k_B T \rho_L \equiv 0$ and $\mu_S - \mu_L \equiv 0$). We determine the minimum number of reciprocal-lattice vectors $\{\mathbf{q}\}$ needed to accurately describe the crystal phase for the fcc and hcp lattices empirically, and find it to be approximately 6000 for both lattice types. Only the ideal hcp lattice was considered, so we set $c/a = (8/3)^{1/2}$ in Eq. (5.4).

As our interests concern the influence of the bond stiffness on the relative stability of the fcc and hcp lattices, we calculate the freezing densities for fcc and hcp at different values of the parameter ξ . Figure 5.1 gives the liquid freezing density of chains of degree of polymerization 100 for both lattices as a function of the parameter ξ at $\Gamma = 5$. The figure clearly demonstrates the hcp structure to be more stable than the FCC structure in the range $0 < \xi/\sigma \leq 0.6$, *i.e.*, if the bonds are sufficiently stiff. Interestingly, the polymers then freeze at a lower density than hard monomers do. Apparently, in that case connectivity stabilizes the (hcp) crystal phase. Although the differences in the densities at the freezing for both lattices seem modest (less than 5%), they do exceed our numerical accuracy, which is about 0.5%. In the opposite limit of floppy bonds, with $\xi/l \gg 1$, the hcp and fcc structures are equally stable within the numerical accuracy of the calculations. In this limit the freezing of the polymer occurs at roughly the same density as that of hard monomers. For certainty, we also investigated a possible fcc-hcp transition deep in the crystal phase by directly comparing free energies, but did not find such a transition between the two lattice structures.

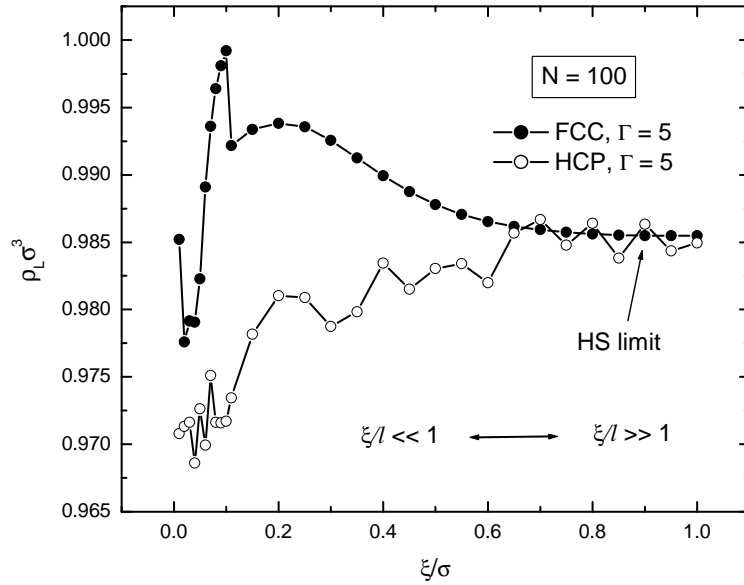


Figure 5.1: The liquid density at the freezing point as a function of the dimensionless parameter ξ/σ measuring the stretching stiffness of the bonds for the fcc and hcp lattices, given at a value of the fusion parameter $\Gamma = 5$ and degree of polymerization $N = 100$. The fusion parameter $\Gamma = l_K/\sigma$ is a measure for the bending stiffness of the chain. The hcp structure is preferable in the range $0 < \xi/\sigma \leq 0.6$. At large ξ , both fcc and hcp structures are equally probable.

The relative stability of the hcp and fcc crystals not only depends on the stretching stiffness of the bonds ξ , but also on the value of the fusion parameter Γ , which (in a way) measures the bending stiffness of the chain. To illustrate this, the percentage difference of the liquid densities at freezing between the fcc and hcp lattices is given as a function of ξ/σ for different values of the fusion parameter Γ in Figure 5.2. The values of Γ used here are chosen arbitrarily to represent the full range of the fusion parameter. For large Γ or large ξ , there is no significant difference between the two close-packed structures. The influence of the fusion parameter on the relative stability of two crystal types becomes evident from a comparison of the results for $\Gamma = 3.25$ (when the fcc structure is more stable at $0.1 \leq \xi/\sigma \leq 0.6$) and the results for $\Gamma = 5$ (when the hcp structure is favorable for $\xi/\sigma \leq 0.6$).

It is important to point out that the somewhat erratic dependence of the freezing density on the bond stiffness is not caused by numerical errors, but by so-called lattice frustration effects. These are especially prominent when the bonds are stiff, and are caused by a geometrical mismatch between the effective bond length and the distance between two neighboring lattice sites. We refer to Chapters 3 and 4 for a closer examination of this phenomenon for the fcc model polymeric solid. Note that the hcp lattice, being less symmetric than the fcc lattice, the effects of the lattice frustration for a given ξ or Γ are different

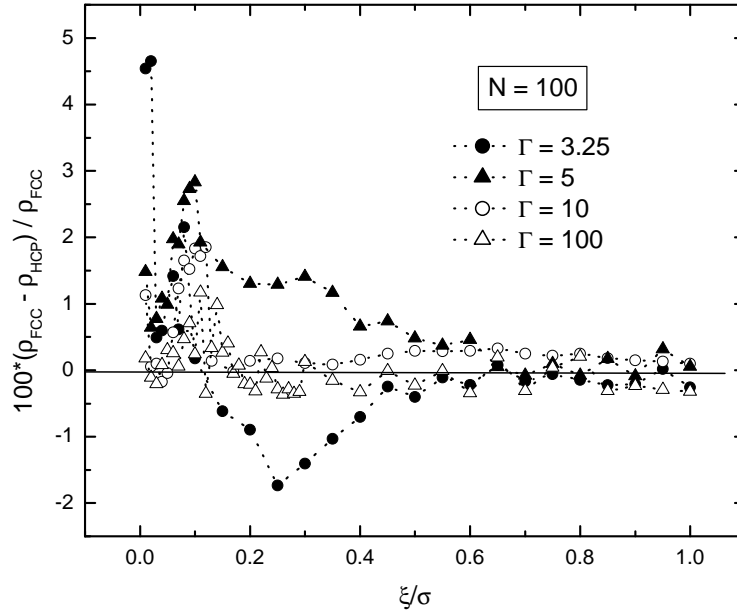


Figure 5.2: The relative density difference of the melt at freezing into the fcc and hcp structures, $100 (\rho_{fcc} - \rho_{hcp}) / \rho_{fcc}$, for different values of the fusion parameter Γ and the degree of polymerization $N = 100$. In the range $0 < \xi/\sigma \leq 0.6$ the preferred lattice type is dependent on the fusion parameter Γ . For large Γ and/or large ξ both fcc and hcp structures are equally stable.

and that (in effect) lattice frustration dictates which lattice is more stable than the other. So, the geometrical factors other than those due to the shape of the interacting moieties can play an important role in the stability of the polymer crystal. For realistic models of polymers such as polyethylene, the parameter ξ/σ is in order of 0.01 [106], and at this regime the hcp structure seems to be more favorable.

In summary, we have investigated the relative stability of the fcc and hcp crystal types for idealized model polymers using polymeric density functional theory [106]. We conclude from our studies that the most favorable lattice type of the two is determined by both the stiffness of the polymeric bonds and by the fusion parameter. Therefore, we propose that in addition to, say, enthalpic interactions, connectivity does play a significant role in the crystal structure of polymers, and that this is one possible explanation for the diversity of crystal lattices observed for polymers.

Chapter 6

Theory of the crystallization of hard polymeric chains in an orienting field

ABSTRACT

We apply a recently proposed density functional theory (DFT) for hard polymeric chains to study the influence of a quadrupolar orienting field on the freezing of model polymers. We find that a ‘disorienting’ field, mimicking elongational flow, promotes crystallization, whilst an ‘orienting’ field, which corresponds to longitudinal shear flow, destabilizes the crystal phase. We also investigate the relative stability of two close-packed crystal lattice types, face-centered cubic and hexagonal close-packed. Geometrical effects, such as the orientation of the field with respect to the main axes of the crystal, play an important role in stabilizing one crystal type over another.

6.1 Introduction

High-tensile polymeric materials are important in many industrial applications [125], and the problem of producing such materials based on highly oriented samples is of great interest in the field of polymer technology and processing. Oriented polymeric materials can be obtained by different methods from the solid phase (by cold drawing, solid-state extrusion or rolling), or from the melt in an extensional-flow setup in which the material is allowed to crystallize [1]. The high-tensile properties of oriented polymers are caused by the intrinsic anisotropy of polymers, and are connected with their chain-like structure. Along the backbone of the oriented chains the strength is determined by covalent interactions

that are much more energetic than those of the Van der Waals type that predominate in unoriented samples.

It is now well-established that the conformation of a polymer molecule can change significantly in an elongational flow field [126, 127]. In this type of flow the dominant component of the velocity is parallel to the flow direction. Under appropriate conditions, chains can achieve nearly full extension near the stagnation point, where the strain rate is the highest. Theoretically, the influence of this type of flow on an isolated polymeric coil was studied by De Gennes [128], who used in his description an earlier theory of Peterlin [129, 130], and predicted a sharp coil-stretch transition at a critical strain rate. Although theories describing the coil-stretch transition focus on polymer solutions, the same principles apply, *mutatis mutandis*, to polymeric melts.

The coil-stretch transition is important in the context of flow-induced crystallization, for there is experimental evidence [125] that polymeric chains stretched in elongational flow solidify into a fiber core, also known as a ‘shish’, which subsequently acts as a nucleation center that enhances the nucleation of crystallites of chains on it [125, 131]. The crystalline lamellar structures (the so-called ‘kebabs’), in which the chains are *not* completely stretched, have a tendency to attach to this central core upon solidification. This has been observed in many experiments [125], but also in recent computer simulation studies [41, 131].

The competition between the influence of an external field that tends to increase order, and the random-walk nature of the polymers in the melt, which promotes disorder, should be an essential ingredient in any sensible theoretical description of flow-induced solidification. Although an inherently non-equilibrium problem, a kinetic theory that does not account for this through the input of a free energy landscape that explicitly deals with the chain-like nature of polymers is bound to fail. In fact, even in the absence of flow a sensible description of the crystallization of polymers requires a self-consistent coupling between the configurational statistics of the chains and thermodynamics of the crystallization transition [132].

In this context it may be useful to refer to the idea of Flory [17] that chain stiffness in combination with packing effects must be at the root of the solidification of polymers. Despite being largely ignored by the polymer crystallization community, this has been confirmed by means of computer simulations [18]. Indeed, repulsive interactions are sufficient to induce crystallization in model polymeric systems — even the familiar lamellar structure is reproduced [18, 41].

Here, we consider the role of an external field mimicking elongational flow on the entropy-driven solidification of model polymers. We shall not be focusing on strong flows in which the chains strongly deform, but instead deals with how a weak flow affects the packing effects that ultimately promote crystallization. As we shall see, even at this level of approach a strong impact on the stability of the crystal phase is observed. Depending on the flow

type and the crystal symmetry, the crystal phase may be either stabilized or destabilized, or one crystal symmetry be favored over another.

We note that the coupling of flow fields to phase transitions has attracted a considerable attention from both theorists and experimentalists, in particular in the field of the isotropic-to-nematic phase transition of stiff polymers or other rod-like particles [133, 134, 135, 136, 137, 138]. This transition is also entropy dominated. From these studies we infer that an external flow field (shear or elongational flow) promotes liquid-crystalline ordering, because the external field increases the degree of order in the system. Another point of interest in the context of our studies is that even a weak flow has noticeable effect on the demixing of polymeric systems. On the basis of a theoretical thermodynamical analysis Bhattacharjee *et al.* [139] found that in sufficiently weak two-dimensional elongational flow, *i.e.*, far from coil-stretch transition, there are flow-induced shifts of the θ -point and of the coexistence curve for polymers in solution.

In this work we present a mean-field analysis of the role of a weak orienting field on the crystallization of a model polymeric melt. We assume that the system is in a state of local equilibrium, and that the flow is steady and of a potential type, in order to be able to apply Kramers-potential description [140] of the flow. Our aim is not to reproduce shish-kebab or any other type of supramolecular structure that are often found after a crystallization in flow. Instead, we aim to shed light on the possible impact that a flow field may have on the coupling of chain configurations, packing effects and the stability of the crystal phase. To this end we make use of an amalgamation of the Green-function description of a polymer chain in a self-consistent field, and classical density functional theory. The Kramers potential we use mimics two types of flow, elongational flow and longitudinal shear. We show that a weak elongational flow field stabilizes the polymeric crystal, whilst longitudinal shear destabilizes the crystalline state.

The remainder of this chapter is organized as follows. In Section 2 we first briefly describe the model polymers considered and the theoretical formalism used to study the influence of an external orientational field on the crystallization. The application of the calculation method to the face-centered cubic (fcc) and hexagonal close-packed (hcp) crystal geometry is explained in Section 3. The results of our numerical calculations are given in Section 4, and our conclusions are presented in Section 5.

6.2 Polymeric density functional theory

We apply a recently proposed [106] polymeric density functional theory (DFT). The model polymers consist of N beads that interact through a hard-core repulsive potential, and that are connected by freely-hinged phantom bonds with an adjustable bond stiffness. The single-chain partition function, or Green function, [85] of a chain with its ends fixed at the

positions \mathbf{r} and \mathbf{r}' , can be written as

$$Z_N(\mathbf{r}', \mathbf{r}; 1, N) = \int \left(\prod_{j=1}^N d\mathbf{r}_j \right) \delta(\mathbf{r}_1 - \mathbf{r}') \delta(\mathbf{r}_N - \mathbf{r}) \times \left(\prod_{j=2}^N g(\mathbf{r}_j, \mathbf{r}_{j-1}) \exp[-\beta U_{scf}(\mathbf{r}_j) - \beta U_{ext}(\mathbf{r}_j, \mathbf{r}_{j-1})] \right) \quad (6.1)$$

with $U_{scf}(\mathbf{r}_j)$ the self-consistent molecular field that a monomer labelled $j = 1, \dots, N$ on an arbitrary test chain experiences due to the presence of other polymeric chains, and $U_{ext}(\mathbf{r}_j, \mathbf{r}_{j-1})$ an external orienting field that couples to pairs of neighboring monomers j and $j - 1$. Note that the self-consistent molecular field is a function of the only one positional coordinate, because we study the freely-hinged model chains that interact via pairs of single site-site interactions only. As usual, $\beta \equiv 1/k_B T$, where T denotes the absolute temperature, and k_B Boltzmann's constant.

In Eq. (6.1) the “kernel” $g(\mathbf{r}, \mathbf{r}')$ represents the bonded interactions between consecutive beads on a chain through the normalized *a-priori* probability that a bond that starts at position \mathbf{r}' ends at position \mathbf{r} . It is a model-dependent quantity. For our model polymer we define this probability, which interpolates between the standard Gaussian and Kuhn models, as follows [106]

$$g(\mathbf{r} - \mathbf{r}') = \frac{\sqrt{6}}{8\pi^{3/2}\xi|\mathbf{r} - \mathbf{r}'|l} \left(\exp \left[-\frac{3(|\mathbf{r} - \mathbf{r}'| - l)^2}{2\xi^2} \right] - \exp \left[-\frac{3(|\mathbf{r} - \mathbf{r}'| + l)^2}{2\xi^2} \right] \right), \quad (6.2)$$

where l is a mean length of the bonds, and ξ is a root-mean-square deviation from this length. The effective Kuhn length l_K of the model may be expressed in terms of l and ξ , as $l_K = \sqrt{l^2 + \xi^2}$ [106]. We distinguish two regimes: one where our model behaves like a freely-hinged chain model for $\xi \ll l$ with fixed bond length $l_K = l$, and one where it becomes equivalent to the standard Gaussian-chain model with a root-mean-square bond extension $l_K = \xi$, corresponding to the limit $\xi \gg l$. In this chapter we present results only for the Gaussian-chain limit, although we have performed calculations in the other (freely-hinged, Kuhn) limit as well. However, the somewhat erratic character of the data obtained for the latter limit proved hard to interpret, and in addition required excessive computational effort to remove numerical inaccuracies. (See also below.)

Eq. (6.1) can be rewritten in terms of a recursive equation

$$Z(\mathbf{r}', \mathbf{r}; 1, N + 1) = \exp[-\beta U_{scf}(\mathbf{r})] \int d\mathbf{r}'' g(\mathbf{r}', \mathbf{r}'') \times \exp[-\beta U_{ext}(\mathbf{r}', \mathbf{r}'')] Z(\mathbf{r}'', \mathbf{r}; 1, N), \quad (6.3)$$

subject to the boundary condition $\lim_{N \rightarrow 1} Z(\mathbf{r}', \mathbf{r}; 1, N) = \exp[-\beta U_{scf}(\mathbf{r})] \delta(\mathbf{r}' - \mathbf{r})$. The solution to this recursive equation Eq. (6.3) is a bilinear sum of products of the left and

right eigenfunctions of the integral operation, weighed by the corresponds eigenvalue to the power N [83, 86, 94].

The total partition function of the system of M polymeric chains is $\mathcal{Z} = \frac{1}{M!} Z_N^M$, where $Z_N \equiv \int d\mathbf{r} \int d\mathbf{r}' Z(\mathbf{r}', \mathbf{r}; 1, N)$ is the single-chain partition function. The Helmholtz free energy F of the system can be easily obtained from the thermodynamic relation $\beta F = -\ln \mathcal{Z}$. The molecular field $U_{scf}(\mathbf{r})$ we treat as an external field, and we use the procedure pioneered by Lifshitz [87] in order to determine this field. To this end, the configurational part F_{conf} of the free energy is calculated by a subtraction of the self-consistent field energy $\int d\mathbf{r} U_{scf}(\mathbf{r}) \rho(\mathbf{r})$ from the free energy F of the system. Here $\rho(\mathbf{r})$ notes the number density of segments, given by

$$\rho(\mathbf{r}) \equiv M Z_N^{-1} \int d\mathbf{r}' \int d\mathbf{r}'' \sum_{s=1}^N Z(\mathbf{r}', \mathbf{r}; 1, s) Z(\mathbf{r}, \mathbf{r}''; s, N). \quad (6.4)$$

Within the self-consistent-field method, the actual free energy \mathfrak{F} is a sum of the configurational free energy and the excess free energy, which accounts for the interaction between the segments

$$\mathfrak{F} = F_{conf} + F_{exc}. \quad (6.5)$$

The density dependence of the configurational free energy can be made explicit. We apply a ground-state approximation and use only the largest eigenvalue. For use in a DFT of the crystal phase it turns out useful to expand the density $\rho(\mathbf{r})$ around that of the liquid state $\rho(\mathbf{r}) = \rho_L + \Delta\rho(\mathbf{r})$, and neglect the terms of higher than second order in $\Delta\rho$. Applying the methodology presented in [106] and in Chapter 3, we find for difference between the configurational free energy of the solid and that of the melt

$$\begin{aligned} \beta \Delta F_{conf} &= \int d\mathbf{r} \rho(\mathbf{r}) \ln \rho(\mathbf{r}) - \int d\mathbf{r} \rho_L \ln \rho_L \\ &\quad - \frac{1}{\rho_L} \int d\mathbf{r} \int d\mathbf{r}' \Delta\rho(\mathbf{r}) e^{-\beta U_{ext}(\mathbf{r}, \mathbf{r}')} g(\mathbf{r}, \mathbf{r}') \Delta\rho(\mathbf{r}) + O(\Delta\rho^3), \end{aligned} \quad (6.6)$$

where the first two terms are the free energies of the ideal solid and melt, and the third term enters due to the connectivity of the polymers. A consequence of the ground-state approximation is that Eq. (6.6) only describes positional ordering on short wavelengths, although the coupling to the external field described next does not preclude long-range configurational effects.

For the Kramers potential we write [135, 140]

$$\beta U_{ext} = -\frac{3}{2} u \cos^2 \varepsilon, \quad (6.7)$$

where u is a dimensionless field strength that we later on connect with the actual elongational flow rate, and ε the angle between the direction of a bond of a test chain and the

direction of the field \mathbf{n} , $\cos \varepsilon \equiv \mathbf{n} \cdot (\mathbf{r} - \mathbf{r}')/|\mathbf{r} - \mathbf{r}'|$. Hence, the potential couples not to single monomers, but to pairs of monomers at the positions \mathbf{r} and \mathbf{r}' .

Positive and negative values of u correspond to different flow geometries. The case when u is positive corresponds to inhomogeneous vortex-free longitudinal shear, and when u is negative the quadrupole potential models an hydrodynamic flow acting on the polymers confined within an uniaxially compressed sample.

For computational convenience we do not employ the Helmholtz free energy, but the grand potential [106]. The grand-potential difference $\Delta\Omega[\rho(\mathbf{r})]$ between the crystal and a liquid reference state is [69]

$$\begin{aligned} \beta \frac{\Delta\Omega}{\rho_L V} &\equiv \Delta\omega = \frac{1}{\rho_L V} \int d\mathbf{r} \rho(\mathbf{r}) \ln \rho(\mathbf{r})/\rho_L \\ &\quad - \frac{1}{\rho_L^2 V} \int d\mathbf{r}' g_F(|\mathbf{r} - \mathbf{r}'|) [\rho(\mathbf{r}) - \rho_S][\rho(\mathbf{r}') - \rho_S] \\ &\quad - \frac{1}{\rho_L V} \sum_{p=2}^{\infty} \frac{1}{p!} \int \dots \int C^{(p)}(\mathbf{r}_1, \dots, \mathbf{r}_p) \prod_{i=1}^p d\mathbf{r}_i (\rho(\mathbf{r}_i) - \rho_L) \\ &\quad - \beta(\mu_S - \mu_L) \frac{1}{\rho_L V} \int d\mathbf{r} \rho(\mathbf{r}) - \frac{1}{\rho_L V} \int d\mathbf{r} (\rho(\mathbf{r}) - \rho_L), \end{aligned} \quad (6.8)$$

where we take the configurational term to first order in the density difference between the two phases, and the excess term to arbitrary order in this difference (although below we truncate this term at the third order). In equation (6.8) V is the volume of the system, μ_S is the chemical potential of the solid and μ_L that of the liquid reference phase, and ρ_S and ρ_L are the segment densities of respectively the solid and liquid state.

As we show in previous work [69, 106] and in Chapters 3 and 4, the p -particle direct correlation function of the liquid reference state $C^{(p)}(\mathbf{r}_1, \dots, \mathbf{r}_p) = -\beta \delta^{(p)} F_{exc} / \prod_{i=1}^p \delta \rho(\mathbf{r}_i)$ can be calculated from a similar free energy as given in Eq. (6.8), producing an integral equation analogous to the polymeric reference interaction site model (so-called PRISM) [82]. The chain-connectivity effect is described directly through the second term of Eq. (6.8), and indirectly via the direct correlation functions included into the third term.

The PRISM equation, which connects the total correlation function of two segments on different chains, $h(\mathbf{r}, \mathbf{r}')$, and the associated two-particle direct correlation function, $C^{(2)}(\mathbf{r}, \mathbf{r}')$, reads in Fourier space

$$\widehat{h}(\mathbf{q}) = \widehat{\omega}(\mathbf{q}) \widehat{C}^{(2)}(\mathbf{q}) + \rho_L \widehat{\omega}(\mathbf{q}) \widehat{C}^{(2)}(\mathbf{q}) \widehat{h}(\mathbf{q}), \quad (6.9)$$

where the hats indicate Fourier-transformed quantities, \mathbf{q} the wave vector and ρ_L the average melt density. The intramolecular correlations between segments on a single chain are described by the form factor $\widehat{\omega}$,

$$\widehat{\omega}(q) = \frac{1 - \widehat{g}_F^2 - \frac{2}{N} \widehat{g}_F + \frac{2}{N} \widehat{g}_F^{N+1}}{(1 - \widehat{g}_F)^2}, \quad (6.10)$$

where \widehat{g}_F is the Fourier transform of the bond probability in the presence of the orienting field. To calculate this quantity, we assumed this field to be weak so that $g_F(\mathbf{r}, \mathbf{r}') \equiv \exp[-\beta U_{ext}(\mathbf{r}, \mathbf{r}')]g(\mathbf{r}, \mathbf{r}') \simeq g(\mathbf{r}, \mathbf{r}')(1 - \beta U_{ext}(\mathbf{r}, \mathbf{r}'))$ in the limit $\xi \gg l$, *i.e.*, for the standard Gaussian model. We find

$$\begin{aligned} \widehat{g}_F(q) = & \exp\left[-\frac{q^2 l_K^2}{6}\right] \left\{ 1 + \frac{1}{2}u(1 + 2P_2(\cos \gamma) + 18q^{-2}l_K^{-2}P_2(\cos \gamma)) \right\} \\ & - 9uq^{-3}l_K^{-3}\sqrt{6\pi}P_2(\cos \gamma)\frac{\text{erf}(ql_K)}{2\sqrt{6}}, \end{aligned} \quad (6.11)$$

where q is the length of the vector in Fourier space and γ the angle between the direction of field \mathbf{n} and the vector \mathbf{q} in Fourier space. The details of calculation of the kernel $g_F(\mathbf{r}, \mathbf{r}')$ in the presence of an external field can be found in the Appendix A. Equation (6.9) is valid at non-zero external field, since the chains remain freely-hinged even when under an external field and bond-order correlations cannot build up on account of the isotropic site-external interactions presumed in this work.

We use the classical Percus-Yevick (PY) closure to solve Eq. (6.9) [22], mimicking a hard-core interaction between the polymeric beads. As for the terms of higher order than second order of the direct correlation functions, below we extract the zero- \mathbf{q} $\widehat{C}^{(3)}$ from $\widehat{C}^{(2)}$ and ignore fourth and higher order terms.

6.3 Solidification into the close-packed-crystal geometry

Ideally, one calculates the equilibrium density profiles in the crystal phase by a functional free-energy minimization. It is computationally more convenient, however, to use an Ansatz for $\rho(\mathbf{r})$ and optimize this Ansatz. For the density distribution $\rho(\mathbf{r})$ in the crystal phase we use the Gaussian profile

$$\rho(\mathbf{r}) = (\pi\epsilon^2)^{-3/2} \sum_{\{\mathbf{R}\}} \exp[-(\mathbf{R} - \mathbf{r})^2/\epsilon^2], \quad (6.12)$$

where $\{\mathbf{R}\}$ is the set of all real-space crystal-lattice vectors, and ϵ is a variational parameter that measures of the width of the Gaussian density distribution around each point of the crystal lattice. It turns out to be useful to write Eq. (6.8) in terms of a Fourier representation of the density distribution Eq. (6.12),

$$\rho(\mathbf{r}) = \rho_L \left[1 + \eta + \sum_{\{\mathbf{q}\}} \zeta(\mathbf{q}) \exp(i\mathbf{q} \cdot \mathbf{r}) \right] \quad (6.13)$$

with $\{\mathbf{q}\}$ the set of the reciprocal-lattice vectors of the crystal lattice under consideration, $\eta = (\rho_S - \rho_L)/\rho_L$ the dimensionless density jump across the crystallization transition, and

$$\zeta(\mathbf{q}) = (1 + \eta) \exp[-\mathbf{q}^2 \epsilon^2 / 4]. \quad (6.14)$$

We insert Eq. (6.13) into Eq. (6.8), truncate the sum containing the direct correlation functions after the third term, and obtain the following expression for the grand potential,

$$\begin{aligned} \Delta\omega = & 1 - (1 + \eta) \left(5/2 + \ln \rho_L + 3/2 \ln \pi \epsilon^2 - \frac{1}{k_B T} (\mu_S - \mu_L) \right) \\ & - \sum_{\{\mathbf{q}\}} \hat{g}_F(\mathbf{q}) \zeta^2(\mathbf{q}) - \frac{1}{2} \eta^2 \rho_L \hat{C}_L^{(2)}(0) - \frac{1}{2} \rho_L \sum_{\{\mathbf{q}\}} \zeta^2(\mathbf{q}) \hat{C}_L^{(2)}(|\mathbf{q}|, \gamma) \\ & - \frac{1}{6} \eta^3 \rho_L^2 \hat{C}_L^{(3)}(0, 0). \end{aligned} \quad (6.15)$$

In our density functional we include only the zero- q part of the three-body direct correlation function [53]

$$\hat{C}_L^{(3)}(q, 0) = \frac{\partial \hat{C}_L^{(2)}(q)}{\partial \rho} \Big|_{\rho=\rho_L}, \quad (6.16)$$

because higher order terms are usually considered to be unimportant [53, 54]. To obtain the optimal density profiles in the crystal phase, we minimize Eq. (6.15) with respect to the liquid density ρ_L , the parameter η and also the width of the density profile ϵ . It should be stressed that as a result of the ground-state approximation, long-range orientational bond order can only develop in our model through the coupling to the external orienting field. In the absence of such a field, the chains behave like random walkers on the crystal lattice [106].

The crystal types we consider are of the face-centered cubic (fcc) and of the hexagonal close-packed (hcp) type. The reciprocal to the fcc lattice is the body-centered cubic (bcc) lattice. The set of the reciprocal vectors $\{\mathbf{q}\}$ that enters the grand potential Eq. (6.15) can be calculated from the following expression

$$\mathbf{G} = \frac{2\pi}{a} [(h - k + l)\mathbf{i} + (h + k - l)\mathbf{j} + (-h + k + l)\mathbf{k}] \quad (6.17)$$

with h, k and l integers, a the nearest-neighbor separation, and $\mathbf{i}, \mathbf{j},$ and \mathbf{k} the basis vectors in the Cartesian system of coordinates. We arbitrarily choose the following bcc axis as the main axis in order to describe the orientation of the crystal in space

$$\mathbf{G}^0 = \frac{2\pi}{a} [\mathbf{i} + \mathbf{j} - \mathbf{k}]. \quad (6.18)$$

The geometry of the model in the case of the fcc lattice is shown in Figure 6.1. In our calculations enters the angle γ between the direction of an external field \mathbf{n} and the vector

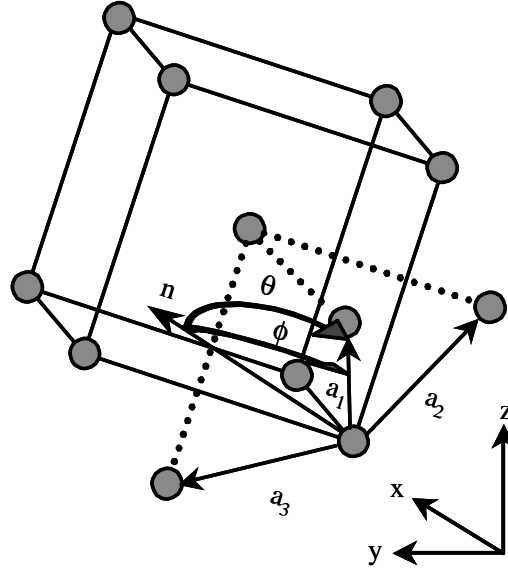


Figure 6.1: The bcc lattice reciprocal to the fcc structure. Shown are also the geometrical parameters of the model under consideration. The vector \mathbf{n} shows the direction of an external field, the vectors \mathbf{a}_1 , \mathbf{a}_2 , \mathbf{a}_3 denote the primitive translation vectors of the bcc lattice, and the angle between the arbitrary chosen main axis $\mathbf{G}^0 \equiv \mathbf{a}_1$ and direction of an external field \mathbf{n} can be expressed in Cartesian coordinates via the usual polar angles θ and ϕ .

\mathbf{q} through the bond probability Eq. (6.11). The angle between the main axis \mathbf{G}^0 of the reciprocal lattice and the direction of an external field \mathbf{n} can be expressed in Cartesian coordinates via usual polar angles θ and ϕ . For the fcc lattice, these angles are connected to the angle γ by a simple trigonometric relation

$$\begin{aligned} \cos \gamma &= \cos \theta \frac{(3h - k - l)}{\sqrt{9(h^2 + k^2 + l^2) - 6(hk + hl + kl)}} + \sin \theta \\ &\times \sqrt{1 - \frac{(3h - k - l)^2}{9(h^2 + k^2 + l^2) - 6(hk + hl + kl)}} \cos \phi. \end{aligned} \quad (6.19)$$

For the case of the hcp lattice, the set of the reciprocal vectors can be calculated from the expression

$$\mathbf{G} = \frac{2\pi}{a} [h\mathbf{i} + \frac{1}{\sqrt{3}}(h + 2k)\mathbf{j} + \frac{a}{c}l\mathbf{k}], \quad (6.20)$$

where $c/2$ is the separation of neighboring hexagonal planes. We choose the following axis as a main one

$$\mathbf{G}^0 = \frac{2\pi}{a} [\mathbf{i} + \frac{1}{\sqrt{3}}\mathbf{j}] \quad (6.21)$$

and the angle γ can be found from the relation

$$\begin{aligned} \cos \gamma = & \cos \theta \frac{\frac{1}{\sqrt{3}}(2h+k)}{\sqrt{\frac{4}{3}(h^2+hk+k^2) + (al/c)^2}} + \sin \theta \\ & \times \cos \phi \sqrt{1 - \frac{(2h+k)^2}{4(h^2+hk+k^2) + \frac{1}{3}(al/c)^2}}. \end{aligned} \quad (6.22)$$

We minimize Eq. (6.15), using the standard quasi-Newton algorithm from the NAG[®] library (Mark 18, E04JYF), at the coexistence between the liquid and solid phases, when the pressures and chemical potentials in both phases are equal.

The number of reciprocal lattice vectors $\{\mathbf{q}\}$ needed to accurately describe the fcc and/or hcp crystal phase we determine empirically. (In the absence of an external field, 5832 reciprocal lattice vectors are needed to get accurate results [106].) In the presence of the field the direct correlation function has to be evaluated for each value of the angle γ , which is different for every reciprocal lattice vector, in order to reach the desired precision. We perform calculations of the direct correlation function for a few thousand reciprocal lattice vectors. Fortunately, the direct correlation function is only a sensitive function of the angle γ , and therefore of the field, in the small- \mathbf{q} -regime. Thus, the direct correlation function in the presence of the field needs to be evaluated only for the first few shells of the reciprocal lattice. For the remaining shells the field-free results for the direct correlation function are sufficiently accurate. That this is so, is shown in Figure 6.2 for the fcc lattice, where we plot the freezing density of the liquid for the case when the angle-dependencies of the first 5 shells (29 reciprocal lattice vectors), the first 10 shells (88 reciprocal lattice vectors) and for the first 20 shells (228 vectors) are included. The total number of reciprocal lattice vectors we use is 9260. It seems sufficient to take into account the values of the angle γ only for the first 88 reciprocal lattice vectors.

In the next section we discuss the results of our calculations.

6.4 Results and discussion

Before discussing the results, it seems useful to clarify the physical meaning of the parameter u , which in our calculation denotes the strength of an external field acting on a single bond. To connect this parameter with a flow rate, we presume that the chains are not very long so that they obey Rouse dynamics. The relaxation time and radius of gyration can be determined analytically for a test chain in a weak Kramers potential flow from the Smoluchowski equation for the configurational distribution function [141]. Comparing the radius of gyration of our model and that obtained by Frisch *et al.* [141] for the Rouse model, we conclude that the parameter u must be equal to $2\tau_0^2 s^2$, where s is the flow rate and τ_0

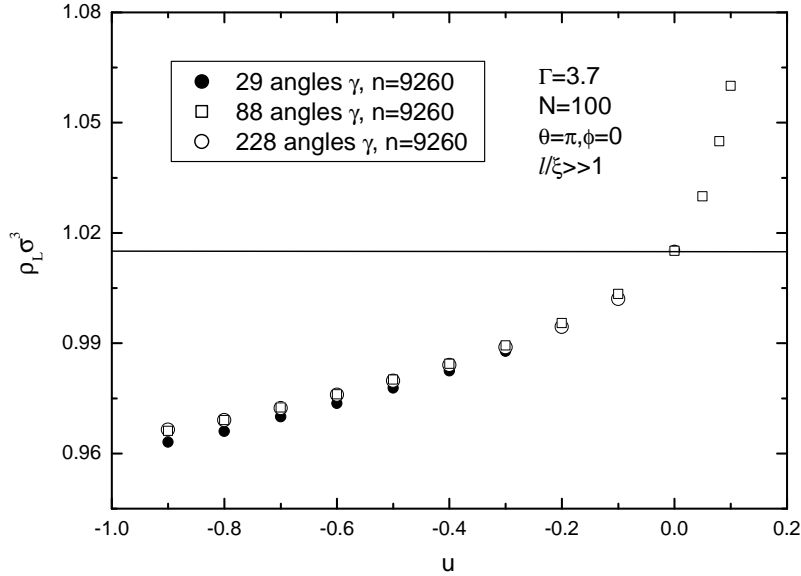


Figure 6.2: Freezing density of the polymeric liquid in the Gaussian-chain limit $\xi/l \gg 1$ if the solid phase has a fcc lattice, as a function of the strength of external field u . Orientation angles $\theta = \pi$ and $\varphi = 0$ of the lattice. See Figure 6.1. Chain parameters $\Gamma = 3.7$ and $N = 100$.

the characteristic relaxation time of the chain, often called the Kramers relaxation time. This relaxation time τ_0 is proportional to the square of the number of monomeric units per chain and corresponds, apart from an uninteresting numerical multiplicative constant, to the well-known Rouse time of the chain [141].

Apart from the field strength (flow rate) u and the degree of polymerization N , the only control parameter that we have is a quantity that we call the fusion parameter $\Gamma \equiv l_K/\sigma$, where l_K is the effective Kuhn length of the chains and where σ indicates the range of the hard-core interactions. We calculated the dependence of the freezing density on the parameter u for the standard Gaussian model, $\xi/l \gg 1$, for different orientations of the crystal lattice relative to the main axis of the flow field at fixed degree of polymerization $N = 100$ and fusion parameter $\Gamma = 3.7$, and show the results in the Figure 6.3. (The crystal type is fcc.) It shows that the polymeric melt crystallizes more easily under the influence of an external ordering field than in the absence of this field at all values of the polar angles of orientation θ and ϕ between the direction of the external field and the main axis of the lattice, but only when the parameter u is negative. If it is positive, the freezing density goes up.

A possible cause for this is the following. For positive u , the orientation of the induced anisotropy of polymeric melt is parallel to the direction of the field. This makes it more difficult for a polymeric bead to occupy a free lattice site in the presence than in the absence of this field. When u is negative, the anisotropy is induced in the easy plane, with

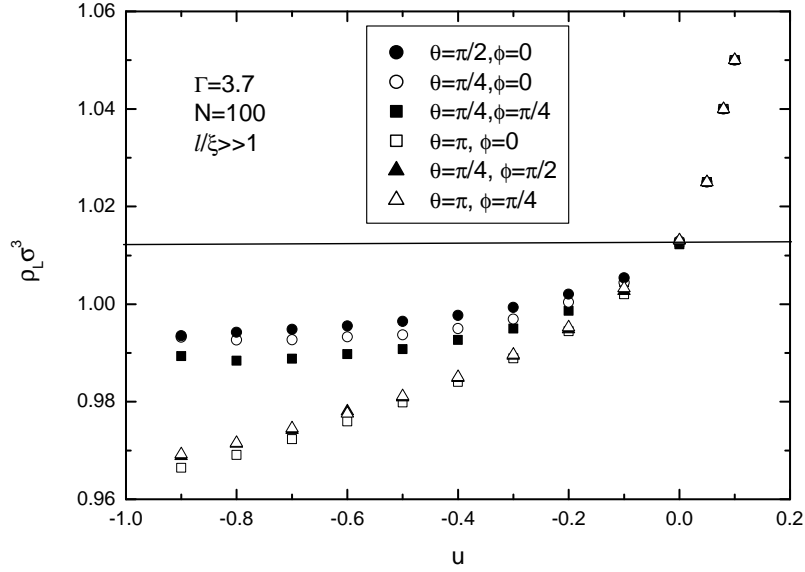


Figure 6.3: Freezing density of the polymeric liquid in the Gaussian-chain limit ($\xi/l \gg 1$) as a function of the strength of external field u , for different values of the orientation angles θ and φ of the fcc lattice, at fixed $\Gamma = 3.7$ and $N = 100$.

a symmetric distribution of the polymeric segments relative to the lattice axes. Hence, in the present crystal geometry it is easier to crystallize fcc lattice, when u is a negative.

Figure 6.4 presents a structural explanation of the stability of the crystal phase for different values of u , and for different orientations of the lattice with respect to the field. The difference $\Delta g(r)$ between the pair-correlation function of the polymeric melt in the absence of an external field and the pair-correlation function of the melt in the presence of this field is positive when $u < 0$ and $\gamma = \pi/2$. In other words, the orienting field induces stronger positional correlations in the melt if $u < 0$, diminishing the structural difference between the melt and the crystal phase, thereby stabilizing the latter. Conversely, when $u > 0$ this difference is negative for all angles γ : the field destroys local positional order in the melt with the opposite effect of destabilizing the crystal phase.

The next, three-dimensional plot of Figure 6.5 shows the orientation dependence of the freezing density at fixed value of the parameter $u = -0.5$ and fusion parameter $\Gamma = 3.7$, again for $N = 100$. The dependence on the angles θ and φ of the lattice orientation has a nontrivial character. There is an obvious periodicity, albeit that this effect is small and the difference between the maximal and minimal values for the freezing densities found is just a few percent. Global minima in the freezing density are found for the angles $\theta = \pi k$ and $\phi = \pi k/2$, with k an integer. Figure 6.5 demonstrates the importance of geometrical effects in the determination of the freezing density of the polymeric melt.

Now we compare the freezing of the fcc and hcp structures under an external field for the

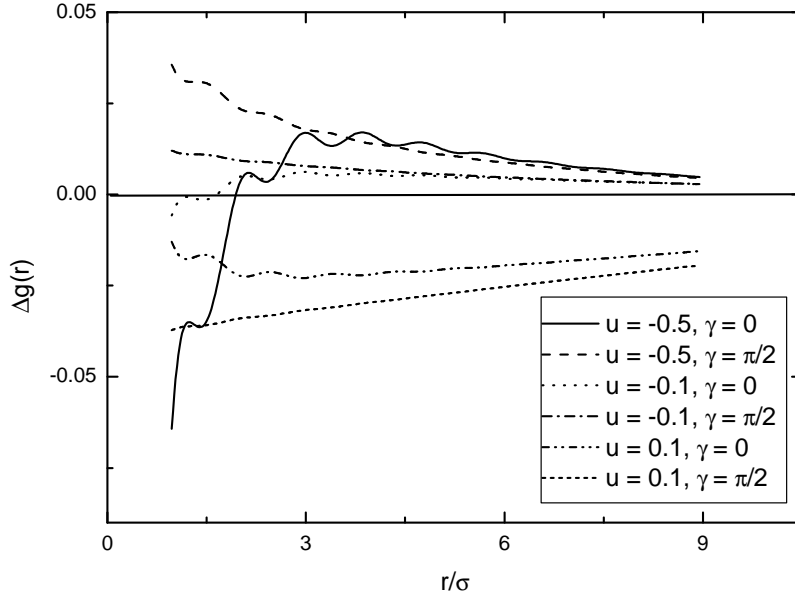


Figure 6.4: The difference $\Delta g(r)$ between the pair-correlation function of the polymeric melt in the absence of an external field and the pair-correlation function of the melt in the presence of this field as a function of a dimensionless distance r/σ , for different values of the strength of an external field u and the angle γ (see the main text). The density $\rho_L = 0.96\sigma^3$ and the chain parameters are fixed at $\Gamma = 3.7$ and $N = 100$.

arbitrarily chosen angles $\theta = \pi/4$ and $\phi = \pi/4$, again in the Gaussian chain limit $\xi/l \gg 1$ (see Figure 6.6). In the absence of an external field the fcc and hcp structures are equally probable within our DFT, and within the accuracy of the numerics that we estimate to be about 0.5%. When the external field is switched on, both lattices crystallize at a lower density than in the absence of the field, but the hcp structure crystallizes at a lower density (and lower free energy density) and should therefore be more stable. Thus, not only the mean length and the stretching stiffness of the bonds can determine the lattice type, as we concluded in earlier work [69], but also the presence of an external field. (The crystal type may remain metastable if the field is turned off.)

In Figure 6.7 we show the dependence on the fusion parameter Γ of the fcc and hcp freezing densities in the presence of an external field with $u = -0.5$, and without this field. The orientation of the crystal was fixed at the arbitrary angles $\theta = \pi/4$ and $\phi = \pi/4$. The difference in freezing densities is significant only in the small- Γ regime. In this regime the system crystallizes more easily under the influence of an external field. In the large- Γ regime the behavior of the polymeric system is monomer-like and the external orientational field cannot influence the stability of the crystal phase.

Finally, in Figure 6.8 we examine how the degree of polymerization N affects the crystallization density of the model polymers in an external orientational field, at fixed fusion parameter of $\Gamma = 3.7$ and at fixed angles $\theta = \pi/4$ and $\phi = \pi/4$. From Figure 6.8 it can

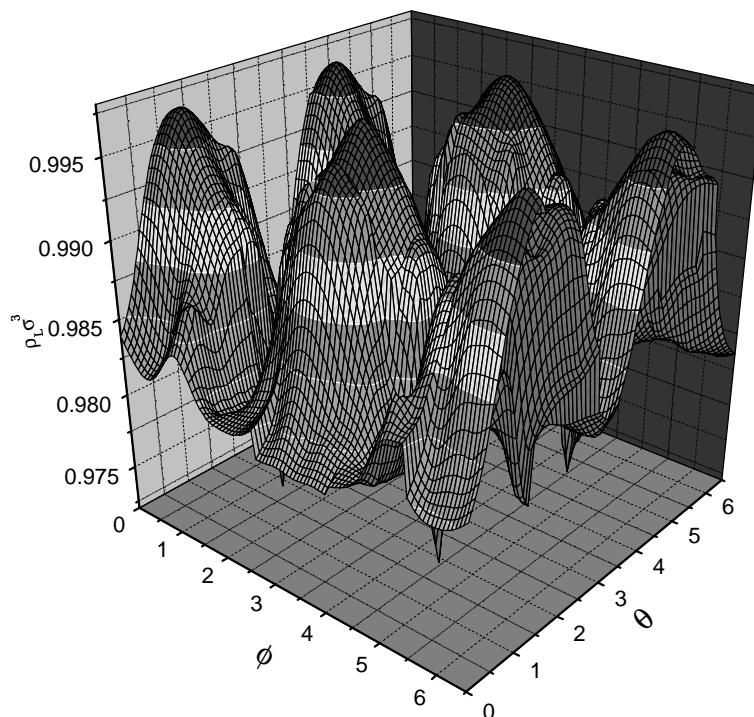


Figure 6.5: The freezing density of the polymeric liquid as a function of the lattice orientation angles θ and φ . The Figure shows results for the fcc lattice for the parameter values $\Gamma = 3.7$, $u = -0.5$, and degree of polymerization $N = 100$ in the Gaussian chain limit $\xi/l \gg 1$.

be seen that in the absence of an external field an increase in the degree of polymerization destabilizes the crystal [106]. It turns out that the dependence of the crystallization density on N in the presence of the external field becomes nonmonotonic. For long chains ($N \geq 200$) the freezing density saturates, while for relatively short chains ($N \leq 10$) there is no significant influence of an orienting field. We have no explanation for this.

6.5 Conclusions

We find that our model polymers crystallize more easily in an external field of the quadrupole type than in absence of that field, but only if it corresponds to a so-called disorienting field, *i.e.*, longitudinal shear. Geometric effects, such as the direction of the field with respect to the orientation of the lattice, play an important role in the stability of the crystal phase. We find that the competition between the configurational entropy of

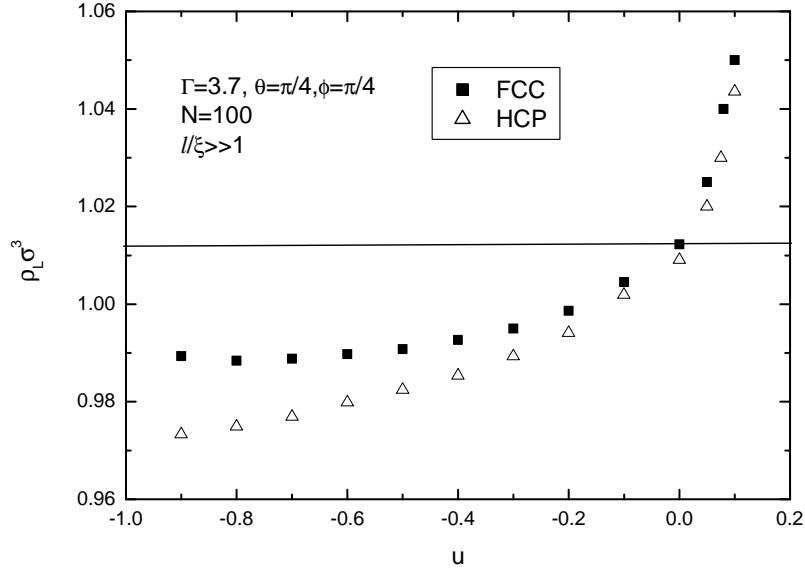


Figure 6.6: Comparison of the freezing density of the polymeric liquid in the Gaussian chain limit $\xi/l \gg 1$ for the fcc and hcp lattices as a function of the strength of external field for the angles $\theta = \pi/4$ and $\varphi = \pi/4$, at fixed $\Gamma = 3.7$ and $N = 100$. The hcp lattice crystallizes at lower density if under an external field.

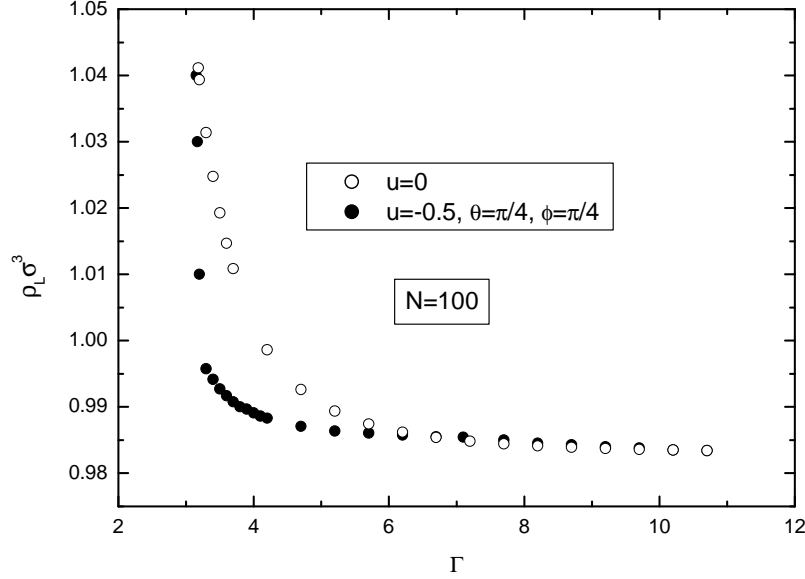


Figure 6.7: Freezing density of the polymeric liquid in the Gaussian chain limit $\xi/l \gg 1$ as a function of the fusion parameter Γ for the fcc lattice. Compared are values in the absence of the field and when $u = -0.5$ and angles $\theta = \pi/4, \varphi = \pi/4$.

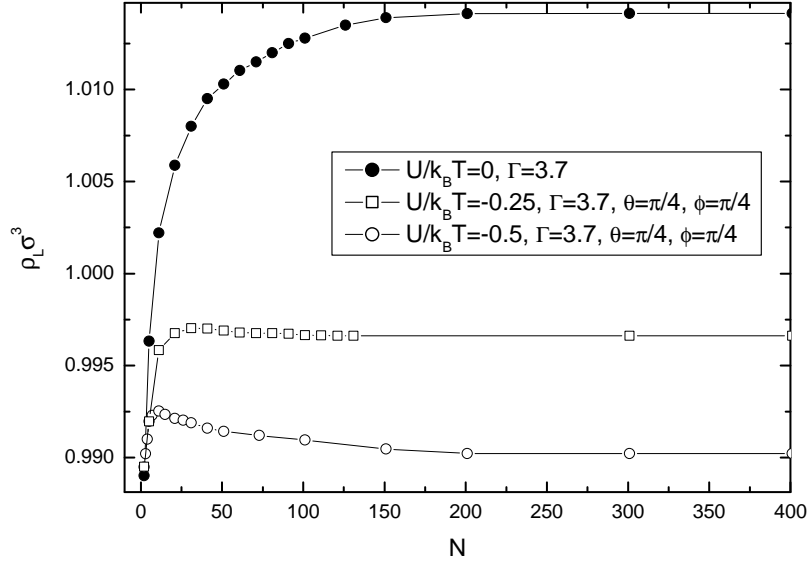


Figure 6.8: Freezing density of the polymeric liquid in the Gaussian-chain limit $\xi/l \gg 1$ for the fcc lattice as a function of degree of polymerization N for different values of u at fixed $\Gamma = 3.7$ and angles $\theta = \pi/4$, $\varphi = \pi/4$.

the chain and the strength of a field that couples to individual bonds leads to a non-trivial flow dependency of the stability of the model polymeric solid. Finally, it appears that the presence of an external field can stabilize one lattice type over another.

6.6 Appendix: The Fourier transform of the bond probability in the presence of an external orientational field

In this appendix we calculate the Fourier transform of the bond probability in the presence of a quadrupole field. In the presence of a weak enough external field, it can be expressed as

$$g_F = g(\mathbf{r}, \mathbf{r}') e^{-\beta U_{ext}(\mathbf{r}, \mathbf{r}')} \simeq g(\mathbf{r}, \mathbf{r}') (1 - \beta U_{ext}(\mathbf{r}, \mathbf{r}')). \quad (6.23)$$

For U_{ext} we use the Kramers potential, Eq. (6.7). We presume that the external field does not change the length of a single polymeric bond, and only changes the orientation of this bond. This assumption seems to be quite reasonable for weak enough external fields, *i.e.*, far from the coil-stretch transition [142].

We apply the following geometry. The angle between the director of a field \mathbf{n} and the vector \mathbf{q} in Fourier space we denote as γ , the angle between vector $\mathbf{r} - \mathbf{r}'$ and \mathbf{n} we mark as

ε , and, finally, the angle between $\mathbf{r} - \mathbf{r}'$ and \mathbf{q} we denote as α . The following trigonometric relationship in spherical coordinates (r, α, ψ) holds

$$\cos \varepsilon = \cos \gamma \cos \alpha + \sin \gamma \sin \alpha \cos \psi. \quad (6.24)$$

We perform the Fourier transformation of the full function of ξ in Eq. (6.2),

$$\begin{aligned} \widehat{g}_F = & \int_0^{2\pi} d\psi \int_{-\pi}^{\pi} \sin \alpha d\alpha \int_0^{\infty} r^2 dr g(r) \left(1 + \frac{3}{2} u (\cos^2 \gamma \cos^2 \alpha \right. \\ & \left. + \sin^2 \gamma \sin^2 \alpha \cos^2 \psi + \sin 2\gamma \cos \alpha \sin \alpha \cos \psi) \right) \exp[iqr \cos \alpha] \end{aligned} \quad (6.25)$$

to obtain

$$\begin{aligned} \widehat{g}_F(q) = & \exp[-q^2 \xi^2 / 6] \left\{ \sin(ql) + 3/4 u q^{-1} l^{-1} \sin(ql_K) (1 + \cos 2\gamma) \right. \\ & \left. + \frac{9}{4} u q^{-3} l^{-1} \xi^{-2} \sin(ql_K) (1 + 3 \cos 2\gamma) \right\} q^{-1} l^{-1} \\ & - \frac{9}{16} u \sqrt{6\pi} q^{-3} \xi^{-3} \exp[-3/2 l_K^2 / \xi^2] \\ & \times \left\{ \operatorname{erf} \frac{\xi^2 q - 3il}{\sqrt{6}\xi} + \operatorname{erf} \frac{\xi^2 q + 3il}{\sqrt{6}\xi} \right\} (1 + 3 \cos 2\gamma), \end{aligned} \quad (6.26)$$

where erf denotes the standard error function. Note that the sum of error functions in the last term is always real. In the absence of an external field the expression above simplifies to the familiar expression $\widehat{g}_F(q) = q^{-1} l^{-1} \exp[-q^2 \xi^2 / 6] \sin ql$ [106]. In the limit $\xi \gg l$ we get

$$\begin{aligned} \widehat{g}_F(q) = & \exp[-q^2 l_K^2 / 6] \left\{ 1 + \frac{1}{2} u (1 + 2P_2(\cos \gamma) + 18q^{-2} l_K^{-2} P_2(\cos \gamma)) \right\} \\ & - \frac{9}{2\sqrt{6}} u q^{-3} l_K^{-3} \sqrt{6\pi} P_2(\cos \gamma) \operatorname{erf}(ql_K), \end{aligned} \quad (6.27)$$

which in the absence of the field leads to the regular expression of the standard Gaussian model $\widehat{g}_F(q) = \exp[-q^2 l_K^2 / 6]$. In this last formula $P_2(\cos \gamma) = \frac{1}{2}(3 \cos^2 \gamma - 1)$ is the second Legendre polynomial. In the limit $ql_K \ll 1$ this expression simplifies to

$$\widehat{g}_F(q) = 1 + \frac{1}{2} u - \left(\frac{1}{6} + \frac{1}{12} u + \frac{1}{15} u P_2(\cos \gamma) \right) q^2 l_K^2. \quad (6.28)$$

Chapter 7

Beyond the polymeric reference interaction site model: angular correlations

ABSTRACT

In this chapter we present the general principles of a description of a model polymeric melt with angular correlations between the chain segments. We find that the classical polymer interaction site model (PRISM) is a limiting case of our theory, where the angular dependence of the direct correlation function of the interaction sites along the chains are averaged out, or absent altogether.

Angular correlations between different chains, brought about by anisotropic interactions, can play a very important role in the physics of polymers leading, *e.g.*, to liquid-crystalline states in polymeric fluids [1]. It seems reasonable to suggest that the coupling between angular and positional degrees of freedom also impacts upon the chain packing at higher densities, and that this coupling can stabilize the crystal phase [17]. Evidence from computer simulations supports this expectation [36].

The problem of the coupling between angular and positional degrees of freedom has been studied at various levels of approximation with the aid of highly coarse-grained polymer models in the context of the quasi one-dimensional crystallization to a (liquid-crystalline) smectic A phase [143, 144]. The link between the angular and positional degrees of freedom in true polymeric crystals, on the other hand, has not received a great deal of attention, presumably because for these more accurate polymer models seem to be required [19]. The most realistic polymeric model that one would use with this application in mind is the rotational isomeric state model (RIS) [23].

At present, there is no formalism that self-consistently deals with angular correlations between interacting chains, be it in isotropic melts, anisotropic melts, or crystalline phases. The purpose of this Chapter is to provide a first step towards such a formalism, and go beyond what is currently the state of the art in the description of polymeric melts, being the polymer reference interaction site model (PRISM) [82].

PRISM, developed by Chandler and Andersen [82], has become one of the most widely used theoretical tools for the description of polymeric melts. This model describes the microscopic structure of isotropic polymeric fluids reasonably well, except perhaps on very large length scales [88] as well as on very small ones where the microscopic details of the monomers come to the fore [88]. It may well be that angular correlations between bonds on different chains are at the root of the apparent discrepancy between theory and experiment in the limit of zero wave vector. There are indeed indications from computer simulation studies that angular correlations between chains impact upon the compressibility of the melt [36].

It so happens that PRISM as usually implemented cannot straightforwardly deal with angular degrees of freedom, although some time ago Pickett and Schweizer [145, 146] did adapt the PRISM formalism in their study of liquid crystallinity in semi-flexible polymers. To this end, they chose a specific form of scattering function in an *ad hoc* way. Such an approach obviously lacks self-consistency, and in fact does not reduce to well-established theoretical predictions for hard rods and hard semi-flexible chains in the limit where the second virial approximation becomes valid [143].

Here we formally *derive* the equivalent of an ‘aPRISM’ (or anisotropic PRISM) theory that should make possible the description of interacting polymers with angular memory under melt conditions. It is based on the Green-function formalism for the description of the freely-hinged polymeric models described in Chapter 3, and reduces to the standard PRISM formalism if the direct correlations between interaction sites on different chains are independent of any angular degrees of freedom, or if these dependencies are averaged out.

We introduce the following concise notation of coordinates in a single polymeric test chain that do have an angular memory (see Figure 7.1.)

$$\mathbf{1} = (\mathbf{r}_1, \mathbf{u}_1); \mathbf{2} = (\mathbf{r}_2, \mathbf{u}_2), \text{ etc.}, \quad (7.1)$$

where $\{\mathbf{r}_i\}$ denotes the positional and $\{\mathbf{u}_i\}$ angular degrees of freedom. The polymer Green function satisfies the following recursive equation [85]¹

$$Z(\mathbf{2}, \mathbf{1}; N + 1) = \exp(-\beta U_{scf}(\mathbf{2})) \int d\mathbf{3} Z(\mathbf{3}, \mathbf{1}; N) g(\mathbf{3}, \mathbf{2}) \quad (7.2)$$

with U_{scf} the self-consistent field the test chain experiences from the presence of the other chains, which we will treat as an external field [83], $g(\mathbf{3}, \mathbf{2})$ the so-called bond-probability

¹This is within a first-order Markov approach. Higher-order Markov descriptions follow trivially.

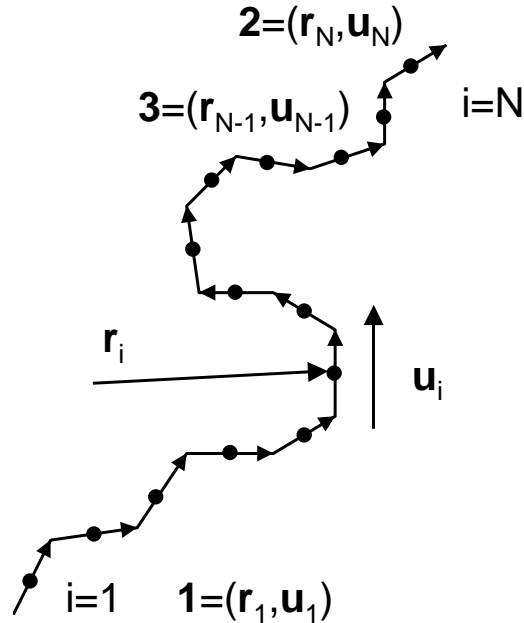


Figure 7.1: The geometry of the model polymer under consideration. Each point within the polymeric chain has the positional coordinate \mathbf{r} and coordinate \mathbf{u} associated with angular degrees of freedom. Note that $\mathbf{u}_i^2 \equiv 1$. See also main text.

‘kernel’, similar to those which we introduced in the previous chapters [86], and $\beta \equiv 1/k_B T$, where T denotes the absolute temperature and k_B Boltzmann’s constant. The coordinates $\mathbf{1}$ and $\mathbf{2}$ are those of the first and last bond, and $\mathbf{3}$ that of the last but one. (See Figure 7.1.)

The partition function of a single chain of N segments, Z_N , reads

$$Z_N = \int d\mathbf{1} \int d\mathbf{2} Z(\mathbf{2}, \mathbf{1}; N), \quad (7.3)$$

whilst the partition function \mathcal{Z} of a system consisting of M chains can, within a self-consistent field approximation, be calculated from

$$\mathcal{Z} = \frac{1}{M!} Z_N^M. \quad (7.4)$$

The free energy \mathfrak{F} is a function of \mathcal{Z} [106]

$$\beta\mathfrak{F} = -\ln \mathcal{Z} - \beta \int d\mathbf{1} U_{scf}(\mathbf{1})\rho(\mathbf{1}) + \beta \int d\mathbf{1} \phi(\mathbf{1})\rho(\mathbf{1}) + \beta F_{int}, \quad (7.5)$$

with ϕ the external potential, $\rho(\mathbf{1}) = \rho(\mathbf{r}, \mathbf{u})$ a mean segment density at position \mathbf{r} and with orientation \mathbf{u} , and F_{int} the free energy due to the interactions between the beads.

The mean segment density is connected to the polymer Green function according to

$$\rho(\mathbf{1}) \equiv M Z_N^{-1} \int d\mathbf{2} \int d\mathbf{3} \sum_{s=1}^N Z(\mathbf{2}, \mathbf{1}; 1, s) Z(\mathbf{1}, \mathbf{3}; s, N). \quad (7.6)$$

Note we have removed the self-consistent field contribution from the free energy, as it should.

The chemical potential of the monomers follows from minimization of the full free energy [94],

$$\mu = \frac{\delta \mathfrak{F}}{\delta \rho(\mathbf{1})} = -U_{scf}(\mathbf{1}) + \phi(\mathbf{1}) + \frac{\delta F_{int}}{\delta \rho(\mathbf{1})}. \quad (7.7)$$

In order to make the contributions from interactions explicit, we functionally expand the third term of Eq. (7.7), assuming the external field to be sufficiently weak, giving

$$\beta \frac{\delta F_{int}}{\delta \rho(\mathbf{1})} = -C^{(1)}(\mathbf{1}) - \int d\mathbf{3} C^{(2)}(\mathbf{1}, \mathbf{3}) \int d\mathbf{2} \chi(\mathbf{3}, \mathbf{2}) \phi(\mathbf{2}) + \dots \quad (7.8)$$

with $\chi(\mathbf{3}, \mathbf{2}) \equiv \delta \rho(\mathbf{3}) / \delta \phi(\mathbf{2})$ the response function that we later identify with the structure factor [49], $C^{(1)}(\mathbf{1}) \equiv C^{(1)}$ the zero-field one-particle direct correlation function, which is a constant for homogeneous isotropic systems, and $C^{(2)}(\mathbf{1}, \mathbf{3})$ the zero-field two-particle direct correlation function. For isotropic melts the following identities are valid:

$$\begin{aligned} C^{(2)}(\mathbf{1}, \mathbf{3}) &\equiv C^{(2)}(\mathbf{r}_1 - \mathbf{r}_3, \mathbf{u}_1, \mathbf{u}_3), \\ C^{(1)}(\mathbf{1}) &\equiv C^{(1)}, \\ \chi(\mathbf{3}, \mathbf{2}) &\equiv \chi(\mathbf{r}_3 - \mathbf{r}_2, \mathbf{u}_2, \mathbf{u}_3), \end{aligned} \quad (7.9)$$

where the indices $\mathbf{1}$, $\mathbf{2}$ and $\mathbf{3}$ now refer to the generalized co-ordinates of arbitrary segments.

It is much easier to manipulate the above equations in Fourier space. The Fourier transform of the self-consistent field, derived from Eqs. (7.7) and (7.8), reads

$$\begin{aligned} \widehat{U}_{scf}(\mathbf{q}, \mathbf{u}_1) &= \widehat{\phi}(\mathbf{q}, \mathbf{u}_1) - \mu \delta(\mathbf{q}) - C^{(1)} \delta(\mathbf{q}) \\ &\quad - \int d\mathbf{u}_2 \int d\mathbf{u}_3 \widehat{C}^{(2)}(\mathbf{q}, \mathbf{u}_1, \mathbf{u}_2) \widehat{\chi}(\mathbf{q}, \mathbf{u}_2, \mathbf{u}_3) \widehat{\phi}(\mathbf{q}, \mathbf{u}_3), \end{aligned} \quad (7.10)$$

where the hats indicate Fourier-transformed quantities.

From Eqs. (7.2) and (7.6) we can now (in principle) calculate in Fourier space the response of the angle-dependent density to the external field

$$\widehat{\delta \rho}(\mathbf{q}, \mathbf{u}_1) = \int d\mathbf{u}_2 \widehat{\chi}(\mathbf{q}, \mathbf{u}_1, \mathbf{u}_2) \widehat{\phi}(\mathbf{q}, \mathbf{u}_2), \quad (7.11)$$

where $\widehat{\delta \rho}(\mathbf{q}, \mathbf{u}_1) = \widehat{\rho}(\mathbf{q}, \mathbf{u}_1) - \rho_0 \delta(\mathbf{q}) / 4\pi$, and ρ_0 is the uniform segment density in the absence of the field, $\rho_0 \equiv \frac{1}{V} \int d\mathbf{r} \int d\mathbf{u} \rho(\mathbf{r}, \mathbf{u})$ with V the volume of the system. By applying

the Yvon equation that also holds for polymers [83], we find for the generalized structure factor of the polymeric melt

$$S(\mathbf{q}) = -\frac{1}{\rho} \int d\mathbf{u}_1 \int d\mathbf{u}_2 \widehat{\chi}(\mathbf{q}, \mathbf{u}_1, \mathbf{u}_2). \quad (7.12)$$

See also [147] and [148].

The external field $\widehat{\phi}(\mathbf{q}, \mathbf{u})$ has to be chosen such that it couples to number-density fluctuations of the interaction sites, producing the usual structure factor that measures correlations between pure density fluctuations. These remain influenced by translation-rotation coupling through the self-consistent field Eq. (7.10).

Clearly, to calculate $S(\mathbf{q})$ we need to establish $\widehat{\chi}$ first. To establish $\widehat{\chi}$, we in turn need to calculate the response of $\widehat{\rho}$ to the external field. The latter can only be calculated by solving the operator equation (7.3), which depends, through the self-consistent field Eq. (7.10), on $\widehat{\chi}$. Clearly, we are dealing with a highly non-trivial, self-consistent calculation that can only be executed provided $\widehat{C}^{(2)}$ is known. In practice, $\widehat{C}^{(2)}$ needs to be determined self-consistently too, through some closure. (See also below.)

A simpler route to achieve the same is as follows. We first switch off the interactions between the segments. In that case $\widehat{C}^{(n)} \equiv 0$, and we obtain for the self-consistent field

$$\widehat{U}_{scf}^0(\mathbf{q}, \mathbf{u}_1) = \widehat{\phi}(\mathbf{q}, \mathbf{u}_1) - \mu\delta(\mathbf{q}). \quad (7.13)$$

Here the superscript 0 indicates the absence of any interactions. From Eqs. (7.7) to (7.13) we calculate the response of $\widehat{\rho}^{(0)}$ to the field and find

$$\widehat{\delta\rho}^{(0)}(\mathbf{q}, \mathbf{u}_1) = \int d\mathbf{u}_2 \chi_0(\mathbf{q}, \mathbf{u}_1, \mathbf{u}_2) \widehat{\phi}(\mathbf{q}, \mathbf{u}_2) \quad (7.14)$$

with $\widehat{\chi}_0$ the response function for the case where the interactions are switched off, allowing us to calculate the form factor ω ,

$$\omega(\mathbf{q}) = -\frac{1}{\rho} \int d\mathbf{u}_1 \int d\mathbf{u}_2 \widehat{\chi}_0(\mathbf{q}, \mathbf{u}_1, \mathbf{u}_2), \quad (7.15)$$

which again follows from a generalization of the well-known Yvon equation [49]. (See again [147].)

If we switch on the interactions, it is obvious from Eq. (7.10) that, in line with the usual RPA-arguments, we merely have to replace $\widehat{\phi}$ by $\widehat{\phi} - \int d\mathbf{u}_2 \int d\mathbf{u}_3 \widehat{C}^{(2)}(\mathbf{q}, \mathbf{u}_1, \mathbf{u}_2) \widehat{\chi}(\mathbf{q}, \mathbf{u}_2, \mathbf{u}_3) \widehat{\phi}(\mathbf{q}, \mathbf{u}_3)$ in Eq. (7.14) to obtain the relevant response function [94, 106]. We obtain the equality

$$\begin{aligned} \widehat{\delta\rho}(\mathbf{q}, \mathbf{u}_1) &= \int d\mathbf{u}_2 \widehat{\chi}_0(\mathbf{q}, \mathbf{u}_1, \mathbf{u}_2) \\ &\left[\widehat{\phi}(\mathbf{q}, \mathbf{u}_2) - \int d\mathbf{u}_3 \int d\mathbf{u}_4 \widehat{C}^{(2)}(\mathbf{q}, \mathbf{u}_2, \mathbf{u}_3) \widehat{\chi}(\mathbf{q}, \mathbf{u}_3, \mathbf{u}_4) \widehat{\phi}(\mathbf{q}, \mathbf{u}_4) \right]. \end{aligned} \quad (7.16)$$

Rearranging the above expression, we get

$$\begin{aligned} \widehat{\delta\rho}(\mathbf{q}, \mathbf{u}_1) = & \int d\mathbf{u}_2 \widehat{\phi}(\mathbf{q}, \mathbf{u}_2) [\widehat{\chi}_0(\mathbf{q}, \mathbf{u}_1, \mathbf{u}_2) \\ & - \int d\mathbf{u}_3 \int d\mathbf{u}_4 \widehat{\chi}_0(\mathbf{q}, \mathbf{u}_1, \mathbf{u}_4) \widehat{C}^{(2)}(\mathbf{q}, \mathbf{u}_4, \mathbf{u}_3) \widehat{\chi}(\mathbf{q}, \mathbf{u}_3, \mathbf{u}_2)] , \end{aligned} \quad (7.17)$$

and, finally, obtain from Eq. (7.11) the identity

$$\begin{aligned} \widehat{\chi}(\mathbf{q}, \mathbf{u}_1, \mathbf{u}_2) = & \widehat{\chi}_0(\mathbf{q}, \mathbf{u}_1, \mathbf{u}_2) \\ & - \int d\mathbf{u}_3 \int d\mathbf{u}_4 \widehat{\chi}_0(\mathbf{q}, \mathbf{u}_1, \mathbf{u}_4) \widehat{C}^{(2)}(\mathbf{q}, \mathbf{u}_4, \mathbf{u}_3) \widehat{\chi}(\mathbf{q}, \mathbf{u}_3, \mathbf{u}_2). \end{aligned} \quad (7.18)$$

To explicitly solve Eq. (7.18) requires $\widehat{C}^{(2)}$ to be known. At the level of a second virial theory, $\widehat{C}^{(2)}$ may presumably be replaced by a Mayer function [49]. The approximation of Shimada, Doi and Okano [149] is in essence a second virial approximation, and they found by similar arguments Eq. (7.18) with $\widehat{C}^{(2)}$ replaced by a constant $-\omega$, showing the coarse-grained nature of their polymeric model.

Ideally, one obtains $\widehat{C}^{(2)}$ self-consistently from Eqs. (7.11), (7.12) and (7.18), and a suitable closure, analogous to the procedure followed in the PRISM formalism [82], albeit of course that in our case $\widehat{\chi}$ has to be calculated self-consistently as well. To calculate $\widehat{C}^{(2)}$ and $\widehat{\chi}$ self-consistently, we first have to calculate the response function $\widehat{\chi}_0$ in the absence of interactions, *e.g.*, by invoking the above described procedure in which is applied a suitably chosen external field that couples to pure density fluctuations.

By way of application of the described formalism, we make connection with the *classical* PRISM equation and show that it (implicitly) ignores angular direct correlations between segments. To this end, we define the following two-particle direct correlation function

$$\overline{C}(\mathbf{q}) = \widehat{C}^{(2)}(\mathbf{q}) \quad (7.19)$$

if the interactions between the sites are isotropic, or, if the interactions are not isotropic,

$$\overline{C}(\mathbf{q}) = \frac{1}{(4\pi)^2} \int d\mathbf{u}_1 \int d\mathbf{u}_2 \widehat{C}^{(2)}(\mathbf{q}, \mathbf{u}_1, \mathbf{u}_2). \quad (7.20)$$

Replacing $\widehat{C}^{(2)}$ by \overline{C} , Eq (7.18) can be written as

$$\begin{aligned} \widehat{\chi}(\mathbf{q}, \mathbf{u}_1, \mathbf{u}_2) \simeq & \widehat{\chi}_0(\mathbf{q}, \mathbf{u}_1, \mathbf{u}_2) \\ & - \overline{C}(\mathbf{q}) \int d\mathbf{u}_3 \widehat{\chi}(\mathbf{q}, \mathbf{u}_3, \mathbf{u}_2) \int d\mathbf{u}_4 \widehat{\chi}_0(\mathbf{q}, \mathbf{u}_1, \mathbf{u}_4). \end{aligned} \quad (7.21)$$

For the isotropic melt, the last term invoking the integration over \mathbf{u}_4 must be a constant. This implies that the entire integral is a constant of \mathbf{u}_1 and \mathbf{u}_2 , and that the isotropic response function can be written as

$$\widehat{\chi}(\mathbf{q}, \mathbf{u}_1, \mathbf{u}_2) = \widehat{\chi}_0(\mathbf{q}, \mathbf{u}_1, \mathbf{u}_2) + A \quad (7.22)$$

with a constant

$$A = -\frac{\overline{C}(\mathbf{q}) \left(\frac{1}{(4\pi)} \int d\mathbf{u}_1 \int d\mathbf{u}_2 \widehat{\chi}_0(\mathbf{q}, \mathbf{u}_1, \mathbf{u}_2) \right)^2}{1 + \overline{C}(\mathbf{q}) \int d\mathbf{u}_1 \int d\mathbf{u}_2 \widehat{\chi}_0(\mathbf{q}, \mathbf{u}_1, \mathbf{u}_2)} \quad (7.23)$$

that follows upon insertion. Thus, the structure factor becomes

$$S(\mathbf{q}) = \omega(\mathbf{q}) + \frac{\rho\omega^2(\mathbf{q})\overline{C}(\mathbf{q})}{1 - \rho\overline{C}(\mathbf{q})\omega(\mathbf{q})} = \frac{\omega(\mathbf{q})}{1 - \rho\overline{C}(\mathbf{q})\omega(\mathbf{q})}, \quad (7.24)$$

equivalent to the classical PRISM equation. We therefore conclude that PRISM is a limiting case of Eq. (7.18), where the orientational correlations between bonds on different chains are either absent from the onset because of isotropic site-site interactions, or because they are averaged out. This implies that within PRISM an interacting chain has the same angular correlations as a non-interacting one, which cannot be very accurate [36].

We conclude that the full Eq. (7.18) has to be used for the (RPA-like) description of the polymeric melt with bond-order correlations [149].

Chapter 8

Summary and proposals for future work

ABSTRACT

In this chapter we conclude the thesis, and give the outlook for future theoretical studies of polymer crystallization.

8.1 Summary and conclusion

An analysis of the crystallization of model polymers from the perspective of density functional theory was the main objective of our work. Although crystallization is an ultimate kinetic phenomenon, a free-energy landscape is vital as input for any reasonable kinetic theory of crystallization. Therefore, equilibrium studies of the crystallization aiming to obtain the free energy are, at least for shallow temperature quenches, of interest.

In this thesis we addressed the following questions:

- What is the main driving force for polymer crystallization?
- What is the role of polymer connectivity?
- Is it possible to predict with reasonable accuracy the elastic properties of polymeric solids on the basis of highly simplified models?
- What are the possible explanations for the variety of lattice types found in polymeric crystals?

- What is the influence of an external orienting flow on the stability of polymeric crystals?
- What can be done for a more realistic description of the angular-dependent polymeric systems?

In reply to these questions, we first presented in Chapter 3 an amalgamation of the Green-function description of the conformation of polymer chains and the density-functional theory of simple liquids into a self-consistent Green-function method for the chain-configuration statistics of polymer melts. It allowed us to study the stability of the polymer melt against non-uniform density distributions such as arise in the ordering of the chains in a crystal. We have shown that without internal chain stiffening by a configurational freezing of the intra-chain degrees of freedom, polymeric chains crystallize only if the effective Kuhn length in the chains is sufficiently large compared with the range of the hard-core interactions between the segments; in that case the densities of the coexisting phases are – apart from lattice frustration effects when the bonds are fully stiff – largely determined by the behavior of the monomeric hard spheres. We conclude that the packing entropy is the main driving force for the formation of polymeric crystal. The role of connectivity in the crystallization for the models under consideration is relative small, except if the effective Kuhn length is not large enough, then no crystal is observed. We found that short chains stabilize the crystal phase; hence, long chains crystallize at higher densities than short ones.

In Chapter 4 we derived from the crystal free energy an expression for the solid-polymer elastic moduli. It turns out that our predictions are already of the right order of magnitude, without adding any enthalpic contributions to the interactions between the chains, indicating once more the dominant role of entropy and of steric forces. The elastic moduli are weakly dependent on connectivity effects, only via the stabilization of the crystal phase. Our results for the Poisson ratio, the bulk and the Young's moduli are of the same order of magnitude as the experimental values, an indication of the importance of the interchain interactions to the elasticity of polymeric solids. We also improved significantly the RY DFT (see also Chapter 2) results for the hard sphere crystal, obtaining the physically realistic elastic moduli.

We studied the relative stability of two different lattice types for model polymeric solids in Chapter 5. The most stable crystal-lattice type appears to be determined by the mean length and the stretching stiffness of the bonds as well as by the size of the segments. We suspect that these effects are one possible explanation for the variety of crystal lattices observed for different polymers, apart from lattice frustration effects.

We find in Chapter 6 that our model polymers crystallize more easily if under the influence of an external field of the quadrupole type than in absence of that field, but only if an external field mimics elongational flow. The direction of the field with respect to the orientation of the lattice plays an important role in polymer crystallization. Another effect we discovered is that the presence of an external field can stabilize one lattice type over another.

We conclude in Chapter 7 that the often-used polymeric reference site model is a limiting case of a random phase approximation-like treatment derived for the angular-dependent polymeric systems, when the orientational correlations are averaged out. Our work can be used for the description of anisotropic liquid-crystalline polymeric melts.

8.2 Outlook

It is beyond doubt that for the more accurate description of polymer crystals more realistic polymeric models are needed. The rotational isomeric state model, which we mention in Chapter 1, seems to be a good candidate for such model. However, models with angular bond correlations are not easy to describe not least because the structure factor cannot be obtained in closed form as is the case in the classical PRISM theory. Therefore, in Chapter 7, we made a first step towards a more accurate description of the melts which exhibit angular correlations. The next step is the development of an angular-dependent density functional theory similar in spirit to those that are used to model liquid crystalline phases of low molecular weight substances. Unfortunately, also these theories are fraught with difficulty. Ultimately, we would like to address the role of anisotropy in the crystallization of polymers. Also we are looking for non-perturbative, easy-to-use DFTs for polymers that are better than the one used in the current work. The more accurate theories might shed light on the possibility of a metastable nematic phase hidden in the region where the crystalline state is stable.

Bibliography

- [1] U. W. Gedde, *Polymer Physics* (Chapman & Hall, London, 1992).
- [2] K. Herman, O. Gerngross, and W. Z. Abitz, *Phys. Chem.* **B10**, 371 (1930).
- [3] P. J. Flory, *J. Chem. Phys.* **17**, 223 (1949).
- [4] P. J. Flory, *J. Amer. Chem. Soc.* **84**, 2857 (1962).
- [5] D. Y. Yoon and P. J. Flory, *Faraday Disc. Royal Soc. Chem.* **68**, 288 (1979).
- [6] K. H. Storcks, *J. Am. Chem. Soc.* **60**, 1753 (1938).
- [7] W. Schlesinger and H. M. Leeper *J. Polym. Sci.* **11**, 203 (1953).
- [8] R. Jaccodine, *Nature* **176**, 305 (1955).
- [9] A. Keller, *Phil. Mag.* **2**, 1171 (1957).
- [10] P. H. Till, *J. Polym. Sci.* **24**, 301 (1957).
- [11] E. W. Fischer, *Z. Naturforsch* **12a**, 753 (1957).
- [12] K. D. Jandt, M. Buhk, M. J. Miles, and J. Petermann, *Polymer* **35**, 2458 (1994).
- [13] A. Keller and G. Goldbeck-Wood, in: 'Comprehensive Polymer Science', Suppl. Vol. II, S.L. Aggarwal and S. Russo (eds.), (Pergamon Press, Oxford, 1996).
- [14] T. Ezquerra, E. Lopez-Cabarcos, B. S. Hsiao, and F. J. Balta-Calleja, *Phys. Rev. E* **54**, 989 (1996).
- [15] G. R. Strobl, *The physics of polymers : concepts for understanding their structures and behavior* (Springer, Berlin, 1996).
- [16] P. D. Olmsted, W. C. K. Poon, T. C. B. McLeish, A. J. Ryan, and N. J. Terrill, *Phys. Rev. Lett.* **81**, 373 (1998).
- [17] P. J. Flory, *Proc. R. Soc. London, Ser. A* **234**, 60 (1956).

- [18] H. Meyer and F. Müller-Plathe, *Macromolecules* **35**, 1241 (2002).
- [19] J. D. McCoy, K. G. Honnell, K. S. Schweizer, and J. G. Curro, *J. Chem. Phys.* **95**, 9348 (1991).
- [20] C. W. Bunn, *J. Polym Sci.* **16**, 323 (1955).
- [21] B. Wunderlich, *Crystal Structure, Morphology, Defects* (Academic, New York, 1973).
- [22] K. S. Schweizer and J. G. Curro, *Phys. Rev. Lett.* **58**, 246 (1987).
- [23] P. J. Flory, *Statistical Mechanics of Chain Molecules* (Oxford Univ. Press, New York, 1988).
- [24] L. Onsager, *Ann. N. Y. Acad. Sci.* **51**, 627 (1949).
- [25] M. L. Huggins, *Ann. N. Y. Acad. Sci.* **43**, 1, (1942).
- [26] J. H. Gibbs, E. A. DiMarzio, *J. Chem. Phys.* **28**, 373 (1958).
- [27] P. D. Gujrati, *J. Phys. A: Math. Gen.* **13**, L437 (1980).
- [28] P. D. Gujrati and M. Goldstein, *J. Chem. Phys.* **74**, 2596 (1981).
- [29] P. D. Gujrati, *J. Stat. Phys.* **28**, 441 (1982).
- [30] J. F. Nagle, P. D. Gujrati, and M. Goldstein, *J. Phys. Chem.* **88**, 4599 (1984).
- [31] J. I. Lauritzen and J. D. Hoffman, *J. Res. Natl. Bur. Stand.* **64**, 73 (1960).
- [32] J. D. Hoffman and R. L. Miller, *Polymer* **38**, 3151 (1997).
- [33] D. M. Sadler and G. H. Gilmer, *Phys. Rev. Lett.* **56**, 2708 (1986).
- [34] D. M. Sadler and G. H. Gilmer, *Phys. Rev. B* **38**, 5684 (1988).
- [35] D. C. Bassett and A. Keller, *Philos. Mag.* **7**, 1553 (1962).
- [36] J. M. Polson and D. Frenkel, *J. Chem. Phys.* **109**, 318 (1998).
- [37] J. P. K. Doye and D. Frenkel, *Phys. Rev. Lett.* **81**, 2160 (1998).
- [38] T. Yamamoto, *J. Chem. Phys.* **115**, 8675 (2001).
- [39] P. Welch and M. Muthukumar, *Phys. Rev. Lett.* **87**, 218302-1 (2001).
- [40] C. Liu and M. Muthukumar, *J. Chem. Phys.* **109**, 2536 (1998).
- [41] I. Dukovski and M. Muthukumar, *J. Chem. Phys.* **118**, 6648 (2003).
- [42] A. Matsuyama, Y. Sumikawa, and T. Kato, *J. Chem. Phys.* **107**, 4711 (1997).

-
- [43] P. Hohenberg and W. Kohn, Phys. Rev. **136**, B864 (1964).
- [44] W. Kohn and L.J. Sham, Phys. Rev. **140**, A1133 (1965).
- [45] C. Ebner, W. F. Saam, and D. Stroud, Phys. Rev. A **14**, 226 (1976).
- [46] N. Mermin, Phys. Rev. **137**, A1441 (1965).
- [47] R. Evans, Adv. Phys. **28**, 143 (1979).
- [48] V. I. Kalikmanov, *Statistical Physics of Fluids* (Springer, Berlin, 2001).
- [49] J. P. Hansen and I. R. McDonalds, *Theory of Simple Liquids* (Academic Press, New York, 1986).
- [50] J. T. Chayes, L. Chayes, and E. H. Lieb, Commun. Math. Phys. **93**, 57 (1984).
- [51] J. T. Chayes and L. Chayes, J. Stat. Phys. **36**, 471 (1984).
- [52] T. V. Ramakrishnan and M. Yussouff, Phys. Rev. B **19**, 2775 (1979).
- [53] B. B. Laird, J. D. McCoy, and A. D. J. Haymet, J. Chem. Phys. **87**, 5449 (1987).
- [54] A. D. J. Haymet and D.W. Oxtoby, J. Chem. Phys. **74**, 2559 (1981).
- [55] B. Groh and B. Mulder, Phys. Rev. E **59**, 5613 (1999).
- [56] P. Tarazona, Phys. Rev. A **31**, 2672 (1985); Phys. Rev. E **32**, 3148(E) (1985).
- [57] R. L. Jacobs, J. Phys. C **16**, 273 (1983).
- [58] P. Tarazona, Mol. Phys. **52**, 81 (1984).
- [59] W. A. Curtin and N. W. Ashcroft, Phys. Rev. A **32**, 2909 (1985).
- [60] A. R. Denton and N. W. Ashcroft, Phys. Rev. A **39**, 4701 (1989).
- [61] M. Baus and J. L. Colot, Mol. Phys. **55**, 653 (1985).
- [62] M. Baus, J. Phys.: Condens. Matter. **2**, 2111 (1990).
- [63] Y. Rosenfeld, Phys. Rev. Lett. **63**, 980 (1989).
- [64] P. Tarazona, Phys. Rev. Lett. **84**, 694 (2000).
- [65] W. G. Hoover and F. H. Ree, J. Chem. Phys. **49**, 3609 (1968).
- [66] Y. Rosenfeld, M. Schmidt, H. Löwen, and P. Tarazona, Phys. Rev. E **55**, 4245 (1997).
- [67] D. Frenkel and A. J. C. Ladd, Phys. Rev. Lett. **59**, 1169 (1987).

- [68] M. V. Jarić, U. Mohanty, Phys. Rev. B **37**, 4441 (1988).
- [69] N. Sushko, P. van der Schoot, and M.A.J. Michels, J. Chem. Phys. **118**, 6098 (2003).
- [70] E. Velasco and P. Tarazona, Phys. Rev. A **36**, 979 (1987).
- [71] B. B. Laird, J. Chem. Phys. **97**, 2699 (1992).
- [72] H. Xu and M. Baus, Phys. Rev. A **38**, 4348 (1988).
- [73] A. Yethiraj and C. E. Woodward, J. Chem. Phys. **102**, 5499 (1995).
- [74] A. Yethiraj, J. Chem. Phys. **109**, 3269 (1998).
- [75] D. Chandler, J. D. McCoy, and S. J. Singer, J. Chem. Phys. **85**, 5971 (1986); **85**, 5977 (1986).
- [76] J. D. McCoy, S. J. Singer, and D. Chandler, J. Chem. Phys. **87**, 4953 (1987).
- [77] D. E. Sullivan, Phys. Rev. B **20**, 3991 (1979).
- [78] D. E. Sullivan, J. Chem. Phys. **74**, 2604 (1981).
- [79] W. E. McMullen and K. F. Freed, J. Chem. Phys. **92**, 1413 (1990).
- [80] E. Kierlik and M. L. Rosinberg, J. Chem. Phys. **97**, 9222 (1992).
- [81] J. G. Curro and K. Schweizer, J. Chem. Phys. **87**, 1842 (1987).
- [82] D. Chandler and H. C. Andersen, J. Chem. Phys. **57**, 1930 (1972).
- [83] P. van der Schoot, Macromolecules **33**, 8497 (2000).
- [84] K. G. Honnell and C. K. Hall, J. Chem. Phys. **90**, 1841 (1998).
- [85] S. F. Edwards Proc. Phys. Soc. **85**, 613 (1965).
- [86] A. Yu. Grosberg, and A. R. Khokhlov, *Statistical Physics of Macromolecules* (AIP Press, New York, 1994).
- [87] I. M. Lifshitz, A. Yu. Grosberg and A. R. Khokhlov, Rev. Mod. Phys. **50**, 3 (1978).
- [88] K. S. Schweizer, and J. G. Curro, Adv. Pol. Sci. **116**, 319 (1994).
- [89] K. G. Honnell, J. G. Curro and K. S. Schweizer, Macromolecules **23**, 3496 (1990).
- [90] L. Verlet, Phys. Rev. **163**, 201 (1968).
- [91] G. Jones and U. Mohanty, Mol. Phys. **54**, 1241 (1985).
- [92] J. P. Hansen and L. Verlet, Phys Rev. **184**, 151 (1969).

-
- [93] H. Takeuchi and R.-J. Roe, *J. Chem. Phys.* **94**, 7446 (1991).
- [94] P.-G. de Gennes, *Scaling Concepts in Polymer Physics* (Cornell University Press, Ithaca 1979).
- [95] I. Stakgold, *Green's Functions and Boundary Value Problems* (John Wiley & Sons, New York, 1998).
- [96] L. R. G. Treloar, *Polymer* **1**, 95 (1960).
- [97] *Solid Phase Processing of Polymers*, I. M. Ward, P. D. Coates, M. M. Dumoulin (Editors), Series Editor : Kun S. Hyun, Hanser Gardner Publications (2000).
- [98] K. Tashiro, M. Kobayashi, and H. Tadokoro, *Macromolecules* **10**, 731 (1977).
- [99] K. Tashiro, M. Kobayashi and H. Tadokoro, *Macromolecules* **11**, 908 (1978).
- [100] K. Tashiro, M. Kobayashi, and H. Tadokoro, *Macromolecules* **11**, 914 (1978).
- [101] M. S. Miao, M.-L. Zhang, V. E. van Doren, C. van Alsenoy, and J. L. Martins, *J. Chem. Phys.* **115**, 11317 (2001).
- [102] J. C. L. Hageman, J. W. van der Horst, and R. A. de Groot, *Polymer* **40**, 1313 (1999).
- [103] H. Löwen, *Phys. Reports* **237**, 249 (1994).
- [104] G. L. Jones, *Mol. Phys.* **61**, 455 (1987).
- [105] M. V. Jarić, U. Mohanty, *Phys. Rev. Lett.* **59**, 1170 (1987).
- [106] N. Sushko, P. van der Schoot, and M. A. J. Michels, *J. Chem. Phys.* **115**, 7744 (2001).
- [107] D. C. Wallace, *Solid State Physics* **25**, 301, (1970).
- [108] J. H. Weiner, *Statistical Mechanics of Elasticity* (Wiley, New York, 1983).
- [109] K. S. Schweizer and J. G. Curro, *J. Chem. Phys.* **89**, 3342 (1988).
- [110] J. M. Powers and R. M. Caddell, *Polymer Engineering and Science* **12**, 432 (1972).
- [111] *Physical Properties of Polymers Handbook*, ed. J. E. Mark, AIP Press (1996).
- [112] S. Alexander and J. McTague, *Phys. Rev. Lett.* **41**, 702 (1978).
- [113] B. J. Alder, W. G. Hoover, and D. A. Young, *J. Chem. Phys.* **49**, 3688 (1968).
- [114] K. W. Kratky, *Chem. Phys.* **57**, 167 (1981).

- [115] P. B. Bolhuis, D. Frenkel, S. Mau, and D. Huse, *Nature (London)* **388**, 235 (1997).
- [116] A. D. Bruce, N. B. Wilding, and G. J. Ackland, *Phys. Rev. Lett.* **79**, 3002 (1997).
- [117] P. N. Pusey, W. van Meegen, P. Bertlett, B. J. Ackerson, J. G. Rarity, and S. M. Underwood, *Phys. Rev. Lett.* **63**, 2753 (1989).
- [118] C. Dux and H. Versmold, *Phys. Rev. Lett.* **78**, 1811 (1997).
- [119] M. O. Robbins, K. Kremer, and G. S. Grest, *J. Chem. Phys.* **88**, 3286 (1988).
- [120] F. Igloi, *J. Phys. C* **19**, 6907 (1986).
- [121] F. Igloi, G. Kahl, and J. Hafner, *J. Phys. C* **20**, 1803 (1987).
- [122] M. Yussouff, *Phys. Rev. B* **23**, 5871 (1981).
- [123] J. L. Colot and M. Baus, *Mol. Phys.* **56**, 807 (1985).
- [124] B. B. Laird, J. D. McCoy, and A. D. J. Haymet, *J. Chem. Phys.* **88**, 3900 (1988).
- [125] *Processing of Polymers* edited by H. E. H. Meijer, Vol. 18 (VCH, New York, 1997).
- [126] S. P. Carrington and J.A. Odell, *J. Non-Newtonian Fluid Mech.* **67**, 269 (1996).
- [127] D. E. Smith and S. Chu, *Science* **28**, 1335 (1998).
- [128] P. G. De Gennes, *J. Chem. Phys.* **60**, 5030 (1974).
- [129] A. Peterlin, *Pure Appl. Chem.* **12**, 273 (1966).
- [130] A. Peterlin, *Adv. Macromol. Chem.* **1**, 225 (1968).
- [131] W. Hu, D. Frenkel, and V. B. F. Mathot, *Macromolecules* **35**, 7172 (2002).
- [132] K. de Moel, E. Flikkema, I. Szleifer, and G. ten Brinke, *Europhys. Lett.* **42**, 407 (1998).
- [133] A. Yu. Zubarev, *Colloid J.* **58**, 189 (1996).
- [134] D. Thirumalai, *J. Chem. Phys.* **84**, 5869 (1986).
- [135] A. R. Khokhlov and A. N. Semenov, *Macromolecules* **15**, 1272 (1982).
- [136] A. Ziabicki and L. Jarecki, *J. Non-Newtonian Fluid Mech.* **97**, 31 (2001).
- [137] A. Ziabicki and L. Jarecki, *J. Non-Newtonian Fluid Mech.* **54**, 269 (2001).
- [138] L. Jarecki and A. Ziabicki, *J. Non-Newtonian Fluid Mech.* **68**, 43 (1997).

- [139] S. M. Bhattacharjee, G. H. Fredrickson, and E. Helfand, *J. Chem. Phys.* **90**, 3305 (1989).
- [140] H. A. Kramers, *J. Chem. Phys.* **14**, 415 (1946).
- [141] H. L. Frisch, N. Pistorio, A. Sariban, K. Binder, and S. Fesjian, *J. Chem. Phys.* **89**, 5194 (1988).
- [142] S.-Q. Wang and W. M. Gelbart, *J. Chem. Phys.* **90**, 597 (1989).
- [143] P. van der Schoot, *J. Phys. II France* **6**, 1557 (1996).
- [144] A. V. Tkachenko, *Phys. Rev. Lett.* **77**, 4220 (1996).
- [145] G. T. Pickett and K. S. Schweizer, *J. Chem. Phys.* **112**, 4869 (2000).
- [146] G. T. Pickett and K. S. Schweizer, *J. Chem. Phys.* **110**, 6597 (1999).
- [147] M. Doi, T. Shimada, and K. Okano *J. Chem. Phys.* **88**, 4070 (1988).
- [148] V. A. Ivanov and A. N. Semenov, *Polymer Science U.S.S.R.* **30**, 1827 (1988).
- [149] T. Shimada, M. Doi, and K. Okano *J. Chem. Phys.* **88**, 2815 (1988).

Samenvatting

De belangrijkste doelstelling van ons werk is het maken van een analyse van de kristallisatie van modelpolymeren, vanuit het perspectief van de dichtheidsfunctionaaltheorie. Hoewel kristallisatie uiteindelijk een kinetisch bepaald proces is, is het vrije-energie landschap uitermate belangrijk als invoer voor elke redelijke kinetische theorie van de kristallisatie. Daarom is onderzoek dat evenwicht veronderstelt, met als doel de bepaling van de vrije energie, van belang, tenminste voor ondiepe temperatuur quenches.

In dit proefschrift hebben we de volgende vragen behandeld:

- Wat is de belangrijkste drijvende kracht achter polymeerkristallisatie?
- Wat is de rol van de connectiviteit van het polymeer?
- Is het mogelijk om, met sterk versimpelde modellen, een redelijke voorspelling te geven van de elastische eigenschappen van polymere vaste stoffen?
- Wat zijn de mogelijke verklaringen voor de diversiteit aan roostertypes die gevonden zijn in polymeerkristallen?
- Wat is de invloed van een externe oriënterende stroming op de stabiliteit van polymeerkristallen?
- Hoe kan een relativistische beschrijving van de hoekafhankelijke eigenschappen van polymersystemen verkregen worden?

In antwoord op deze vragen hebben we eerst in Hoofdstuk 3 een samensmelting gepresenteerd van een Green-functie beschrijving van polymeerketens en de dichtheidsfunctionaaltheorie van eenvoudige vloeistoffen in een zelfconsistente Green-functie methode voor de statistische eigenschappen van de ketenconfiguratie van polymere smelten. Deze methode stelde ons in staat om de stabiliteit van het polymeer te bestuderen in de aanwezigheid van niet-uniforme dichtheidsverdelingen, zoals die optreden bij het ordenen van ketens in een kristal. We hebben laten zien dat polymeerketens, in afwezigheid van interne ketenverstijving door het invriezen van de intra-keten vrijheidsgraden, alleen kristalliseren als de effectieve Kuhn lengte van de ketens groot genoeg is, vergeleken met de afstand waarover de harde-deeltjes interacties tussen de ketensegmenten hun werking hebben. In dit geval

worden de dichtheden van de coëxisterende fasen - afgezien van roosterfrustratie-effecten waar de bindingen volledig stijf zijn - grotendeels bepaald door het gedrag van de monomere harde bollen. We concluderen dat de pakkingsentropie de belangrijkste drijvende kracht is achter de vorming van een polymeerkristal. De rol van de connectiviteit op de kristallisatie is voor de beschouwde modellen relatief klein, behalve wanneer de effectieve Kuhn-lengte niet groot genoeg is, in welk geval geen kristalvorming waargenomen wordt. We hebben gevonden dat korte ketens de kristalfase stabiliseren, waardoor lange ketens bij hogere dichtheden kristalliseren dan korte.

In Hoofdstuk 4 hebben we uit de vrije energie van het kristal een uitdrukking voor de elastische moduli van het vaste polymeer afgeleid. Het blijkt dat onze voorspellingen, zelfs zonder het toevoegen van enthalpische bijdragen aan de interactie tussen de ketens, al van de juiste grootte-orde zijn, hetgeen weer wijst op de dominante rol van de entropie en sterische krachten. De elastische moduli hangen zwak af van connectiviteitseffecten, enkel via de stabilisatie van de kristalfase. Onze resultaten voor de Poisson ratio en de bulk- en Young-moduli zijn van dezelfde orde van grootte als de experimentele waarden, een aanwijzing voor het belang van de interketen-interacties voor de elasticiteit van polymere vaste stoffen. We hebben tevens de resultaten van RY DFT (zie Hoofdstuk 2) voor harde bollen significant verbeterd en daarbij fysisch realistische waarden voor de elastische moduli verkregen.

We hebben in Hoofdstuk 5 de relatieve stabiliteit van twee verschillende roostertypen voor modelpolymeren bekeken. Het stabielste kristalrooster lijkt bepaald te worden door de gemiddelde lengte en de stijfheid bij het strekken van de bindingen, evenals door de grootte van de segmenten. We vermoeden dat deze effecten, naast het roosterfrustratie-effect, een mogelijke verklaring geven voor de variëteit aan kristalroosters die voor verschillende polymeren zijn waargenomen.

In Hoofdstuk 6 vinden we dat onze modelpolymeren gemakkelijker kristalliseren onder invloed van een veld van het quadrupool type dan in de afwezigheid van dat veld, maar alleen als het veld elongatiestroming nabootst. De richting van het veld ten opzichte van de oriëntatie van het rooster speelt een belangrijke rol in polymeerkristallisatie. Verder vinden we dat een extern veld bepaalde roostertypes kan stabiliseren ten opzichte van andere.

We concluderen in Hoofdstuk 7 dat het vaak gebruikte polymeric reference site model een limietgeval is van een random phase approximation-achtige beschrijving afgeleid voor hoekafhankelijke polymeersystemen, wanneer de oriëntationele correlaties uitgemiddeld worden. Ons werk kan gebruikt worden om smelten van anisotrope, vloeibaar-kristallijne polymeren te beschrijven.

Er is geen twijfel mogelijk dat realistischer modellen nodig zijn voor een preciezere beschrijving van polymeerkristallen. Het rotational isomeric state model, dat we beschrijven in Hoofdstuk 1, lijkt een goede kandidaat te zijn voor een dergelijk model. Modellen met hoekcorrelaties zijn echter niet eenvoudig te beschrijven, niet in de laatste plaats omdat de structuurfactor niet in een gesloten vorm verkregen kan worden, zoals wel het geval is

in bijvoorbeeld de klassieke PRISM theorie. Daarom hebben we in Hoofdstuk 7 de eerste stap gezet naar een preciezer beschrijving van smelten die hoekcorrelaties vertonen. De volgende stap is de ontwikkeling van een hoekafhankelijke dichtheidsfunctionaaltheorie in de geest van die, welke gebruikt worden om vloeibaarkristallijne fasen van stoffen met een laag molecuulgewicht te modelleren. Helaas zijn ook deze theorieën erg gecompliceerd. Uiteindelijk zouden we de rol van anisotropie of de polymeerkristallisatie willen bespreken. Verder zijn we op zoek naar DFTs die niet gebaseerd zijn op perturbatie, die makkelijk in het gebruik zijn en bovendien beter dan degene die we in dit werk gebruiken. Preciezer theorieën zouden met name licht kunnen werpen op de mogelijkheid van een metastabiele nematische fase, verborgen in het gebied waar de kristallijne toestand stabiel is.

Acknowledgements

I would like to thank the people who played an important role in the creation of this thesis. First of all I want to thank my supervisor Thijs Michels, who gave me an opportunity to study and to work in The Netherlands. Also I would like to express my sincere gratitude to my direct supervisor, Paul van der Schoot, from whom I have learned a lot, and who helped me during all four years of my work, being not only a great teacher but also a good friend. His sense of humor and his view on the different, not only scientific, problems created a very interesting environment for my studies. I am really grateful for motivating me and without his help I would not manage to finish this thesis.

I would like to thank the members of my reading committee for the careful reading and for the valuable remarks and the corrections.

I am grateful to all my former colleagues from the Polymer Physics Group. Especially I want to thank my office mate Jeroen van Gestel for his kindness and help during my stay in Eindhoven. Also I want to thank Tanya Nimalasuriya and Peter Prinsen with whom I also shared the office for their help and pleasant discussions. I would like to thank my colleague Alexey Lyulin for his help and support. I am grateful to Frank Pasveer and Ali Nowbakht Irani for nice conversations, help and for being my squash partners and friends. Also I want to express my gratitude to Jan-Willem van der Horst, my former colleague, who became my good friend. I want to thank my friends, Vasily Belokurov, Mikhail Sizov, Ilja Malakhovskiy, and Sergey Trofimov, for their support and kindness.

I would like to thank Ania for being with me during this hard year. Lastly, I want to thank my grandma, aunts, cousin, all my family for supporting me my whole life. Especially, I want to express my gratitude to my parents, who love me so much and helped me a lot in my life. This thesis is dedicated to the memory of my grandfather Leonid Nesterov, to whom I am highly indebted.

Curriculum Vitae

The author was born on March 16, 1975 in Lviv, Ukraine. In September 1992 he started his education at Ivan Franko Lviv State University and graduated in 1997 with honors. From September 1997 to September 1999 he worked as a research assistant at the Institute of Physics, Polish Academy of Sciences, Warsaw, Poland. He performed computer simulations of proteins and simple liquids. From October 1999 to September 2003 he carried out his Ph.D. research at Eindhoven University of Technology, The Netherlands, studying the crystallization of polymers.

List of publications

Theory of the crystallization of hard polymeric chains in an orienting field,
N. Sushko, P. van der Schoot, and M.A.J. Michels,
submitted to *Macromolecules*.

Density functional theory for the elastic moduli of a model polymeric solid,
N. Sushko, P. van der Schoot, and M.A.J. Michels,
J. Chem. Phys. **118**, 6594 (2003).
(Erratum: **119**, 639 (2003).)

On the role of connectivity in the relative stability of crystal types for model polymeric solids,
N. Sushko, P. van der Schoot, and M.A.J. Michels,
J. Chem. Phys. **118**, 6098 (2003).

Density-functional theory of the crystallization of hard polymeric chains,
N. Sushko, P. van der Schoot, and M.A.J. Michels,
J. Chem. Phys. **115**, 7744 (2001).
(Erratum: **116**, 5325 (2001).)

Motion of grains, droplets, and bubbles in fluid-filled nanopores,
N. Sushko and M. Cieplak,
Phys. Rev. E **64**, 021601 (2001).

Dynamical chaos and power spectra in toy models of heteropolymers and proteins,
M. S. Li, M. Cieplak, and N. Sushko,
Phys. Rev. E **62**, 4025 (2000).

Spin analogues of proteins: scaling of 'folding' properties,
T. X. Hoang, N. Sushko, M. S. Li, and M. Cieplak,
J. Phys. A **33**, 3977 (2000).